Piliated *Neisseria gonorrhoeae* induce host cell signaling to stabilize extracellular colonization and microcolony formation

D i s s e r t a t i o n

zur Erlangung des akademischen Grades

d o c t o r r e r u m n a t u r a l i u m

(Dr. rer. nat.)

im Fach Biologie

eingereicht an der

Mathematisch-Naturwissenschaftlichen Fakultät I

der Humboldt-Universität zu Berlin

von

Jan Peter Böttcher

Präsident der Humboldt-Universität zu Berlin

Prof. Dr. Jan-Hendrik Olbertz

Dekan der Mathematisch-Naturwissenschaftlichen Fakultät I

Prof. Dr. Andreas Herrmann

Gutachter: 1. Prof. Dr. Thomas F Meyer

2. Prof. Dr. Dr. h.c. mult. Jörg Hacker

3. Prof. Dr. Thomas Rudel

Tag der mündlichen Prüfung: 08.04.2011

Table of contents

Abstract

The obligate human pathogen *Neisseria gonorrhoeae* causes the sexually transmitted disease gonorrhea. This type-IV-pili (Tfp)-producing bacterium colonizes mucosal epithelia of the human urogenital tract. The early stages of infection with piliated *N. gonorrhoeae* (P^+GC) are characterized by Tfp-mediated adherence to host cells, followed by formation of bacterial microcolonies on the surface of host epithelial cells. This study provides evidence that host cell participation is required for the efficient formation of extracellular microcolonies during *Neisseria* infection. P^+GC infecting fixed host cells demonstrate altered motility and delayed microcolony formation compared to infecting living host cells.

Cortical actin and various signal transducing proteins are recruited to the site of bacterial attachment within host cells, one of them being the major structural protein of plasma membrane caveolae, caveolin-1 (Cav1). Down-regulation of Cav1 results in increased uptake of P^+GC into host cells whereas expression of the protein in Cav1-negative cells blocks bacterial internalization. Host cell entry results in decreased viability of internalized bacteria over time, thus premature uptake is deleterious for the bacteria. In this study Cav1 recruitment is demonstrated to be an immediate and continuous cellular response to P^+GC infection that involves Cav1 phosphorylation on its tyrosine 14 residue. Prevention of bacterial uptake mediated by Cav1 as well as tight association of Cav1 with the cytoskeleton also requires tyrosine phosphorylation. A broad analysis of interaction partners of phosphorylated Cav1 revealed a direct interaction with the Rho-family guanine nucleotide exchange factor Vav2. Both Vav2 and its substrate, the small GTPase RhoA, are involved in preventing bacterial uptake and RhoA activation after P^+GC infection requires Cav1 expression, thus providing evidence for a Cav1-Vav2-RhoA signaling cascade. Moreover, six novel SH2-domain containing interaction partners of tyrosine phosphorylated Cav1 have been identified, all of which have been implicated in modulating the cytoskeleton. This study highlights how Tfp-producing bacteria avoid host cell internalization, as enteropathogenic *E. coli* was also found to recruit Cav1 similar to P^+GC, establishes a mechanistic link between Cav1 phosphorylation and pathogen-induced cytoskeleton reorganization and advance our understanding of caveolin function. The establishment and maintenance of an extracellular state might benefit certain pathogens by providing them time to express virulence factors required for subsequent infection steps.

Zusammenfassung

Das obligat humanpathogene Pathogen *Neisseria gonorrhoeae* ist der Erreger der sexuell übertragbaren Krankheit Gonorrhoe. Es handelt sich dabei um ein Typ-IV-Pili (Tfp) exprimierendes Bakterium, das die Schleimhäute des menschlichen Urogenitaltrakts besiedelt. Die frühen Infektionsstadien piliierter *N. gonorrhoeae* (P^+GC) sind durch die Tfp-vermittelte Adhärenz an Wirtszellen gekennzeichnet. Anschliessend erfolgt die Bildung von bakteriellen Mikrokolonien auf der Oberfläche der Wirtszellepithelien. In dieser Arbeit wird gezeigt, dass auch die Wirtszellen an der effizienten Bildung der extrazellulären Mikrokolonien beteiligt sind. P^+GC die fixierte Wirtszellen infizieren weisen veränderte Bewegungsmuster sowie eine verzögerte Mikrokoloniebildung gegenüber einer Infektion lebender Wirtszellen auf.

Kortikales Aktin wird zusammen mit anderen an verschiedenen Signalwegen beteiligten Proteinen innerhalb der Wirtszellen zu den adhärierten Bakterien rekrutiert, darunter das Haupt-strukturprotein von Caveolae-Membrandomänen, caveolin-1 (Cav1). Eine Reduzierung der Cav1 Proteinexpression führt zu einer verstärkten Aufnahme von P^+GC in die Wirtszellen, wohingegen die Expression von Cav1 in Cav1-negativen Zellen eine Internalisierung verhindert. Internalisierte Bakterien weisen dabei geringere Überlebens-raten auf je länger sie in den Wirtszellen verbleiben, folglich ist diese verfrühte Aufnahme durch die Wirtszellen für die Bakterien schädlich. In dieser Arbeit wird gezeigt, dass die Rekrutierung von Cav1 eine unmittelbare und kontinuierliche zelluläre Antwort auf eine Infektion mit P^+GC ist, welche die Phosphorylierung von Cav1 an Tyrosin 14 bedingt. Zusätzlich erforderte die Cav1-vermittelte Blockierung der Internalisierung der Bakterien und die Verankerung von Cav1 mit dem Zytoskelett eine Tyrosinphosphorylierung von Cav1. Eine umfassende Analyse möglicher Interaktionspartner von phosphoryliertem Cav1 zeigte eine direkte Interaktion mit Vav2, einem Guaninnukleotid-Austauschfaktor für GTPasen der Rho-Familie. Sowohl Vav2 als auch sein Substrat, die kleine GTPase RhoA, blockieren die Aufnahme von Bakterien in die in Wirtszellen. Die Aktivierung von RhoA nach P^+GC Infektion erfordert die Expression von Cav1, was auf einen Cav1-Vav2-RhoA Signalweg hindeutet. Darüber hinaus wurden in dieser Arbeit sechs neue, eine SH2-Domäne-beinhaltende Interaktionspartner von phosphoryliertem Cav1 identifiziert, welche ebenfalls mit der Regulierung zytoskeletaler Veränderungen in Verbindung gebracht wurden. Weiterhin

konnte gezeigt werden, dass auch enteropathogene *E. coli* in der Lage sind Cav1 zu rekrutieren, was daher das Verständnis erweitert wie Tfp-produzierende Bakterien einer frühen Internalisierung durch Wirtszellen entgehen. Des Weiteren wurde eine mechanistische Verbindung zwischen der Phosphorylierung von Cav1 und einer Pathogen-vermittelten Umordnung des Zytoskeletetts etabliert und eine Beitrag zur Klärung der zellbiologischen Funktionen von caveolin geliefert. Die beschriebene Etablierung und Aufrechterhaltung des initialen extrazellulären Infektionsschrittes könnte den pathogenen Mikroorganismen Zeit zur Expression von im weiteren Verlauf der Infektion benötiger Virulenzfaktoren verschaffen.

INTRODUCTION

1 Introduction

1.1 Host-bacteria interactions

The major goal of infection biology is to elucidate the molecular mechanisms involved in host-bacteria interactions. This interplay between pathogenic microorganisms and their hosts is a complex multi-step process, which has been extensively shaped by evolution. Bacteria utilize virulence factors to establish successful host colonization, which are expressed simultaneously or consecutively during all phases of infection. Virulence factors mediate processes such as cell adherence, cell invasion, immunoevasion and immunosuppression. The host relies on the innate and the adaptive immune responses to counter microbial infection strategies. The evolutionary race between host defenses and bacterial virulence factors often results in a high molecular specificity of host-bacteria interactions and thus a strict host tropism of these pathogens. The host tropism is mostly determined by the adherence of the pathogens to the host cells by binding to specific receptors, which consequently triggers specific host cell responses and signal cascades within the infected cell.

1.1.1 Adherence of bacteria to host cells

Attachment of bacteria to mucosal surfaces is the initial event required for pathogenesis of most infectious diseases (*4*). Bacteria can reach mucosal epithelia at body/environment interfaces that are present in the respiratory, digestive and urogenital tract. To evade mechanical unspecific immune responses such as microvilli activity, peristaltic movement and body fluid flows, bacteria need to attach quickly and firmly to their host cells. For that purpose pathogenic bacteria express adhesive molecules, called adhesins, to specifically bind to receptors present in the host cell membrane. Pathogenic bacteria target receptor molecules that typically fulfill essential host functions and therefore have to be expressed by the host cell (*5*). Bacteria utilize hairlike, polymeric pili and fimbriae as well as monomeric adhesive membrane-bound molecules to attach to host cells (*6*). Filamentous pili and fimbriae allow initial interactions at a distance beyond a protective bacterial capsule, which enables the bacteria to escape phagocytic immune cells.

Consequently, polymeric pili and fimbriae are found in many Gram-negative bacteria such as pathogenic *E. coli*, *Yersinia spp., Salmonella spp., Shigella spp., Vibrio spp., Pseudomonas spp.* and *Neisseria spp*. as well as Gram-positive bacteria such as *Corynebacterium spp.* and *Streptococcus spp*. (*6*). In Gram-negative bacteria different types of pili exist, such as type I pili, P pili, type IV pili (Tfp) and curli. Pili are typically formed by non-covalent interactions between subunits of pilin, the major pilus protein. In contrast, Gram-positive bacteria mainly form pili by covalent polymerization of adhesive pilin subunits (*7*). Adherence to host cells is normally mediated by the end or tip of the pilus at which the actual fimbriae or pili (*8, 9*) or a pilus-associated protein (e.g. FimH of *E. coli* type I pili or PilC of Tfp of pathogenic *Neisseria* (*10, 11*)) can function as the adhesin to host receptors. After initial pilus-mediated binding, many bacteria can establish a secondary, more intimate binding with additional host-cell receptors via adhesive membrane-bound molecules, such as the opacity associated (Opa) proteins of pathogenic *Neisseria* (*12*). This binding can strengthen the host-pathogen association and/or mediate subsequent infection steps, such as bacterial invasion into host cells. In addition, adhesin-ligand interactions during adherence can initiate host cell signaling cascades that may affect bacterial uptake or invasion and also promote pro- or anti-inflammatory events.

1.1.2 Invasion of pathogenic bacteria into host cells

Adhesion to host cells may result in bacterial internalization, either by bacterial-induced endocytosis (termed invasion) or phagocytosis. Invasion either enables the pathogen to accommodate and replicate within host cells, as in the case of *Chlamydia*, *Salmonella*, *Yersinia*, *Legionella*, *Listeria* and *Burkholderia*, or to pass through the epithelial layer to reach further extracellular niches, as observed in pathogenic *Neisseria* and enteropathogenic *E. coli* (EPEC). Some bacteria, such as *Chlamydia* (*13*) and *Rickettsia* (*14*) are obligate intracellular pathogens and rely on cellular internalization to replicate and establish a successful infection. Invasion to epithelial and endothelial host cells is mediated by virulence factors called invasins. Binding of invasins to specific host cell receptors triggers cellular signaling cascades leading to actin cytoskeleton rearrangements that drive bacterial invasion (*10*). Invasin, a surface protein of *Yersinia enterocolitica* and *Yersinia pseudotuberculosis* was the first bacterial invasion protein identified (*15*). It binds with high

affinity to various members of the β1 chain integrin family (*16*). Upon Invasin binding, the cytoplasmic part of β1 integrins then recruits focal adhesion kinase (FAK) or Src family kinases, which enables *Yersinia* to invade non-phagocytic cells (*17, 18*). In *Neisseria*, the Opa outer membrane proteins function as tight adhesins but are also known to induce invasion. To exploit host cell components and signaling pathways in order to gain entry into their host cells represents a common scheme among invading pathogens.

1.2 Pathogenic *Neisseria*

Two important human pathogens, *N. gonorrhoeae* (gonococci, GC) and *N. meningitidis* (meningococci), which cause gonorrhea and meningitis, respectively (*19, 20*), are part of the genus *Neisseria*, that belongs to the *Neisseriaceae* family within the class of β-proteobacteria. *Neisseria* are Gram-negative, strictly aerobic, 0.6-1.5 µm long diplococci colonizing the mucosa of humans and other endotherms. The closely related, obligate human pathogens *N. gonorrhoeae* and *N. meningitidis* cannot survive outside the human host and thus rely completely on humans for disease transmission. The genus also contains non-pathogenic species including *N. mucosa, N. sicca, N. flava, N. lactamica* and *N. cinerea,* which are commensals living in the mucosa of the human oro- and nasopharynx and rarely cause opportunistic infections (*21*).

1.2.1 Meningococcal pathogenesis

N. meningitidis colonizes the mucosa of the upper respiratory tract and does not cause diseases in the vast majority of carriers. As the prevalence in the population is around 10-35% in non-epidemic geographic areas (*22*), meningococci can be regarded as a normal part of the nasopharyngeal flora. The bacteria are transmitted from person to person through droplets of respiratory or throat secretions. It is likely that, at some time during life, most individuals are colonized with meningococci. A disease outbreak therefore represents a failed or dysfunctional relationship with the host. For unknown reasons, meningococci invade and pass the mucosal epithelium in these cases, reach the bloodstream, multiply intravascularly and disseminate in the body, resulting in acute meningococcal sepsis. The bacterium eventually passes the blood-brain barrier, causing fulminant meningitis (*23*).

Meningococcal meningitis is characterized by high fever, rash, nausea, severe headache and a stiff neck and if left untreated the disease can cause death within hours (*19, 24*), exhibiting a fatality rate of ~10% (*25*). Despite the reported high rates of meningococcal carriage in many human populations, the disease is rare, exhibiting annual incidence rates varying from 1 to 1000 cases per 100,000 individuals in different countries (*22*). Based on different capsular polysaccharide structures of *N. meningitidis* 13 serogroups have been classified, but only six serogroups (A, B, C, W-135, X and Y) cause the life-threatening disease. The disease can also cause epidemics which are currently confined to the so-called "meningitis belt", which reaches from Ethiopia to Senegal. Epidemics in sub-Saharan Africa have been associated with serogroups A, Y and W135 whereas in Europe disease is mainly caused by serogroup B and by serogroup Y in North America. However, cases associated with Serogroup C are reported worldwide (*22*).

1.2.2 Gonococcal pathogenesis

N. gonorrhoeae causes gonorrhea (colloquial "the clap"), one of the most common sexually transmitted infections (STIs) in the world and the WHO estimates that the global annual incidence rate is around 62 million cases (*26*). Gonococci typically colonize the mucosal epithelia of the urethra and the cervix, but also the rectum, the throat and the conjunctiva of the eye can be infected (*20*). In addition to highly contagious sexual transmission among adults, infants of infected mothers are prone to eye infection during delivery. Most cases of gonorrhea are uncomplicated genital tract infections: cervicitis in women and urethritis in men. The bacteria cause a local mucosal infection that is followed by an infiltration of large numbers of polymorphonuclear leukocytes (PMN), leading to sloughing of the epithelium, submucosal microabscesses and exudation of pus (*20*). Exudates from infected individuals contain PMNs with large numbers of ingested gonococci. However, clearance of the bacteria by PMNs is incomplete as a small gonococcal subpopulation is able to survive and also replicate in the PMNs (*27, 28*). Typical clinical symptoms of gonorrhea are purulent urethral discharge and dysuria in men and vaginal discharge, pelvic pain, dysuria and abnormal uterine bleeding in women (*29*). However, 15% of infected men and 80% of infected women remain without symptoms, yet are infectious and can transmit the disease (*20*). As the majority of infected women are asymptomatic,

many receive treatment only after referral from a symptomatic male partner. An untreated infection can cause complications as it can extend to the fallopian tubes and result in pelvic inflammatory disease and salpingitis, finally leading to infertility. Uncomplicated gonorrhea can be treated successfully with antibiotics such as the third generation of cephalosporins. Disseminated gonococcal infection (DGI) represents a rare systemic complication of the disease where bacteria have entered the bloodstream. In 0.5-3% of total gonorrhea cases, DGI can lead to more severe disease manifestations that include septic arthritis and dermatitis or even endocarditis, perihepatitis and meningitis (*30-32*).

1.2.3 *Neisseria* virulence factors

Neisseria possess a set of virulence factors required for successful human infection and transmission to a new host. These pathogenicity factors, including Tfp, Opa-proteins, lipooligosaccharide (LOS), IgA1 protease, Porin and the meningococcal polysaccharide capsule, will be further discussed in this chapter. These virulence factors can be expressed consecutively or simultaneously during the infection process. Tfp and Opa proteins frequently undergo prominent antigenic and phase variation to avoid detection by the host immune system. Phase variation of bacterial proteins is defined by random high-frequency on-off switching of their expression within a bacterial population, whereas antigenic variation alters the properties of a protein through gene-pseudogene recombination. Antigenic and phase variation of neisserial surface proteins contribute to the virulence of the bacteria by generating heterogeneity among the population thus promoting immune evasion.

Type-IV-pili

Tfp are filaments on the surfaces of *Neisseria* and many other Gram-negative bacteria that mediate an extraordinary set of functions, such as initial adhesion to host cells, bacterial aggregation, twitching motility, microcolony (MC) formation and DNA uptake during transformation (*33*). Tfp are found in many different bacteria such as *Vibrio cholerae* (*34*), *Salmonella enterica* (*35*), *Pseudomonas aeruginosa* (*36*), *Moraxella bovis* (*37*) and EPEC (*38*). In case of *Neisseria*, pili are important virulence factors that are required for a

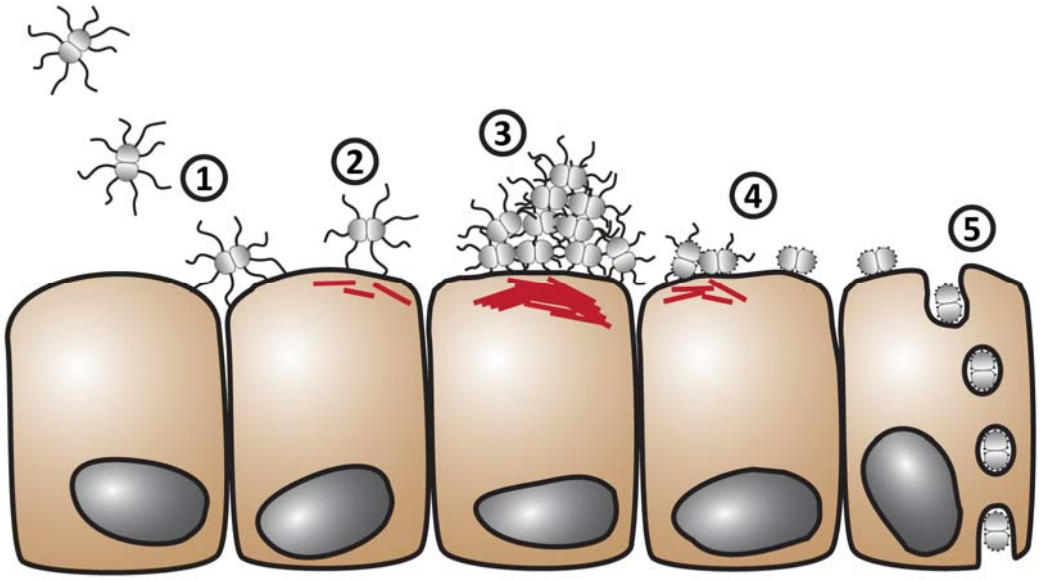

Figure 1-1. Early stages in the interaction of *N. gonorrhoeae* with host cells epithelia (1) Initial adhesion to host cells is mediated by Tfp. (2) Tfp binding and retraction leads to recruitment of diverse host cell proteins and induction of signaling pathways. (3) Piliated bacteria aggregate to large extracellular MCs while host cells form dynamic networks of cytoskeletal and signaling proteins underneath bacterial attachment sites. (4) Intimate contact of bacteria with the host cell surface is mediated by binding of Opa adhesins to HSPG or CEACAM receptors (5) Opa-mediated binding can trigger invasion of individual diplococci which is followed by epithelial cell transcytosis, enabling the bacteria to spread to deeper tissues. Figure adapted from (*2*).

successful infection (*39, 40*) as they mediate adherence to different cell types, such as epithelia, endothelia, sperm cells, erythrocytes, granulocytes and macrophages. Neisserial Tfp are dynamic molecular machines which execute complex processes such as fiber assembly and extension, fiber adhesion, fiber disassembly and retraction in order to fulfill above mentioned functions. Tfp are polymeric structures, mainly composed of the 18-22 kDa pilE protein (synonymous pilin), which are 6 nm in diameter and up to several micrometers in length (*33*). In addition to pilin, many other pilus-associated proteins are required for pilus formation. Pilin is synthesized as a prepilin precursor protein that has to be processed by the PilD prepilin peptidase/transmethylase before the polymeric pilus fiber can be assembled. PilD processing results in the mature pilin subunit with a characteristic α-methylated phenylalanine residue at its N-terminus (*41, 42*). Mature Pilin is then assembled into the pilus fiber by a molecular machinery and forms a right-handed helical cylinder with a fivefold symmetry around the helix axis (*43, 44*). Different pilus-associated proteins are required for functional pilus assembly by this molecular motor: PilF, a putative

ATPase, is mediating *Neisseria* pilus fiber formation in the periplasm (*42*). A dodecamer of the minor pilus protein PilQ forms a gated channel in the outer membrane through which the pilus fiber is elongated (*45*). PilT mediates pilus disassembly from the fiber base and thus is responsible for pilus retraction (*33, 46*). PilT function relies on ATP hydrolysis and ATP depletion reduces the rate of retraction (*47*). Knockout mutants of PilT are hyperpiliated, do not exhibit twitching motility or natural competence and form abnormal extracellular bacterial MCs (*48, 49*). The high molecular weight protein PilC was described to regulate PilT-mediated pilus retraction and thus functions in elongation of the pilus (*50, 51*). There are two gene copies of PilC in *Neisseria*, PilC1 and PilC2, and full PilC null mutants have been reported to be defective for pilus biogenesis (*52*). Also PilC was found to be localized at the pilus tip and to function as the pilus adhesin (*11*). In other studies, PilC was also shown to be associated with the bacterial cell surface, regardless of piliation (*53*). Lastly, minor pilus proteins including PilV, which is essential for adherence to epithelial cells (*54*), as well as PilU and PilX, which have a function in bacterial aggregation (*55*), have been described. As mentioned above the virulence factor pilin undergoes recombinase A-dependent antigenic recombination to increase bacterial variety, which occurs between one of several silent pilS pilin pseudogenes and the pilE expression locus (*56-58*).

The nature of the host cell pilus receptor is discussed controversially. At first the surface protein CD46 was proposed to serve as the pilus receptor. Expression of human CD46 resulted in Tfp-mediated binding to hamster cells and cell treatment with purified CD46 as well as anti-CD46 antibodies inhibited binding of piliated *Neisseria* (*59*). However, opposing studies could not demonstrate differences in adherence of piliated *Neisseria* or the pilus adhesin PilC after cell treatment with anti-CD46 antibodies, CD46-expression in animal cells or after siRNA-mediated down-regulation of CD46 *(60, 61).* Alternatively, I-domain-containing integrins have been proposed recently as pilus receptors in urethral epithelial cells (*62*).

Opacity-associated proteins

The second class of neisserial adhesins is encoded by the multigene, phase-variable *opa* gene family, which mediates a more intimate association with the host cell and triggers

bacterial invasion (*63*). The expression of neisserial Opa proteins leads to a change in plate colony opacity and color due to an increase in bacterial aggregation (*64*). Gonococcal strains normally have 11 Opa loci, whereas meningococcal strains typically harbor 3 to 4 Opa loci (*65, 66*). These loci are highly scattered within the genome and show independent phase-variation. High-frequency phase variation results from varying numbers of 5' tandem repeats $[CTCTT]_n$ in all *opa* genes, which affect in-frame protein translation (*67*). *Neisseria* can express no Opa protein, one Opa protein at a time or several different Opa proteins simultaneously.

All Opa proteins are integral outer membrane proteins of around 30 kDa, which have 70% amino acid sequence identity but contain two hypervariable and one semi-variable domain in four surface-exposed loops (*68, 69*). Two Opa proteins classes can be distinguished in pathogenic *Neisseria*, based on their binding specificity to host cell receptors. The smaller group of Opa proteins interacts with heparan sulfate proteoglycans (HSPGs) (*70*). A prominent member of this group is Opa50 that mediates an efficient invasion into epithelial cells after binding to HSPGs by at least two different ways (*71*). Invasion into some epithelial cell lines (e.g. Chang conjunctiva cells) relies on phosphatidylcholine-dependent Phospholipase C and acidic sphingomyelinase activation (*72*). In other epithelial cell lines (e.g. HeLa cervix carcinoma cells) an alternative HSPG-dependent invasion is triggered in the presence of serum, as the serum-derived extracellular matrix protein vitronectin stimulates bacterial internalization (*73*). The second and larger Opa protein class binds to members of the carcinoembryonic antigen cellular adhesion molecule (CEACAM) family, which have a wide range of important cellular functions including migration, cell adhesion and activation of signaling pathways. Different Opa proteins interact with different CEACAM receptors, e.g. Opa52 binds to CEACAM1, 3, 5 and 6 (*74-76*). However, the broad majority of Opa proteins can interact with CEACAM1 and CEACAM5 (*63*). Opa protein binding to CEACAMs occurs via protein–protein interactions incorporating residues on the CC'FG face in the N-terminal domain of the receptors (*77, 78*).

Other neisserial virulence factors

Lipooligosaccharide (LOS) is a main component of the outer membrane of *Neisseria*. LOS is distinguished from lipopolysaccharide (LPS) of other Gram-negative bacteria by its highly branched basal oligosaccharide structure and the absence of repeating O-antigen subunits. Thus, LOS consists of different core oligosaccharide subunits bound to lipid A, which is anchored in the outer membrane. The lipid A domain is one of the key factors responsible for the toxicity of *Neisseria* as membrane fragments of lysed bacteria containing lipid A stimulate inflammation after recognition by CD14, but can also lead to an endotoxic shock (*79*). The carbohydrate part of LOS is undergoing phase variation, resulting in bacterial populations with distinct types and numbers of carbohydrates in their LOS (*80*). LOS can interact with asialoglycoprotein receptors on the cell surface of macrophages, hepatocytes and sperm cells (*81*), which allows *Neisseria* to be transmitted between hosts. Interestingly, LOS was also shown to be able to promote gonococcal invasion into ME-180 cells in the absence of Opa proteins in vitro (*82*).

Porins account for over 60% of total protein in the outer membrane of *Neisseria* (*83*). These proteins have a size of approximately 30 kDa and are constitutively expressed. They form anion-selective ion channels in the outer membrane which are crucial for survival of *Neisseria* (*84*). *N. meningitidis* expresses two Porins, PorA and PorB, whereas *N. gonorrhoeae* only expresses PorB. Gonococcal porin can be further differentiated serologically in $PorB_{IA}$ and $PorB_{IB}$. $PorB_{IA}$ is found in clinical isolates recovered from patients with disseminated gonorrheal disease whereas $PorB_{IB}$ is associated with isolates from patients having localized infections (*85-87*). $PorB_{IA}$-expressing GC strains were also found to be more serum-resistant, indicating increased bacterial survival in the bloodstream (*87*). Gonococcal porin is a major virulence factor as it can translocate into the membranes of infected host cells where it forms ATP/GTP-regulated pores and causes calcium influx from the extracellular milieu, resulting in activation of calpain and apoptotic caspases (*88, 89*). Porin further translocates to the mitochondria of infected cells where it induces pore formation in the mitochondrial membrane, which leads to loss of mitochondrial membrane potential resulting in apoptosis (*90, 91*). Controversially, purified porin as well as gonococcal infection have also been reported to increase expression of anti-apoptotic factors in urethral epithelial host cells (*92*). Similar to gonococcal porin, meningococcal PorB was also

reported to translocate to the mitochondria. In contrast to GC, meningococcal PorB translocation prevents apoptosis in epithelial cells and B-cells (*93, 94*). Porin is additionally involved in maintaining high internalization rates during Opa50-mediated gonococcal invasion (*95*). Also, the serological porin variant $PorB_{IA}$ can mediate an Opa-independent invasion under low-phosphate conditions (*96*). Recently, glycoprotein 96 (Gp96) was identified to be the phosphate-sensitive receptor for $PorB_{IA}$ and the Gp96-associated scavenger receptor was found to mediate the following $PorB_{IA}$-associated uptake (*97*).

Pathogenic *Neisseria* produce a 106 kDa extracellular serine protease which cleaves the mucosal human immunoglobulin IgA1 in the hinge region and is therefore called **IgA1 protease** (*98*). The IgA1 protease is expressed as a 169 kDa precursor protein which is composed of a leader-, protease- and helper domain. Leader and helper domain enable the protein to pass the inner and outer membrane via type-V-secretion and to be excreted as a soluble proform, which then matures into the active protease and a small stable alpha-protein (*99*). IgA1 protease preferentially cleaves human IgA1 both in serum and at mucosal surfaces of the respiratory and urogenital tracts (*100*) but was also shown to cleave the Pro/Ser/Thr-rich hinge region of Lamp1 of epithelial cells *in vitro* (*101*). As *Neisseria* infection reduces Lamp1 levels and less viable intracellular bacteria are found in IgA1 deletion mutants (*102*), it is reasonable to argue that IgA1 protease promotes neisserial intracellular survival by decreasing the structural integrity of lysosomal compartments as a result of protease-mediated LAMP1 degradation. Intracellular survival results in a more efficient transcytosis of *Neisseria* through the epithelial cell layer, thus enabling the bacteria to spread to deeper tissues (*103*).

The **Opc** outer membrane adhesin/invasin protein, which shows weak homology to Opa proteins, is present in many but not all meningococcal strains (*104*). Homologs of unknown function are also found in the gonococcal genome (*105*). In non-capsulated meningococci Opc enables the bacteria to adhere to and invade endothelial cells independently of Opa and pili expression (*106*). Adherence and invasion is mediated by Opc binding to the serum-derived glycoprotein vitronectin and formation of trimolecular complexes with the alpha(v)beta(3)-integrin receptor on the cell surface (*107*).

An exclusive and important virulence factor of meningococci is the protective **polysaccharide capsule**. The vast majority of meningococcal clinical isolates are encapsulated (*108*) and, as mentioned above, meningococcal serogroups are distinguished by their capsular polysaccharide structures. Encapsulated meningococci rely completely on pili-mediated initial host-cell contact as the capsule covers all other meningococcal adhesins but are more resistant to killing in human serum (*109*). Capsules of disease-associated serogroups contain sialic acid which down-regulates the activity of the alternative complement pathway and reduces amplification of C3b production, thereby decreasing C3b opsonization and subsequent phagocytosis of the bacteria (*110, 111*). Phase-variable controlled capsule expression was found to be shut down before Opa-mediated invasion of epithelial cells (*112*). Due to the exposure and accessibility of the capsule, recently licensed vaccines against meningococci usually contain capsular polysaccharides from 1-4 serogroups conjugated to a protein carrier (*113*).

1.2.4 Microcolony formation

Tfp-mediated attachment of *Neisseria* proceeds in distinct stages, comprising the (A) initial attachment of individual diplococci, followed by (B) MC formation and host cell microvillus deformation and (C) subsequent MC dispersal leading to intimate bacterial attachment (*114*). Typical neisserial MCs formed in the infection process are round dome-shape three-dimensional clusters of approximately 10-100 bacteria. MCs move over the host cell surface and can fuse with other MCs to form large motile structures during prolonged *in vitro* infections (*49*). MCs can be observed *in vitro* but are also detected by immunohistochemistry in patient biopsies; e.g. MCs were detected in the tonsillar epithelial tissue of meningococcal carriers, in skin lesions of children suffering from acute meningococcal sepsis and in the cerebral capillaries of a fatal case of fulminant meningitis (*115-117*).

However, the importance of MCs for successful host colonization is controversial. The densely aggregated bacterial MCs are resistant to shear stress caused by mucus flow or encountered after dissemination in the bloodstream (*117*). Possibly large numbers of shear stress resistant bacterial colonies forming in cerebral blood vessels can favor crossing of the

blood brain barrier which allows bacterial escape from the immune system (*117*), thus MC formation could be an important pathogenicity factor. In addition, MC formation was shown to be a prerequisite for biofilm formation, which shields the bacteria from antibiotics and the host immune system (*118, 119*). Tfp-expression and PilT-mediated pilus retraction are required for MC formation, as these factors allow host cell adherence, bacterial aggregation and twitching motility (*49*). Underneath forming MCs, host cell components such as cytoskeletal and signaling proteins, are dynamically recruited and migrate in conjunction with motile MCs (*49, 120, 121*). This dynamic relationship suggests that host cells are also involved in MC formation.

1.3 Enteropathogenic *Escherichia coli*

Tfp-expressing EPEC is one of the most important pathogens causing infantile persistent diarrhea worldwide (*122*) and was used a second infection model in this study. The extracellular pathogen EPEC can be subdivided into typical and atypical strains based on expression of the *eae* (intimin) and *bfpA* [bundle-forming pilus (Bfp)] genes. *Eae* is encoded in the locus of enterocyte effacement (LEE) pathogenicity island and is present in all EPEC strains; however *bfpA*+ strains are classified as typical and *bfpA*− strains are classified atypical EPEC (*123*). EPEC cause a peculiar histopathology known as the attaching and effacing (A/E) lesion, which is characterized by intimate attachment of the bacteria to the host epithelial surface and destruction of intestinal microvilli. EPEC pathogenesis can be divided in three stages: (A) initial adherence to intestinal epithelial cells, (B) translocation of bacterial proteins via the Type III secretion system (TTSS) and (C) pedestal formation and consequent intimate bacterial adherence (*124, 125*). Initial adherence is mediated by the plasmid-encoded Bfp, which belong to the Tfp (*38*) and allow the bacteria to form MCs on host cells. Mutant strains that lack this plasmid and thus do not express Bfp demonstrate reduced virulence (*126*), which indicates that the initial adherence and MC formation on host cells are important for EPEC for a successful infection (*127*). The next stage of EPEC pathogenesis involves the production of EPEC-secreted proteins, including EspA, EspB and EspD. These so-called translocator proteins are main components of the TTSS: EspA polymerizes to form a filamentous conduit along which secreted proteins travel to arrive at

the EspB and EspD-formed translocation pore in the plasma membrane of the host cell (*125*). Subsequently 6 known effector proteins such as the translocated intimin receptor (Tir), Map, EspF, EspG, EspH, EspZ, are injected into the host cell (*128*). The well-characterized effector Tir targets the host plasma membrane where it causes actin-pedestal formation and serves as a receptor for the bacterial outer membrane protein intimin, conferring intimate attachment (*129*). EPEC effector proteins demonstrate functional redundancy, interdependence and cooperativity in subverting and exploiting host cell signaling pathways. Effector-mediated host cell subversion contributing to EPEC virulence includes microvilli effacement, pedestal and filopodia formation, disruption of tight junctions, inhibition of transporter activity and induction of apoptosis (*128*).

1.4 Rho family GTPases and infection

Many biological processes, such as embryonic morphogenesis, immune surveillance, angiogenesis and tissue repair, base on cell functions controlled by actin cytoskeleton dynamics (*130*). Modulation of the actin cytoskeleton drives the formation of cellular structures such as lamellipodia, filopodia, stress fibers and focal adhesions and is controlled through signaling by Rho family GTPases, such as Rac1, Cdc42 and RhoA (*131*). Rac1 promotes lamellipodia formation and membrane ruffling, as well as the generation of new adhesions at the cell front. Cdc42 stimulates membrane extension to create filopodia. RhoA activity is important for actomyosin contractility, stress fiber formation and the maturation of adhesions (*132-134*). Rho-GTPases switch between an active, GTP-bound form and an inactive, GDP-bound form. The activation of Rho GTPases is effectively regulated by Rho-GDIs, guanine nucleotide exchange factors (GEFs) and GTPase-activating proteins (GAPs) which can be activated by diverse cellular stimuli, e.g. integrin-mediated cell adhesion (*134*). Rho-GDIs sequester and solubilize inactive GDP-bound Rho-GTPases in the cytoplasm. After release from Rho-GDIs, Rho-GTPases are targeted to the plasma membrane where GEFs are promoting GTP loading and therefore activation of Rho-GTPases. Inactivation of Rho-GTPases is induced by GAPs that facilitate GTP hydrolysis to GDP. Interestingly, extracellular signals have been reported to regulate activation of Rho family GTPases predominantly through GEFs (*133*). Activated GTP-bound Rho family GTPases recruit and activate

downstream effector proteins and pathways to mediate actin cytoskeleton dynamics; e.g. GTP-loaded RhoA can interact with mDia1 and Rock, Rac1 activates p21-activated kinases (PAKs) and Wave whereas Cdc42 initiates WASP-dependent pathways (*134*). Until now, more than 40 effectors, 50 GEFs and 40 GAPs have been identified for the Rho family GTPases (*133*).

Several bacteria have been identified to exploit the function of Rho family GTPases during pathogenesis and activating or mimicking the cytoskeleton remodeling Rho-GTPases enables pathogens to effectively bind to, invade and move within host cells. Many pathogenic Gram-negative bacteria utilize a TTSS to inject actin cytoskeleton-modifying virulence proteins into the host cell cytoplasm (*135*). Some by *Salmonella* species injected effector proteins bind directly to actin to modulate its dynamics, whereas others function as GEFs or GAPs to regulate the activity of Rho GTPases (*136, 137*). In EPEC, *Shigella* and *Salmonella* conserved TTSS-secreted proteins were identified that modify the actin cytoskeleton by mimicking the GTP-bound form of Rho family GTPases (*138*). These bacterial proteins, which do not exhibit sequence homology with eukaryotic Rho family GTPases, utilize a conserved WxxxE motif to directly activate downstream effectors of the Rac, Cdc42 and Rho signaling pathways (*138*). Another effective way of bacteria to interfere with actin cytoskeleton rearrangements is through the expression of exotoxins, which target the regulatory cycle of Rho family GTPases. *Clostridium difficile* A and B toxins and *Clostridium sordellii* lethal toxin are glycosyl transferases that glucosylate RhoA family GTPases which blocks proper GTP-loading and effector docking (*139*). The cytotoxic necrotizing factor from *E. coli* and *Yersinia* species and the dermonecrotic toxin from *Bordetella* species block GTP hydrolysis by deamidation or transglutamination of Rho family GTPases, respectively. These aberrations block the intrinsic GTPase activity of Rho proteins, resulting in their constant activation (*140*). Once permanently activated, Rho family GTPases are rapidly ubiquitinylated and degraded by the Ubiquitin proteasome system. The C3 exoenzyme from *Clostridium* species, *Bacillus cereus* and *Staphylococcus aureus* specifically ADP-ribosylates RhoA. This blocks GTP-loading of RhoA by GEFs and also locks the binding to Rho-GDIs, which leads to an accumulation of inactive Rho/Rho-GDI complexes (*141*). In *Neisseria* infection, Rho family GTPases Rac1 and Cdc42 have been described to play an important role by reorganizing the actin cytoskeleton during Opa-mediated invasion after CEACAM3

binding (*142*). Also $PorB_{IA}$-triggered gonococcal invasion under low-phosphate conditions was identified to require Rho family GTPase activity (*97*). The diverse and specific ways bacteria evolved to modulate Rho family GTPase activity reflects the importance actin cytoskeleton rearrangements for the successful infection of host cells by multiple bacteria species.

1.5 Caveolin and caveolae

1.5.1 Structure and function of lipid rafts and caveolae

Lipid rafts are cholesterol- and sphingolipid-enriched microdomains that move within the fluid bilayer of eukaryotic cell membranes and are formed by lipid–lipid interactions (*143*). They represent rigid liquid-ordered domains within the liquid-disordered phase of the bulk of the cell membrane and mediate cellular functions such as signal transduction, membrane trafficking and cell polarization (*144, 145*). These functional lipid microdomains can be further divided morphologically into caveolae and non-caveolar lipid rafts. Caveolae were first identified by electron microscopy and can be observed as omega (Ω)-shaped plasma membrane invaginations of approximately 50-100 nm diameter (*1, 146*). Caveolae are highly abundant in many cell types, such as endothelial cells, fibroblasts, smooth-muscle cells and adipocytes (*1*) and may occur singly or in clusters. Caveolae, in contrast to lipid rafts in general, contain a filamentous cytoplasmic coat formed by the integral membrane protein caveolin-1 (Cav1) (*147*). Association of Cav1 oligomers with cholesterol-rich membrane domains leads to formation of caveolae (*148*), likewise cholesterol depletion using Methyl-β-cyclodextrin (MβCD) or filipin disrupts caveolae structure and results in flattened plasma membranes (*147*).

1.5.2 Molecular features of caveolins

Three hetero- or homo-oligomer complex-forming caveolin proteins have been identified so far, Cav1, caveolin-2 (Cav2) and caveolin-3 (Cav3). Cav1 and Cav2 are found in caveolae-rich non-muscle cells, whereas Cav3 is detected exclusively in skeletal muscle and some smooth-muscle cells (*149*). Cav2, in contrast to Cav1 and Cav3, is not required for, but

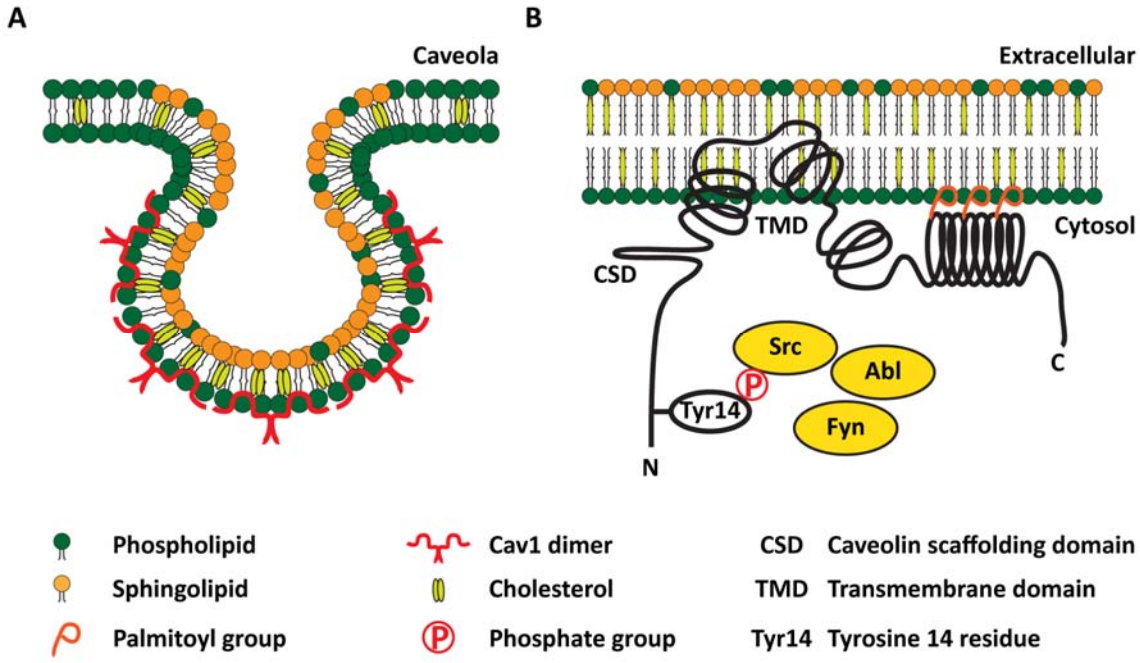

Figure 1-2. Caveolae structure and Cav1 protein domains and membrane topology. (A) Cav1 is the main structural component of caveolae and is inserted into the caveolar membrane. The N- and C-terminus of the protein point to the cytoplasm while the transmembrane domain is embedded in the plasma membrane. (B) Functional domains identified in Cav1. The transmembrane domain (TMD) and the palmitoylated cysteine residues stabilize the association of the protein with the membrane. The caveolin scaffolding domain (CSD) and the phosphorylated tyrosine 14 residue (Tyr14) constitute the protein-protein interaction domains of Cav1. Src, Abl1 and Fyn phosphorylate Cav1 at Tyr14, which can mobilize the protein and locate it to non-caveolar cellular regions. Figure adapted from (*1*) and (*3*).

may contribute to, caveolae formation *in vivo* (*150, 151*). Two isoforms exist of Cav1: Cav1α and Cav1β, the latter lacking the first 31 amino acids (AA) of the N-terminus (*152*). Both isoforms can be found in caveolae, but only the Cav1α isoform forms novel caveolae efficiently in Cav1-negative backgrounds (*153*). Cav1 contains three cysteine residues in the C-terminal region (Cys133, Cys143 and Cys156) that are palmitoylated and stabilize the protein at the membrane (*154*). Furthermore, Cav1 was originally identified as a substrate of Src tyrosine kinase (*155*), which phosphorylates Cav1 on tyrosine 14 (Tyr14) (*156*). Cav1 also contains a scaffolding domain (CSD) of approximately 20 amino acids that mediates interactions with multiple proteins, such as Src family tyrosine kinases, growth factor receptors, G-protein-coupled receptors (GPCRs) and endothelial nitric oxide synthase (eNOS) (*157-159*). Besides being the main structural component of caveolae, Cav1 can also be found in the Golgi complex, recycling endosomes and subapical intracellular regions (*160, 161*). Pools of free Cav1 are important for Cav1-mediated signaling independently of its association with caveolae.

1.5.3 Caveolin-1 and signal transduction

Cav1 can mediate cell signaling events either as cytoplasmic protein or within caveolae, which provide functional platforms containing preorganized and compartmentalized signaling molecules (*162*). Different experimental strategies to characterize caveolae and Cav1 function have been pursued, including cholesterol depletion, coimmunoprecipitation, colocalization and cofractionation (*1*). These approaches introduced many novel Cav1-binding signaling proteins to the field and confirmed the CSD and phospho-Tyr14 as the main protein-protein interacting domains of Cav1. Binding to the CSD via the ligand Cav1-binding motives ϕXϕXXXϕ or ϕXXXXϕXϕ (with ϕ representing an aromatic AA) can regulate signaling of Cav1 interacting partners, such as eNOS, G-protein α-subunits, Ras, Src, epidermal growth factor receptor (EGFR) and protein kinase C (PKC) isoforms (*163-165*). Binding of CSD-derived peptides functionally inactivates the enzymatic activity of G-proteins, Src family kinases and eNOS *in vitro* thus it is believed that CSD interaction generally suppresses activation of binding partners *in vivo*. This tonic caveolin-mediated inactivation might be a stalling mechanism of a diverse group of signaling molecules within caveolae, which can be followed by specific regulated stimulation of these signaling molecules by receptor ligands.

Signaling can also occur through caveolae internalization during caveolae-mediated, GTP hydrolysis-, dynamin- and actin-dependent endocytosis (*166-168*). Cav1 and caveolae have been implicated to function in different endocytic processes, such as potocytosis (*169*) and transcytosis (*170*). Caveolae-mediated endocytosis is triggered by loss of contact with the extracellular matrix and has been demonstrated to suppress the integrin-mediated activation of the small GTPase Rac1 as well as the Ras–Erk and the phosphoinositide 3-kinase (PI3K)-Akt pathways (*171, 172*). Interestingly, caveolae internalization and consequent inhibition of above-mentioned pathways requires phosphorylation of Cav1 on Tyr14 (*173*). Cav1 Tyr14 phosphorylation has been suggested previously to play a major role in cellular signaling since it is triggered by various cellular stimuli such as growth factor and hormonal stimulation (*174-176*), cellular stress (*177, 178*) and hyperosmotic shock (*179*). These stimuli utilize the tyrosine kinases Src, Fyn and Abl1 to phosphorylate Cav1 at Tyr14. In addition to integrin-regulated caveolae internalization, phospho-Tyr14-Cav1 was also shown to be required for Cav1 anterior polarization in transmigrating cells (*180*) and for

regulation of FAK transposition between focal adhesions and cytosolic pools (*181*). However, the downstream binding partners of phospho-Tyr14-Cav1 remain elusive, and so far the identified phosphotyrosine-dependent binding partners cannot account fully for all of the functions mentioned above as phosphotyrosine-dependent protein interaction screens only identified the Src-homology 2 (SH2)-containing proteins Grb7 (*175*) and C-terminal Src kinase (Csk) (*182*) as phospho-Tyr14-Cav1 interaction partners .

Cav1 and phospho-Tyr14-Cav1 were also linked repeatedly to cytoskeletal reorganization and activation of small GTPases, which links Cav1 signaling to a modulation of the actin cytoskeleton. Cav1 directly binds to the F-actin cross-linking protein filamin (*183*) and the Rho-associated serine/threonine kinase (Rock) (*184*). Furthermore, Cav1 was shown to be able to associate with multiple small GTPases and regulate their activity. The small GTPase RhoA was shown to localize to caveolae-enriched membrane domains in endothelial cells and to coimmunoprecipitate with Cav1 *in vitro*, suggesting an interaction of these proteins (*185*). Importantly, Cav1-RhoA colocalization and increased levels of phosphorylated Cav1 were recently associated with elevated levels of activated RhoA and RhoA/Rock signaling (*186-188*). First, phospho-Tyr14-Cav1 binds to and activates Csk (*182*) which is known to negatively regulate Src kinase by phosphorylation. Src kinase inactivation then decreases activity of the p190 Rho GTPase-activating protein (p190RhoGAP) which leads to increased levels of active GTP-bound RhoA, thus promoting RhoA signaling (*186*). Therefore the activation of RhoA by phospho-Tyr14-Cav1 is hypothesized to function in an indirect way. Indeed, levels of active RhoA are reduced in Cav1-negative cells, however, levels of active Rac1 and Cdc42 are increased in the absence of Cav1 (*186, 189-191*). These findings were also linked to the CSK-mediated inactivation of Src, as Src kinase is involved in Rac and Cdc42 activation (*192-196*). Similarly to RhoA, Rac1 and Cdc42 have also been found to directly interact with Cav1. Cav1 is hypothesized to function as a Rho protein GDP dissociation inhibitor (Rho-GDI) on Cdc42 after direct binding to the GDP-bound form of Cdc42 (*190*). Rac1 binding through the CSD is thought to be part of a signaling pathway finally leading to ubiquitylation and degradation of activated Rac1 (*191*).

1.5.4 Lipid rafts and caveolae in bacterial pathogenesis

Various interactions between bacterial pathogens and lipid rafts and caveolae have been established in recent years (*197*) and the functions of lipid rafts, caveolae and Cav1 in cellular signaling and modulation of the actin cytoskeleton suggests that they can also play important roles in host-microbial interplay. In fact, cholesterol and raft-associated proteins accumulate at *Shigella* entry foci on host cells, assisting and enhancing *Shigella* host cell binding and cellular entry (*198*). In bone marrow-derived mast cells, CD48, a receptor for FimH-expressing *E. coli* is recruited to caveolae-rich membrane domains, resulting in increased bacterial entry within *E. coli*-encapsulating caveolar chambers (*199*). Similarly, disrupting caveolae by cholesterol depletion significantly reduces the ability of *Campylobacter jejuni* to enter Caco-2 colon epithelial cells (*200*). Cav1 also associates with early and late inclusions of the obligate intracellular pathogen *Chlamydia trachomatis* and this pathogen was found to enter host cells via caveolin-containing sphingolipid and cholesterol-enriched plasma membrane microdomains (*201, 202*). Thus, lipid rafts and caveolae have been generally associated with increased cellular invasion by microbiological pathogens (*203, 204*). Furthermore, bacterial toxins, such as anthrax toxin, listeriolysin O and cholera toxin, have been reported to target lipid domains (*205-207*).

In line with these findings Kirchner et al. monitored the cellular localization of Cav1 in ME-180 epithelial cells following infection with piliated gonococci (P^+GC) in our group. She previously found that endogenous Cav1 colocalizes with attached diplococci and P^+GC MCs after two hours of infection (*208*). Interestingly, down-regulation of Cav1 by siRNA resulted in bacterial uptake into host cells. This uptake was identified to be Tfp-specific, as Opa-mediated bacterial uptake remained unaltered by Cav1 expression, and independent of pilus retraction. The observed epithelial cell entry of P^+GC resulted in a drastic decrease over time in the viability of internalized bacteria. Thus, Cav1 was identified to block premature and for the bacteria deleterious uptake of P^+GC into host cells (*208*).

1.6 Aim of the study

Like for many bacterial pathogens, successful attachment of *N. gonorrhoeae*—the causative agent of the sexually transmitted disease gonorrhea—to host cells depends on

specialized structures on the bacterial surface called type IV pili. After Tfp-mediated attachment to host cells, the bacteria form MCs on the cell surface, which was thought to depend entirely on bacterial factors. The contribution of host cells to extracellular MC formation will be investigated in this study using high-resolution live cell microscopy. Moreover, P^+GC infection and attachment induce changes within host cells that facilitate and promote infection. However, little is known regarding the cellular signaling events elicited by these interactions. The cytoskeleton protein actin and a range of signaling proteins are recruited underneath bacterial attachment sites. Kirchner et al. discovered that the host cell protein Cav1 is recruited to P^+GC infection sites and that recruited Cav1 blocks the premature uptake into host cells, which is deleterious for the bacteria (*208*). To extend these findings in another infection model with piliated bacteria, Cav1 recruitment in EPEC infection will be investigated, as initial adherence of EPEC to intestinal epithelial cells is conducted by type IV bundle-forming pili. Kirchner and De Graaf further investigated cellular processes upstream of Cav1 recruitment and reported that Cav1 recruitment to bacterial infection sites is abrogated by cholesterol depletion (*208*), blockage of tyrosine phosphorylation (*208*) and protein kinase A inhibition (*209*). However, important characteristics of Cav1 recruitment after P^+GC infection still require investigation, such as the temporal dynamics and progression of the recruitment, the spatial distribution of recruited Cav1 within host cells and the molecular features of Cav1 required for its recruitment. These questions will be addressed by expressing fluorescent Cav1 constructs as well as Cav1 mutants and monitoring Cav1 recruitment after P^+GC infection using live-cell imaging, three-dimensional image reconstruction and electron microscopy. Furthermore, the relevance of tyrosine-phosphorylation of Cav1 during P^+GC infection will be investigated by monitoring Cav1 phosphorylation levels by immunoblotting and immunofluorescence experiments. As it was reported that a functional actin cytoskeleton is required for inhibition of bacterial internalization (*208*), one of the main goals of this work is to identify a possible functional link between Cav1 and cytoskeletal components. Cav1 phosphorylation at Tyr14 has repeatedly been reported to mediate cell signaling and to be required for activation of small GTPases; however, only very few binding partners of phospho-Tyr14-Cav1 have been characterized so far. Therefore, the identification of novel phospho-Tyr14-Cav1 signaling partners is a prime objective of this study, which will lead to a better understanding of reported Cav1-mediated signaling pathways. Therefore, a broad and

unbiased analysis of potential SH2-/PTB-domain-containing interaction partners for Tyr14-phosphorylated Cav1 will be performed. Identified interactions involved in downstream Cav1 signaling will be confirmed biochemically and subsequently tested in the $P^{+}GC$ infection model to investigate host cell signaling pathways exploited by *N. gonorrhoeae*.

MATERIAL AND METHODS

2 Materials and Methods

2.1 Materials

2.1.1 Bacteria

Strains:	**Collection No.:**	**Genotype / properties:**
***N. gonorrhoeae* strains:**		
P^+GC	N280	MS11-F3-54b; *opaC::cat*; P^+ Opa^- (*210*)
P^+GC-GFP	N1174	MS11-F3-54b; *opaC::cat*; Hermes-8 plasmid pMKGFP conjugated from N1081, P^+ Opa^-, GFP
P^+GC-RFP	N1175	MS11-F3-54b; *opaC::cat*; P^+ Opa^- Hermes-8 plasmid pMKRFP conjugated from N1082, P^+ Opa^-, RFP
***E. coli* strains:**		
EPEC	E256	EPEC 2348/69 (O127:H6), EPEC wild type
EPEC ΔTTSS	E257	EPEC 2348/69 CVD452, EPEC TTSS mutant (*211*)
DH5α		F- ϕ80lacZΔM15 Δ(lacZYA-argF)U169 recA1 endA1 hsdR17(rk^-, mk^+) phoA supE44 thi-1 gyrA96 relA1 λ-

2.1.2 Cell lines

Cell line:	**Collection No.:**	**Properties:**	**Media and Supplements:**
ME-180		ATCC CRL-7932, human cervix epidermoid carcinoma	McCoy's 5A (Gibco), 10% FCS
ME-180 shLuci	JPB002	ME-180, shRNA mediated stable knockdown of firefly luciferase	McCoy's 5A (Gibco), 10% FCS
ME-180 shCav1	JPB004	ME-180, shRNA mediated stable knockdown of Caveolin1	McCoy's 5A (Gibco), 10% FCS
ME-180 shVav2	JPB006	ME-180, shRNA mediated stable knockdown of Vav2	McCoy's 5A (Gibco), 10% FCS
ME-180 shPLCγ1	JPB007	ME-180, shRNA mediated stable knockdown of PLCγ1	McCoy's 5A (Gibco), 10% FCS
HeLa		ATCC CCL-2, human cervix adenocarcinoma	RPMI 1640 (Gibco), 10% FCS
AGS		ATCC CRL-1739, human gastric adenocarcinoma	RPMI 1640 (Gibco), 10% FCS
AGS pcDNA3	AGS 3	AGS stably transfected with	RPMI 1640 (Gibco),

		pcDNA3	10% FCS, 0.5 mg/ml G418
AGS Cav1	AGS 179	AGS stably transfected with pcDNA3-Cav1-HA	RPMI 1640 (Gibco), 10% FCS, 0.5 mg/ml G418

2.1.3 Oligonucleotides and oligopeptides

Gene:	**Sequence:**	**Supplier:**
siRNA oligonucleotides:		
firefly Luciferase	5'-AACUUACGCUGAGUACUUCGA-3'	Qiagen
Vav2	5'-CUGAAAGUCUGCCACGAUA-3' 5'-UGGCAGCUGUCUUCAUUAA-3' 5'-GUGGGAGGGUCGUCUGGUA-3' 5'-GCCGCUGGCUCAUCGAUUG-3'	Dharmacon Research, ON-TARGET Plus SMART pool
Cdc42	5'-TTCAGCAATGCAGACAATTAA-3'	Qiagen
Rac1	5'-ATGCATTTCCTGGAGAATATA-3'	Qiagen
RhoA	5'-TAGGCTGTAACTACTTTATAA-3'	Qiagen
Filamin	5'-GTGGAAGAAGATCCAGCAGAA-3'	Qiagen
shRNA oligonucleotides:		
firefly Luciferase	5'-AACTTACGCTGAGTACTTCGA-3'	Metabion
Caveolin1	5'-CAGCAACAATTTATGAATTGA-3'	Metabion
Vav2	5'-GCATGACTGAAGATGACAAGA-3'	Metabion
PLCγ1	5'-GGACTTTGATCGCTATCAAGA-3'	Metabion
Oligopeptides used in SH2-/PTB-domain screening:		
Peptides were labeled with N-terminal 5(6)-carboxytetramethyl-rhodamine [5(6)-Tamra] Purification grade >95%		
Cav1 Tyrosine 14, phosphorylated	N-KYVDSEGHL(p)YTVPIREQG-C	Thermo Electron
Cav1 Tyrosine 14, unphosphorylated	N-KYVDSEGHLYTVPIREQG-C	Thermo Electron
Cav1 Tyrosine 42, phosphorylated	N-ADELSEKQV(p)YDAHTKEID-C	Thermo Electron
Cav1 Tyrosine 42, unphosphorylated	N-ADELSEKQVYDAHTKEID-C	Thermo Electron
Oligopeptides used in Streptavidin-Agarose Pull-Down assay:		

Peptides were labeled with N-terminal biotin
Purification grade >95%

Cav1 Tyrosine 14, phosphorylated	N-VDSEGHL(p)YTVPIREQ-C	Thermo Electron
Cav1 Tyrosine 14, unphosphorylated	N-VDSEGHLYTVPIREQ-C	Thermo Electron

2.1.4 Plasmids

Plasmid:	**Collection No.:**	**Properties:**
Cav1-HA	L306	Full-length Cav1 coding region was amplified from total cDNA of ME-180 cell line and cloned into the expression vector pcDNA3 (Promega) (*208*), plasmid provided by Yury Churin
Y14F-Cav1-HA	L312	Y14F-Cav1-HA was generated by changing tyrosine 14 of cav1 in Cav1-HA to phenylalanine using the QuikChange site-directed mutagenesis kit (Stratagene), plasmid provided by Yury Churin
Cav1-GFP	L322	Cav1 coding region was subcloned from Cav1-HA into pEGFP-N1 (Invitrogen)
Y14F-Cav1-GFP	L324	Cav1 coding region was subcloned from Y14F-Cav1-HA into pEGFP-N1 (Invitrogen)
ΔCav1-HA	L371	Cav1 coding for AA 32-178 (Cav1 isoform beta) was cloned into the vector pcDNA3, plasmid provided by Yury Churin
Y529F-Src	L101	Src-Y527F cloned into pNeoMSV was provided by T. Hunter (*212*)
pEGFP-C2	L367	pEGFP-C2 was provided by Dr. László Buday
GFP-Vav2	L368	Full-length Vav2 cloned into pEGFP-C2 was provided by Dr. László Buday (Semmelweis University, Budapest, Hungary)
pcDNA3.FLAG	L369	pcDNA3.FLAG was provided by Dr. Daniel D. Billadeau (Mayo Clinic, Rochester, MN, USA).
Truncated Vav2	L370	C-terminal SH3-SH2-SH3 domains of Vav2 cloned into pcDNA3.FLAG was provided by Dr. Daniel D. Billadeau (Mayo Clinic, Rochester, MN, USA).
PLCδ-PH-eGFP	H3784	PH-domain of PLCδ fused to GFP was provided by T. Balla (National Institutes of Health, Bethesda, MD) (*208*)

2.1.5 Antibodies

Antibody:	Origin:	Working dilution:	Supplier:
Primary antibodies:			
anti Cdc42	rabbit	1:500 (IB)	Abcam
anti-14-3-3 beta	rabbit	1:2000 (IB)	Santa Cruz
anti-Caveolin-1	rabbit	2µg (IP)	BD Transduction
anti-Caveolin-1, N20	rabbit	1:20000 (IB), 1:100 (IF)	Santa Cruz
anti-Cytokeratin 8	mouse	1:1000 (IB)	Santa Cruz
anti-Filamin, E3	mouse	1:100 (IF)	Santa Cruz
anti-Flag	mouse	1:1000 (IB), 2µg (IP)	Sigma
anti-GFP	mouse	1:2000 (IB), 2µg (IP)	Roche
anti-*Neisseria gonorrhoeae*	rabbit	1:100 (IF)	USBiological
anti-p110	rabbit	1:1000 (IB)	Santa Cruz
anti-p85	rabbit	1:1000 (IB)	Santa Cruz
anti-Phospho-Tyr14-Cav1 3251S	rabbit	1:500 (IB), 1:100 (IF)	Cell Signaling
anti-Phospho-Tyr14-Cav1	rabbit	1:100 (IF)	GenScript
anti-Phospho-Tyr14-Cav1, clone 56	mouse	1:1000 (IB)	BD Transduction
anti-pilus,m346	mouse	1:33 (IF)	MPIIB
anti-PLCγ1	rabbit	1:1000 (IB)	BD Transduction
anti-Rac1	mouse	1:2000 (IB)	Millipore Kit
anti-RhoA	mouse	1:250 (IB)	Cell Biolabs Kit
anti-RhoA	mouse	1:500 (IB)	Cytoskeleton Kit
anti-Vav2, C64H2 monoclonal	rabbit	1:1000 (IB)	Cell Signaling
anti-β-Actin	mouse	1:5000 (IB)	Sigma
Secondary antibodies:			
Cy™2-conjugated anti-mouse IgG	donkey	1:100 (IF)	Jackson Immuno Research
Cy™2-conjugated anti-rabbit IgG	goat	1:100 (IF)	Jackson Immuno Research
Cy™3-conjugated anti-mouse IgG	donkey	1:100 (IF)	Jackson Immuno Research
Cy™3-conjugated anti-rabbit IgG	goat	1:100 (IF)	Jackson Immuno Research
Cy™5-conjugated anti-mouse IgG	donkey	1:100 (IF)	Jackson Immuno Research
Cy™5-conjugated anti-rabbit IgG	goat	1:100 (IF)	Jackson Immuno Research
ECL™ anti-mouse IgG, HRP-linked	sheep	1:3000 (IB)	GE Healthcare
ECL™ anti-rabbit IgG, HRP-linked	donkey	1:3000 (IB)	GE Healthcare

2.1.6 Buffers, solutions and media

SDS-PAGE, Western Blot and Immunoprecipitation

Solution:	**Composition:**
SDS running gel buffer (4x)	60,5 g Tris/HCl, 4 g SDS, add 1000 ml H_2O, adjust to pH 6.8
SDS separating gel buffer (4x)	182 g Tris/HCl, 4 g SDS, add 1000 ml H_2O, adjust pH to 8.8
4x Sample Buffer	40 mL Glycerol (86%), 8 g SDS, 25 mL 1M TrisHCL, pH 6.8, 3,1 g DTT, 4 mg bromphenol blue, add water to final volume of 100 mL
SDS Electrophoresis buffer (10x)	250 mM Tris, 1.92 M Glycine, 1 % SDS
Semi Dry Blot Transfer Buffer (1x)	50 mM Tris-HCl, 40 mM Glycine, 20 % (v/v) Methanol
Wet Blot Transfer Buffer (1x)	25 mM Tris, 190 mM Glycine, 20 % (v/v) Methanol
TBS	10 mM Tris-HCl, 100 mM NaCl, pH 7,5
WB wash buffer (TBS-T)	TBS, 0,1% Tween 20
WB Blocking buffer	TBS-T, 3 % (w/v) BSA, 10 % (w/v) skim milk powder
Stripping buffer	62,5 mM Tris-HCl, pH 6.7, 10 mM β-mercaptoethanol, 2 % (w/v) SDS
Ponceau staining	2 % (w/v) Ponceau S, 30 % (w/v) TCA, 30 % (w/v) sulfosalicylic acid
Coomassie staining	0.25% (w/v) Coomassie Brilliant Blue R250, 50% Methanol, 10% acetic acid
Destaining solution	10% ethanol, 10% acetic acid
Cell lysis buffer for cytoskeletal preparation	1 mM EGTA, 4% PEG 6000, 100 mM PIPES pH 6.9, 0.5% Triton X-100
Wash buffer for cytoskeletal preparation	1 mM EGTA, 4% PEG 6000, 100 mM PIPES pH 6.9
Cell lysis Buffer (1x) for Immunoprecipitation	20 mM Tris (pH 7.5), 150 mM NaCl, 1 mM EDTA, 1 mM EGTA, 1% Triton X-100, 2.5 mM Sodium pyrophosphate, 1 mM beta-glycerophosphate. Just before use add 2mMNa_3VO_4 or Roche – 1:20 PhosSTOP phosphatase inhibitor (Roche) and 1:50 Roche - Complete protease inhibitor (Roche).

Infection and bacterial culture media

Solution:	**Composition:**
LB medium	10 g bacto tryptone, 5 g yeast extract, 5 g NaCl in 1 L ddH_2O,

	pH 7.0
SOC medium	20 g bacto-tryptone, 5 g yeast extract, 0.5 g NaCl, 2.5 ml 1 M KCl in 1 L ddH2O; pH 7.0; autoclave, 20 ml 1 M sterile glucose, 5 ml 2 M MgCl2
LB agar	LB medium, 1.5 % agar
GC agar	7.5 g casein peptone, 7.5 g meat peptone, 1 g KH_2PO_4, 4 g K_2HPO_4, 1 g amylomaize, 5 g NaCl, 10 g Agar in 1 L ddH_2O; after autoclaving, 1% vitamin mixture is added
Skim milk	10 % skim milk powder in ddH_2O
Vitamin mixture	0.01 g vitamin B12, 1 g adenine, 0.03 g guanine, 10 glutamine, 0.03 g thiamine, 25.9 g L-cysteine, 1.1 g L-cysteine, 0.5 g uracil, 0.15 g arginine, 0.02 g $Fe(NO_3)_3$, 0.013 g p-amino benzoic acid, 0.1 g cocarboxylase, 0,25 g nicotinamide adenine dinucleotide, 100 g D-glucose in 1 L ddH_2O
Proteose pepton medium (PP medium)	15 g proteose peptone, 5 g NaCl, 0.5 g starch, 4 g KH_2PO_4, 1 g K_2HPO_4 in 1 L ddH2O; adjust to pH 7.5, before use freshly add 1 % Vitamin mixture and 0.5 % $NaHCO_3$ (8,4 %)
Neisseria conjugation medium	PP medium, 1 % Vitamin mixture, 0.5 % $NaHCO_3$ (8,4 %), 100 µg/ml benzonase
Saponin	1% (w/v) Saponin in RPMI 1640, sterile filtration
Gentamicin	50µg/ml Gentamicin in RPMI 1640
Neisseria lysis buffer	40 mM tris acetate, pH 7.8, 20 mM sodium acetate, 1 mM EDTA, 1 % SDS

Immunofluorescence

Solution:	**Composition:**
4% PFA, pH7.4	4 g of PFA are dissolved in 50 ml ddH_2O. Heat to 65°C while stirring and add 1 M NaOH until the solution clears. 10 ml 10 x PBS are added and pH is adjusted to 7.4. Final volume of 100 ml is reached by adding ddH_2O and aliquots are frozen at -20°C
IF Blocking solution	2 % BSA in PBS
Permeabilization	0,2 % Triton X-100 in PBS
PBS (1x)	155.17 mM NaCl, 2.9 mM Na_2HPO_4, 1.06 mM KH_2PO_4, pH 7.4
Mowiol	2.4 g of Mowiol 4-88 is dissolved in 6 g glycerol and 6 ml ddH_2O at RT for 2h. 12ml 0.2 M Tris/HCL, pH 8.5 is added and solution is stirred at 50°C for 1h. To remove undissolved Mowiol clumps, the solution is centrifuged at 7500x g for 15 min. Stored at 4°C

2.1.7 Fine chemicals

Chemicals not listed separately have been purchased from Biomol, Calbiochem, Fluka, Gibco, Merck, Roth, Serva and Sigma Aldrich.

Chemical:	**Properties:**
Acrylamide	Roth
Agar 100	Agar Scientific Ltd.
Alexa 546-conjugated phalloidin	Invitrogen
Ammonium persulfate (APS)	Roth
Bovine serum albumin (BSA)	Biomol
Bromophenol blue	Biomol
Complete™	Roche
CT04 Rho inhibitor	Cytoskeleton
Cytochalasin D	Sigma Aldrich
ECL substrate	ICN Biomedicals
FCS	Biochrom
GC Agar base	Remel
Geneticin G-418	PAA Laboratories
Gentamicin	Sigma Aldrich
HiPerFect transfection reagent	Qiagen
LB Agar base	Invitrogen
Lipofectamine 2000	Invitrogen
Meat peptone	SIFIN
Mowiol 4-88	Sigma Aldrich
NSC23766 Rac1 inhibitor	Calbiochem
Paraformaldehyde (PFA)	Merck
Pervanadate	Sigma Aldrich
PhosStop	Roche
Polybrene	Sigma-Aldrich
PP2	Calbiochem
PageRuler™ Plus Prestained Protein Ladder	Fermentas
Protein G agarose beads	Calbiochem
Protein marker	New England Biolabs
Proteose Peptone	Becton Dickinson
Saponin	Sigma Aldrich
Skim milk powder	TSI
STI571 (Imatinib)	LC Labs
TEMED	Invitrogen
Tris	AppliChem

Triton X-100	Calbiochem
Trypsin	Invitrogen
Tween 20	Sigma-Aldrich

2.1.8 Laboratory equipment and consumable materials

Binoculars (Olympus), Phase contrast microscope (Olympus), Laser scanning confocal microscope TCS SP (Leica), Laser scanning live cell confocal microscope VT-Infinity system (Visitron Systems), consisting of an Olympus IX81 (Olympus), VT-Infinity galvo scanner confocal head (Visitron Systems) and a Hamamatsu C9100-02 CCD camera (Hamamatsu Photonics K.K), Epifluorescence microscopes (Nikon, Leica), 4700 Proteomics Analyzer (Applied Biosystems), RMC MTX/CRX cryo-ultramicrotome (Boeckeler Instruments, Tucson, AZ, USA), Leo 906E transmission electron microscope (Carl Zeiss, Jena, Germany) equipped with a Morada digital camera (Silicon Integrated Systems, Hsinchu, Taiwan), Centrifuges (Kontron Instruments, Sorvall, Hermle, Eppendorf), Mini-Protean II electrophoresis system (BioRad), Immunoblotting equipment (BioRad), film developing machine (Kodak), ELISA photometer (Molecular Devices), Photometer (Pharmacia Biotech), pH-Meter (inoLab), Agarose gel electrophoresis chamber (MMC-Biotech), PCR Gene Amp PCR System (Perkin Elmer), HERA incubators (Heraeus), Thermocycler (Perkin Elmer), Water bathes (GFL), –80°C freezer (Forma Scientific), pH-meter (WTW), Balances (Sartorius), Laminar flow chambers (Heraeus), Fume hood (Prutscher), Vortex mixer (IKA-Works), PVDF Transfer Membrane (PerkinElmer), Amersham Hyperfilm (GE Healthcare), Whatman chromatography paper (Schleicher and Schüll), cell culture dishes (TPP and Corning Life Sciences), 3.5 cm^2 glass-bottom live-cell dishes (MatTek) sterile cell culture pipettes (Corning Life Sciences), Eppendorf test tubes (Sarstedt), Falcon tubes (Sarstedt), 12 mm coverslips (Roth), microscope slides (Roth).

2.1.9 Kits

BCA Protein Assay (Pierce), Plasmid Mini Kit (Qiagen), QIAfilter Plasmid Maxi Kit (Qiagen), EndoFree Plasmid Maxi Kit (Qiagen), Gel Extraction Kit (Qiagen), PCR Purification Kit (Qiagen), RhoA Activation Assay Kit (Cytoskeleton), Precision Red™ Advanced Protein Assay (Cytoskeleton).

2.1.10 Software

Windows XP (Microsoft), Office 2007 (Microsoft), Photoshop CS3 (Adobe), Illustrator CS3 (Adobe), Acrobat (Adobe), Reference Manager 11 (Thompson ISI research soft), Chromas (Technelysium), Vector NTI (Invitrogen), TCS images acquisition (Leica), MetaMorph 7 (Universal Imaging Corporation), Imaris 6 (Bitplane), ImageJ v1.44a.

2.2 Methods

2.2.1 Bacterial culture techniques

Growth of *N. gonorrhoeae*: Bacteria were grown on GC agar plates at 37°C in a humidified incubator with an atmosphere of 5% CO_2 over night. The colony morphology of the seeded bacteria was checked with a binocular the next day and only bacteria exhibiting the correct observable colony phenotype (P^+Opa^-) were streaked onto fresh GC plates. Selected piliated gonococci (P^+GC) were grown not longer than 16 h to prevent bacterial autolysis and used for infection experiments or stocked.

Stocking of *N. gonorrhoeae:* Overnight cultures were suspended in skim milk and transferred to a cryotube vial containing glass beads. Suspension was aspirated completely to obtain fluid-coated beads and the vial was stored at -80°C.

Conjugation of *N. gonorrhoeae:* The donor strain and the recipient strain were suspended in conjugation medium. The OD_{550} of both suspensions was adjusted to 0.2 and the strains were mixed 1:1. 1 ml of the mixture was concentrated on nitrocellulose filter paper and incubated on GC agar for 3 h at 37°C in a humidified incubator with an atmosphere of 5% CO_2. Subsequently bacteria were resuspended in 400 µl conjugation medium and plated on GC agar plates containing selective antibiotics.

Growth of *E. coli*: For plasmid DNA preparation *E. coli* were cultured overnight in LB broth medium supplemented with the appropriate antibiotic at 220 rounds per minute (rpm) at 37°C. After plasmid transformation *E. coli* were cultured on antibiotic-supplemented LB agar plates at 37°C in a humidified incubator with an atmosphere of 5% CO_2 overnight.

Growth of enteropathogenic *E. coli:* EPEC strains were grown overnight in LB broth without shaking at 37 °C in a humidified incubator with an atmosphere of 5% CO_2. EPEC strains used for infection experiments were diluted 1:100 in serum free Dulbecco's modified Eagle medium (DMEM) and grown for 3.5 h at 37°C without shaking under a 5% CO_2 atmosphere to an OD_{600} of approximately 0.3 to stimulate TTSS expression and create so-called pre-activated cultures, as described previously (*213*). Pre-activation of EPEC by growth in tissue culture media facilitates their rapid binding to host cells (*214*).

Stocking of *E. coli:* *E. coli* were cultured overnight in LB broth medium supplemented with the appropriate antibiotic. 300 µl of glycerol (86%) was added to 700 µl of the fresh overnight culture, mixed vigorously and stored at -80°C.

Transformation of *E. coli* by heat-shock: $CaCl_2$ competent *E. coli* were thawed carefully on ice. 1 µg of plasmid DNA was added to 50 µl competent *E. coli* and incubated for 30 minutes on ice. The reaction tube was subsequently heated shocked at 42°C for 90 seconds and immediately incubated on ice for 2 minutes. 1 ml SOC medium preheated to 37°C was added and the mixture was incubated for 1 h at 37°C and 220 rpm. 50 µl and 250 µl of the reaction were plated onto antibiotic-supplemented LB agar plates and incubated at 37°C in a humidified incubator with an atmosphere of 5% CO_2 over night.

2.2.2 Cell culture methods and infection.

Cell culture propagation and seeding: The human cervix carcinoma cell line ME-180 (ATCC HTB33) was grown in McCoy's 5A medium supplemented with 10% FCS. The human cervix adenocarcinoma cell line HeLa (ATCC CCL-2) and the human gastric adenocarcinoma cell line AGS (ATCC CRL-1739) were grown in RPMI 1640 medium supplemented with 10% FCS. AGS 3 (AGS control) and AGS 179 (AGS Cav1) cells were grown in RPMI 1640 medium supplemented with 10% FCS and 0.5 mg/ml Geneticin G-418. All cell lines cells were grown in 75 cm^2 culture flasks at 37°C in a humidified incubator with an atmosphere of 5% CO_2. Cells were splitted before reaching 100% confluency. Therefore, cells were washed with to 37°C pre-warmed PBS, 1 ml of to 37°C pre-warmed trypsin was added and the cells were incubated in the incubator until they detached from the flask bottom. Cells were diluted with medium according to required working dilution or the next passage date. To determine

the appropriate number of cells to be seeded for experiments, cells were counted using a Neubauer chamber. Cells were then splitted into new flasks for further culturing or seeded in multiwall plates for performing experiments.

Inhibitor treatments: Cell monolayers were washed with warm PBS and incubated in serum free RPMI1640 media containing one of the following inhibitors: 150 µM pervanadate for 30 min, 1 µM Cytochalasin D for 30 min, 10 µM PP2 for 1 h, 10 µM STI571 (Imatinib) for 1h, 20 µM, 100 µM and 300 µM NSC23766 for 1 h and 50 ng/ml, 100 ng/ml, and 250 ng/ml cell permeable Rho inhibitor CT04 for 4 h. After incubation cells were processed for immunoprecipitation experiments or bacteria were added for infection experiments. To obtain pervanadate, 37,5 µl orthovanadate from a 0,2M stock solution was incubated with 70 µl of 3% H_2O_2 and filled up to 500 µl with RPMI. After incubation for 10 min at room temperature, a 1:100 dilution with RPMI was prepared (final concentration 150 µM).

Infection with P^+GC: Cells were washed three times with serum-free medium and fresh serum-free medium was added to the 70-80% confluent cell monolayer 1 h before infection. P^+GC not grown more than 16 h were carefully resuspended in 5 ml serum-free cell culture medium. Bacterial concentration was determined photo spectrometrically measuring the OD_{550} and the bacterial count was approximated using standard growth curves. P^+GC were added to cell monolayers at a multiplicity of infection (MOI) of 100. Infection was synchronized by careful centrifugation of the bacteria onto the cell monolayer for 3 minutes at 300 rpm at room temperature. Infected cells were placed 37°C in a humidified incubator with an atmosphere of 5% CO_2 for the indicated infection time.

Infection with EPEC: Cells were washed three times with serum-free medium and new serum-free medium was added to the 70-80% confluent cell monolayer 1 h before infection. Pre-activated EPEC cultures were added to cell monolayers for 2 h. Infection was performed as described for P^+GC infection.

2.2.3 Gentamicin Protection Assay

Quantification of bacterial binding and entry into host cells was performed using standard gentamicin-based assays with dilution plating to recover viable bacteria. Cell confluency at

infection time was 70-80%. Cells were washed three times in serum-free RPMI 1640 medium prior to infection and incubated in serum-free RPMI 1640 medium 1 h. Bacteria were added to the cells at a multiplicity of infection of 100. Cells were then incubated in RPMI 1640 medium at 37 °C, 5% CO_2 for 2 h. 100 µg/ml gentamicin was then added for an additional 2 h to kill extracellular bacteria. Cells were washed, and 1% saponin was added to permeabilize cells followed by plating of appropriate dilutions of the lysate on GC agar. To quantify adherent bacteria, lysis with saponin was done prior to gentamicin treatment. Intracellular gentamicin-protected (Gm^P) bacteria were determined as a percentage of total cell-associated bacteria. Assays were conducted in triplicate wells, yielding the given mean and the standard deviation.

2.2.4 Transfection of plasmid DNA

Cells were seeded in 12-well-plates, incubated overnight at 37°C in a humidified incubator with an atmosphere of 5% CO_2 and grown to a confluency of 70-80%. Cells were once washed with warmed PBS and fresh 500 µl of warmed OptiMem was added to the cell monolayer. 0.5 µg plasmid DNA was dissolved in 50 µl OptiMem and separately 1 µl of Lipofectamine 2000 was dissolved in 50 µl OptiMem. Both mixtures were incubated for 5 min at RT and then combined, mixed and incubated for 30 min at RT. The solution containing DNA-lipid complexes was then added dropwise to the cells and cells were incubated for 4 h. at 37°C with 5% CO_2. Transfection solution was then replaced with fresh medium and cells were further incubated overnight. The cells were used for experiments 24 h post transfection.

2.2.5 Transfection of siRNA

The transfection of siRNAs was carried out using Hiperfect transfection reagent according to the manufacturer's instructions. Briefly, cells were transfected with 25-50 nM siRNA duplex and used for experiments 72 h after transfection. Therefore, $1.2*10^5$ cells were seeded per 12-well in serum-containing culture medium. Next, 1.5-3 µl of a 20 µM siRNA stock was diluted in 100 µl serum-free culture medium, the solution was mixed and 4 µl Hiperfect was added. The mixture was incubated for 10 min at RT and added dropwise to the cell

suspension. Cells were incubated overnight and the transfection medium was removed the next day. Cells were then grown for 48 h, splitted and seeded to multiple wells. Cells were incubated overnight and used for experiments 72 h post siRNA transfection.

2.2.6 Generation of shRNA Knockdown Cell Lines

shRNA-expressing vectors were constructed by cloning computed shRNA oligonucleotides into the pLVTHM vector. The sequences of the targets of the shRNAs are as follows: human Cav1, 5'-CAGCAACAATTTATGAATTGA-3'; human Vav2, 5'-GCATGACTGAAGATGACAAGA-3'; human PLCγ1, 5'-GGACTTTGATCGCTATCAAGA-3'; firefly luciferase, 5'-AACTTACGCTGAGTACTTCGA-3'. All constructs were verified by sequencing. Viruses carrying the shRNAs were produced by transfecting 293T cells with the generated pLVTHM constructs together with viral packaging vectors (psPAX2, pMD2G, kindly provided by D. Trono, Ecole Polytechnique Fédérale de Lausanne, Switzerland) by calcium phosphate transfection. Viruses were harvested from the supernatant 48 h after transfection, filtrated, and applied to ME-180 cells for lentiviral infection in the presence of polybrene (5 µg/ml). Pools of GFP-positive cells were selected and validated for their ability to knock down protein expression of target genes by more than 70% in comparison with luciferase control cells.

2.2.7 Indirect immunofluorescence

Cells were grown on acid-washed glass coverslips (12 mm diameter), experiment were performed and cells were fixed with 4 % PFA for 20 min at RT. Fixed cells were washed three times with PBS, permeabilized with 0,2 % Triton X-100 in PBS, washed three times with PBS and blocked with 2 % BSA in PBS. The primary antibodies diluted in blocking solution were then carefully added onto the cover slips and incubated at room temperature for 1 h under moist conditions. Cells were washed three times with PBS and the secondary antibodies diluted in blocking solution were added for 1 h. Again cells were washed three times with PBS and mounted onto glass slides using Mowiol. Differential staining of intra- and extracellular bacteria was achieved by double staining of bacteria, primarily without permeabilization of cells and subsequently after cell permeabilization. Samples were

analyzed by confocal laser scanning microscopy using a Leica TCS SP microscope, equipped with an argon/krypton mixed gas laser source. Image stacks were further processed using Photoshop or Imaris.

2.2.8 Live-Cell Confocal Microscopy

ME-180 cells were grown in 3.5 cm^2 glass-bottom dishes overnight under standard conditions. Fresh serum-free RPMI without phenol red was added, and cells were placed in a humidified incubation chamber at 37 °C and 5% CO_2. Images were obtained with the VT-Infinity system. Briefly, the system consists of an Olympus IX81, VT-Infinity galvo scanner confocal head, and a Hamamatsu C9100-02 CCD camera. Bright field images were acquired with a 63× phase contrast objective and a high-speed shutter system. Fluorescent images were acquired with a 488 nm laser beam with an intensity of 250 mW using the 488 nm emission filter set. Images were collected and processed using MetaMorph and Imaris software.

2.2.9 SDS-Gel electrophoresis and Western blotting

Protein electrophoresis was performed using the Biorad Mini-Protean II electrophoresis system. Equal amounts of proteins were separated under reducing conditions for approximately 1 h at 120 V. PVDF membranes were activated by incubation in methanol for 1 min and then washed with TBS-T for 5 min. Gels were blotted for 2 h at 60mA per gel (in case of Semi Dry Blot) or overnight at 100 mA (in case of Wet Blot) onto PVDF membranes. Membranes were then blocked for 1 h in blocking buffer containing 3 % BSA and 10 % skim milk. Subsequently blots were incubated for 1 h with primary antibody dissolved in TBS-T with 3 % BSA. The blot were washed three times for 10 min in TBS-T and incubated for 1 h with the horseradish peroxidase (HRP)-conjugated secondary antibodies. Blots were washed again three times for 10 min and ECL reagent was added. Chemiluminescence was detected by exposing a sensitive photographic film to the membrane. Blots were scanned and quantified using ImageJ software (v1.44a).

Stripping of Western Blots: PVDF membranes were again activated by incubation in methanol for 1 min and washed with TBS-T for 5 min. Blots were incubated in 100 ml stripping buffer at 50°C for 30 min. Blots were then washed three times with TBS-T for 1 h. The stripped blots were blocked again and reprobed with primary and secondary antibodies.

2.2.10 Immunoprecipitation

Cells were lysed in 1× Immunoprecipitation cell lysis buffer containing PhosStop Phosphatase Inhibitor and Complete™ Protease Inhibitor. The lysates were pre-cleared for 4 h with protein G-agarose beads and incubated with 2 µg bait antibody overnight. Protein G-agarose beads were subsequently added for 4 h to precipitate antigen-antibody complexes. After extensive washing, the precipitate was eluted by heating to 95 °C in SDS loading buffer and the individual proteins separated by SDS-PAGE. Western blotting was used to assess the precipitate.

2.2.11 Peptide Synthesis and SH2/PTB-Protein Arrays

Fluorescently labeled peptides with sequences corresponding to residues 5–22 of Cav1 were synthesized, one phosphorylated on Tyr14 and the other not phosphorylated as previously described (*215*), purified to > 95% by preparative reverse phase HPLC, and quality controlled via mass spectrometry and analytical HPLC. Human SH2 and PTB domains were expressed and purified as previously described (*215*), and protein microarrays were fabricated and probed as more recently reported (*216*).

2.2.12 Peptide Synthesis and Streptavidin-Agarose Pull-Down

Peptides were designed as 15-mers (residues 7–21 of Cav1) bearing an N-terminal biotin. Peptides were synthesized as pairs, one phosphorylated on Tyr14 and the other not phosphorylated, purified to > 95% by preparative reverse phase HPLC, and quality controlled via mass spectrometry and analytical HPLC. For affinity pull-downs, 10 nmol of immobilized peptide was added to ~2 mg of cell lysate. ME-180 cells were lysed in 1× Immunoprecipitation cell lysis buffer containing 2 mM sodium orthovanadate, as a

phosphatase inhibitor, and Complete™ Protease Inhibitor. The lysates were pre-cleared for 1 h with streptavidin agarose beads and equal amounts of lysate were incubated overnight at 4 °C with streptavidin agarose beads, pre-saturated with the respective biotinylated peptides. After extensive washing, the streptavidin precipitate was eluted by heating to 95 °C in SDS loading buffer and the individual proteins separated by SDS-PAGE. Separated protein bands of interest were identified by MALDI-TOF-TOF using a 4700 Proteomics Analyzer. Additionally, Western blotting was used to assess the precipitate.

2.2.13 Cytoskeletal Preparation

AGS and ME-180 cells (2×10^7) were washed with PBS at 4 °C and then incubated in cytoskeletal lysis buffer (1 mM EGTA, 4% PEG 6000, 100 mM PIPES pH 6.9, 0.5% Triton X-100) for 5 min at 4 °C to stabilize the cytoskeleton. Supernatant containing cytoplasmic and compartmental proteins were removed and the remaining cytoskeletal proteins washed once, harvested in lysis buffer by scraping, and pelleted by centrifugation (14,000× g, 5 min). Pellets were washed once with 1 ml wash buffer (1 mM EGTA, 4% PEG 6000, 100 mM PIPES pH 6.9), then collected in SDS loading buffer and analyzed by Western blotting.

2.2.14 RhoA Activation Assay

Using an enzyme-linked immunosorbent assay-based RhoA activation assay kit active RhoA was determined according to the manufacturer's protocol. To synchronize Rho activity, cell monolayers exhibiting 60% confluency were grown in culture medium with 0.5% FCS for an additional 24 h and then serum-starved for another 16 h. After infection, cells were lysed at the indicated time points, aliquots snap-frozen in liquid nitrogen, and the protein concentration determined using Precision Red™ Advanced Protein Assay. Cell lysate (37.5 µg protein) from each sample was incubated in microwells coated with the isolated Rhotekin Rho-binding domain. Active RhoA was subsequently measured using immunodetection followed by a colorimetric reaction measured by absorbance at 490 nm. Assays were conducted in triplicate microwells, yielding the given mean and the standard deviation. Data were tested for significance using Student's *t* test.

2.2.15 Generation of Anti-Pilus Antibody

P^+GC pili were purified as described previously (*217*). Purified pili were utilized for immunizing BALB/c mice for the generation of monoclonal antibodies following standard poly-ethylene glycol (PEG) fusion protocol. Briefly, 6–8-wk-old Balb/c mice were primed with 50 µg of purified pili in Freund complete adjuvant followed by two boost injections on day 20 and 40 in Freund incomplete adjuvant. Spleen cells were fused with P3X63Ag8 myeloma cells. Positive hybridomas were screened by standard ELISA against purified pili. Anti-pilin antibody producing hybridomas were subcloned three times by limited dilution.

2.2.16 Immunogold Labeling

Cells were fixed in 2% PFA/1% acrolein in PBS for 2 h at RT. After washing with PBS, the cells were overlaid with warm gelatine (10% PBS) and scraped off the plate. After gelling at 4 °C, the specimens were cut into small blocks, post-fixed in 2% PFA, and infiltrated with a sucrose/PVP solution. Specimens were mounted on a stub, frozen in liquid nitrogen, and 60 nm sections were produced using a RMC MTX/CRX cryo-ultramicrotome. Sections were thawed, blocked, and incubated with anti-Cav1 antibody (rabbit, BD Transduction Laboratories). After washing, bound antibody was detected using anti-rabbit secondary antibodies coupled to 6 nm colloidal gold. The samples were analyzed on a Leo 906E transmission electron microscope equipped with a Morada digital camera.

RESULTS

3 Results:

3.1 Expression and recruitment of Cav1 to infection sites prevent internalization of P$^+$GC by host cells.

Previous studies in our group by Kirchner et al. monitored the cellular localization of the major structural protein of plasma membrane caveolae, Cav1, in ME-180 cells following P$^+$GC infection. Endogenous Cav1 colocalized with P$^+$GC MCs after two hours of infection (*208*) which blocked premature (and for the bacteria deleterious) uptake of P$^+$GC into host cells. Based on these findings, Cav1 localization in P$^+$GC infected ME-180 cells was analyzed utilizing confocal imaging to further investigate the mechanism of Cav1-mediated block of P$^+$GC uptake into host cells. Endogenous Cav1 localized to P$^+$GC infection sites 2h post infection consistent with the prior findings (Figure 3-1) (*208*).

To better understand the dynamics of Cav1 recruitment to the infection sites, live-cell imaging of Cav1-GFP transfected cells was used. A substantial accumulation of the Cav1-GFP was observed at sites of bacterial infection, which could even be induced by single diplococci (Figure 3-2, lower panel). As, during MC formation, individual bacteria aggregated on the host cell surface so did the recruited Cav1-GFP underneath the bacteria (Movie 1). Cav1 recruitment was identified here as an immediate cellular answer; only 50 seconds after P$^+$GC attachment to the host cell Cav1-GFP accumulation was detected at bacterial attachment sites (Figure 3-2, lower panel). The observed Cav1-GFP recruitment continued during the course of the infection, ultimately resulting in a major accumulation of the

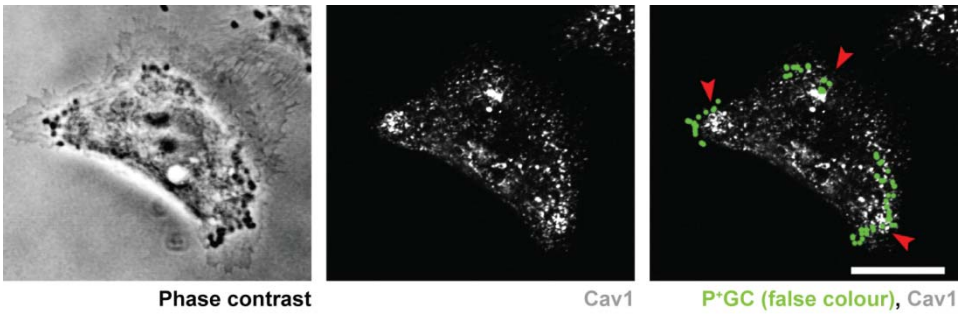

Figure 3-1. ME-180 cells were infected with P$^+$GC and subsequently the distribution of endogenous Cav1 was monitored using immunofluorescence. Recruitment of Cav1 (white, middle panel) to attached P$^+$GC (green, right panel) was observed 2 h post infection. Arrows indicate to P$^+$GC recruited Cav1.

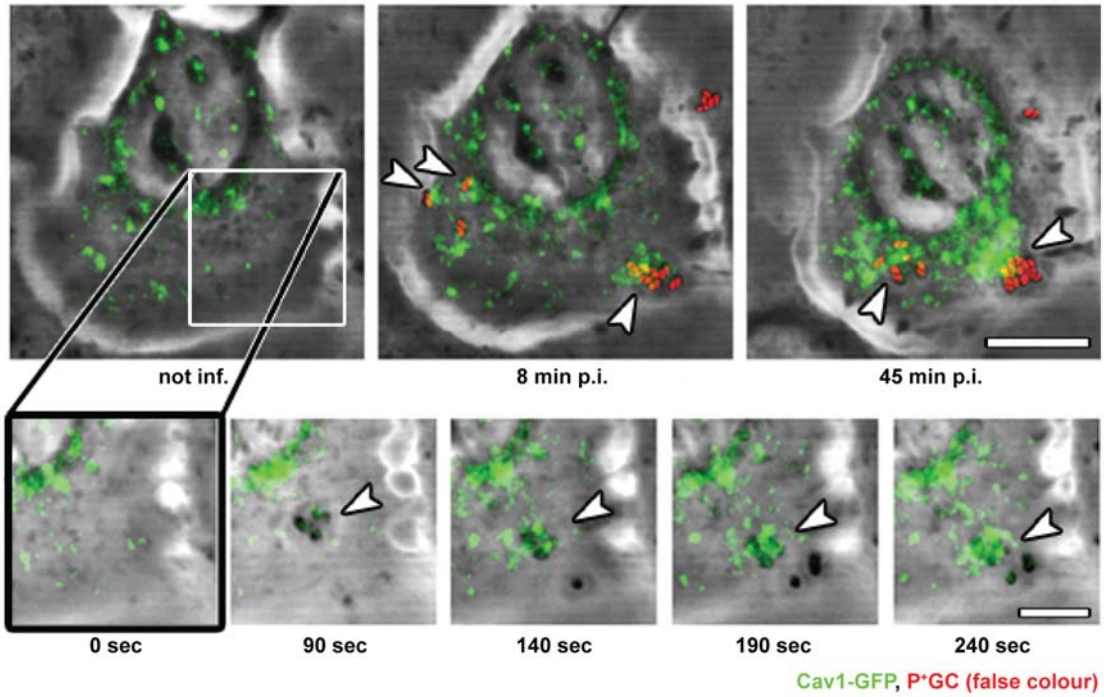

Figure 3-2. Excerpts of Movie 1: ME-180 cells were transfected with Cav1-GFP and subsequently infected with P^+GC. Cav1-GFP (green) is recruited within seconds to individually attached P^+GC (red) in ME-180 cells (lower panels). Recruitment to MCs continues as infection proceeds (upper panels). Attached P^+GC are indicated by arrows.

protein at the infection sites (Figure 3-2, upper panel and Movie 1). Taken together, these data suggest that Cav1 accumulation is an immediate cellular response to P^+GC attachment that occurs throughout the early stages of P^+GC infection.

Cav1 has also been shown to localize to non-caveolar cellular regions where it participates in transport of signaling proteins, in particular after being phosphorylated on its tyrosine 14 residue (Tyr14) (*160, 161, 218*). Therefore it was hypothesized that the Cav1 recruited to P^+GC MCs localizes just outside the caveolae and plays a role in protein trafficking or signaling. To test this, the exact subcellular localization of the recruited Cav1 at the infection sites was analyzed by 3D image reconstruction and transmission electron microscopy (TEM) in different cell lines. To learn if Cav1 recruitment is a general phenomenon during P^+GC infection, Cav1 localization and function during the infection were studied in another cervical epithelial cell line. Therefore Cav1-GFP was expressed in HeLa cells, which were subsequently infected with P^+GC. The bacteria were stained and the localization of the GFP construct was monitored by confocal microscopy. Images were assembled as a 3D reconstruction of the infected host cell and the location of Cav1 was

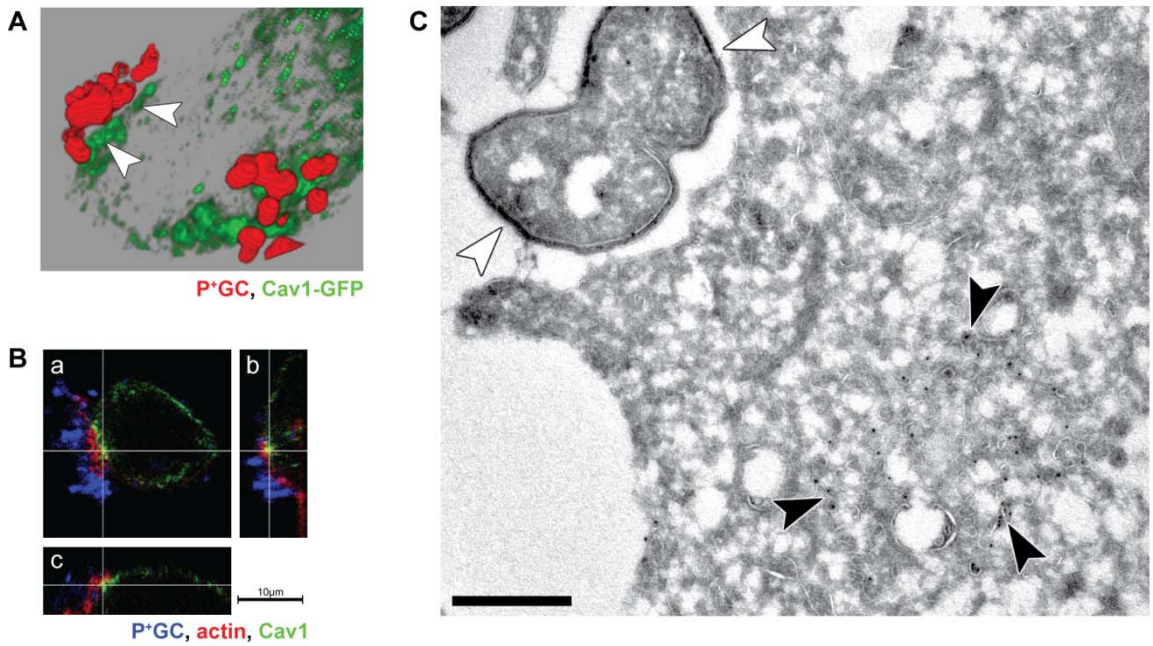

Figure 3-3. Recruited Cav1 is found in the vicinity of P$^+$GC, but not directly at the plasma membrane. (A) 3D reconstruction of confocal images depicting Cav1-GFP (green) recruitment in the host cell 2 h post infection with P$^+$GC (red). Gaps between P$^+$GC and Cav1 are indicated by white arrows. (B) Horizontal (a) and vertical (b, c) confocal image sections show F-actin (red) localization between bacteria (blue) and endogenous Cav1 (green) in infected ME-180 cells. Scale bar: 10 µm. (C) Immunogold labeling of Cav1 in ME-180 cells after infection with P$^+$GC. Cav1 is 6-nm-gold-labeled (black arrows). P$^+$GC are observed as diplococci attached to the cell membrane (white arrows). Scale bar: 500 nm.

mapped. A small gap was observed between Cav1-GFP and the bacteria (Figure 3-3A, white arrows) indicating that Cav1 accumulates in the vicinity of P$^+$GC, but not directly below the plasma membrane (Figure 3-3A). A small interspace was observed between Cav1-GFP and the bacteria (Figure 3-3A, white arrows). This result was then confirmed through TEM by immunogold labeling of Cav1 in P$^+$GC infected ME-180 cells. TEM micrographs revealed that the gold particles representing Cav1 (Figure 3-3C, black arrows) were located in the vicinity of the diplococci (Figure 3-3C, white arrows) but not directly at the plasma membrane.

To compare endogenous Cav1 localization with cytoskeletal proteins known to be recruited to cortical plaques (*121*), F-actin and Cav1 recruitment were monitored simultaneously. Analysis of horizontal sections of confocal image stacks revealed that F-actin structures in P$^+$GC-infected cells localized at the plasma membrane and endogenous Cav1 was found right below these F-actin structures (Figure 3-3B). These results indicate that recruited Cav1 localizes upon P$^+$GC infection not only close to the bacteria but also in a defined position within a set of proteins, one of them being F-actin.

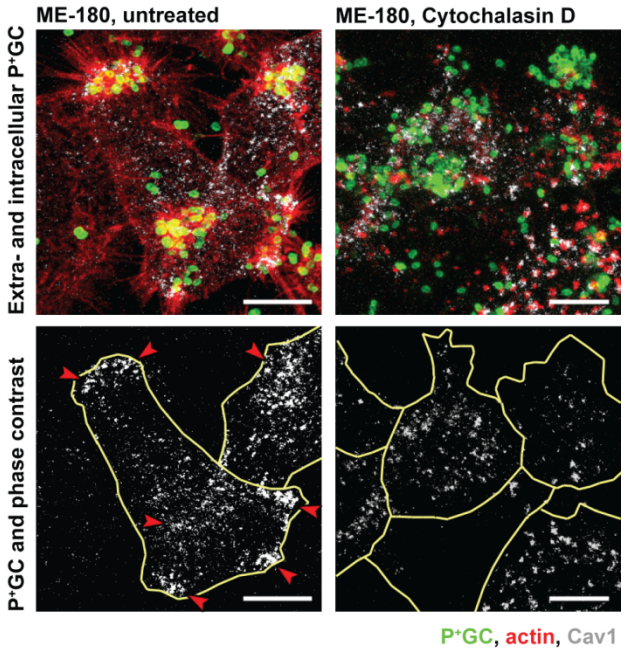

Figure 3-4. Disruption of F-actin filaments with cytochalasin D (CytD) prevents Cav1 recruitment to P$^+$GC attachment sites. P$^+$GC (green) infection induced Cav1 (white, lower panels) and F-actin (red) recruitment to attachment sites in untreated control cells (left panels, to P$^+$GC recruited Cav1 indicated by arrows), whereas CytD treatment disrupted F-actin filaments and inhibited Cav1 recruitment (right panels). Scale bars: 20 µm.

Given the co-localization of the F-actin and Cav1 at the infection sites, the importance of a functional actin cytoskeleton for Cav1 recruitment was analyzed next. As previously reported (*121*), attachment of P$^+$GC to epithelial cells induced the assembly of F-actin structures at sites of bacterial attachment (Figure 3-4, left panels). ME-180 cells were then treated with cytochalasin D (Cyt D), which inhibits actin polymerization thereby disrupting actin filaments. This treatment prevented Cav1 accumulation at P$^+$GC infection sites (Figure 3-4, right panels) consistent with earlier findings of our group that actin filament disruption with Cyt D or latrunculin A induced premature bacterial internalization (*208*). Thus, recruitment of Cav1 and inhibition of bacterial internalization both require a functional actin cytoskeleton.

Kirchner et al. discovered that Cav1 is essential to prevent the internalization of P$^+$GC into host cells (*208*). To confirm these finding and further explore the functional role of Cav1 in P$^+$GC infection, a stable ME-180 Cav1-knockdown cell line was created. Therefore ME-180 cells were infected with a lentivirus expressing a short hairpin RNA (shRNA) targeting the Cav1 mRNA, resulting in the stable knockdown cell line ME-180 shCav1. As control a cell line expressing a shRNA targeting firefly luciferase mRNA was used (ME-180 shLuci). The

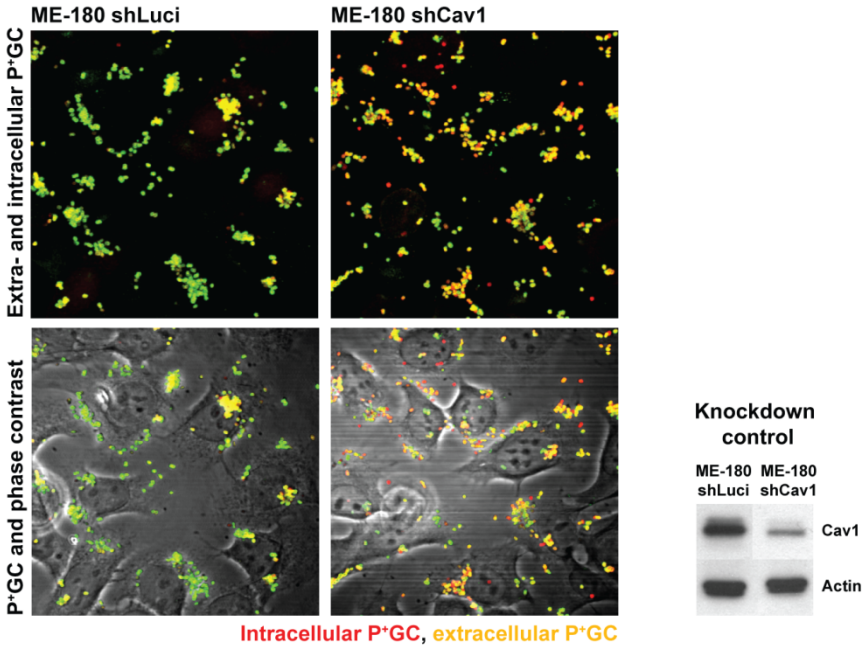

Figure 3-5. ShRNA-mediated down-regulation of Cav1 in ME-180 cells results in P$^+$GC internalization. Intracellular bacteria (red) are detected in ME-180 shCav1 cells (right panels) whereas only extracellular bacteria (yellow-green) are detected in ME-180 shLuciferase control cells (left panels). Efficiency of Cav1 knockdown in ME-180 cells after lentiviral transduction of luciferase (control) or Cav1 shRNA constructs (side panel). Scale bar: 20 µm.

knockdown of Cav1 protein levels was confirmed by Western blot analysis (Figure 3-5, side panel). Consequently, the generated cell lines were tested in the P$^+$GC infection model. Consistent with previous findings (*208*), infection of the ME-180 shCav1 cell line with P$^+$GC resulted in internalization of the bacteria as demonstrated by confocal microscopy (Figure 3-5). The total number of cell-associated bacteria was similar in the shCav1 and shLuci cells and was thus unaffected by Cav1 expression. However, differential fluorescent staining of intracellular and extracellular bacteria revealed that internalized bacteria could only be found in the shCav1 knockdown but not in the shLuci control cells.

Taken together, these results demonstrate that Cav1 recruitment to the vicinity of attached P$^+$GC is an immediate actin-dependent cellular response that plays an important role in preventing the internalization of P$^+$GC by host epithelial cells.

3.2 Tyrosine phosphorylation of Cav1 is required for Cav1 association with the cytoskeleton and to prevent internalization of P$^+$GC by host cells.

Previous reports showed that Cav1 phosphorylation on Tyr14 leads to mobilization of the protein to non-caveolar regions and promotes signaling events (*173, 219*). To learn more about a possible role of Cav1 phosphorylation during infection, the cellular amounts of Tyr14-phosphorylated Cav1 and the localization of Tyr14-phosphorylated Cav1 (phospho-Tyr14-Cav1) as well as its kinase Src were investigated following P$^+$GC infection.

First, the cellular localization of phospho-Tyr14-Cav1 was determined using immunofluorescence staining and confocal imaging (Figure 3-6). To identify if the Cav1 recruited to P$^+$GC attachment sites is phosphorylated, a phospho-Tyr14-Cav1 specific antibody was utilized for immunofluorescent staining. Despite the low levels of immunostaining for Tyr14-phosphorylated Cav1 (green), it could be detected in the vicinity of attached P$^+$GC (red), as observed previously for non-phosphorylated Cav1 (Figure 3-1 - 3-4). This suggests a possible link between P$^+$GC infection and Cav1 phosphorylation.

To confirm Cav1 phosphorylation during P$^+$GC infection, ME-180 cells were treated with the phosphotyrosine phosphatase (PTP)-inhibitor pervanadate before infection. Pervanadate treatment prevented a possible dephosphorylation of Cav1 and thus resulted in the accumulation of the phosphorylated state of Cav1, which allowed an easier detection of the phosphorylated Cav1 by immunofluorescence. Thus cells were immunostained and the localization of Cav1 and phospho-Tyr14-Cav1 was monitored using confocal microscopy (Figure 3-7A). Again, phospho-Tyr14-Cav1 could be detected in the vicinity of attached P$^+$GC

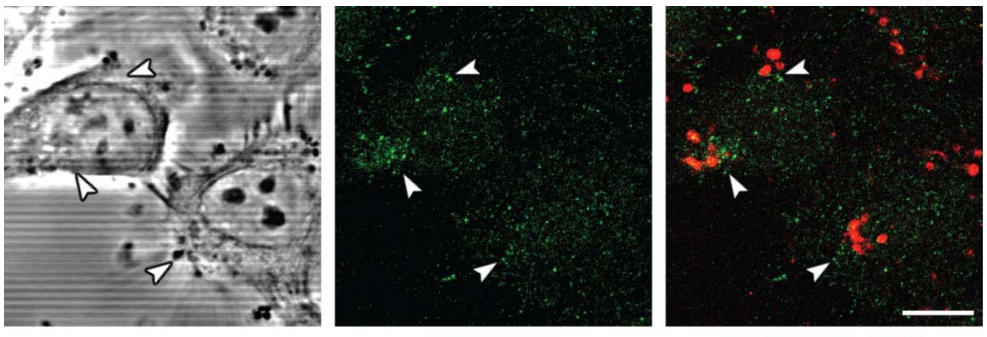

Figure 3-6. Cav1 is tyrosine-phosphorylated during P$^+$GC infection. Recruitment of phospho-Tyr14-Cav1 (green, middle panel, arrows) to attached P$^+$GC (red, right panel) in ME-180 cells 2 h post-infection. Scale bar: 10 µm

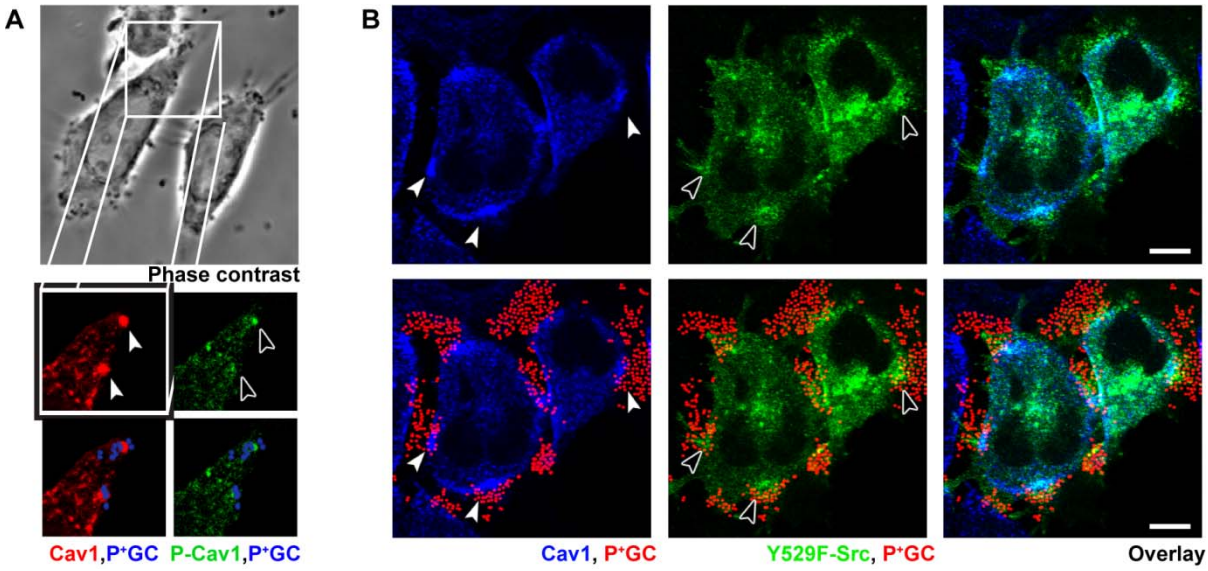

Figure 3-7. Src kinase is involved in Cav1-tyrosine-phosphorylation during P^+GC infection. A) phospho-Tyr14-Cav1 (green, black arrows) is found in PTP-inhibitor pervanadate-treated ME-180 cells at P^+GC infection sites (blue). Recruited phospho-Tyr14-Cav1 colocalizes with Cav1 (red, white arrows). (B) Transiently expressed constitutively active Src kinase (Y529F-Src, green, black arrows) is recruited in HeLa cells to attached P^+GC (red) during infection. Recruited Y529F-Src shows a high degree of colocalization with recruited Cav1 (blue white arrows).

using confocal analysis; however, even after pervanadate-treatment the recruited Cav1 was only partially phosphorylated.

Cav1 is known to be phosphorylated at Tyr14 by Src family kinases, consequently the localization of Src kinase was investigated during P^+GC infection. Unfortunately immunofluorescence staining of endogenous Src was not successful; therefore constitutively active Src kinase (Y529F-Src), in which the tyrosine-529 residue has been replaced by phenylalanine, was expressed in HeLa cells. After transfection, the cells were then infected with P^+GC and localization of Cav1 as well as Y529F-Src was monitored by immunofluorescence staining and confocal analysis. However, the localization of the endogenous Src protein could only be approximated through the localization of the constitutively active Src mutant after infection. Nonetheless, confocal analysis demonstrated that Cav1 and Y529F-Src were recruited jointly to P^+GC infection sites (Figure 3-7B). This Cav1-Y529F-Src co-localization in close vicinity of the P^+GC infection sites indicates that phospho-Tyr14-Cav1 and active Src kinase can be recruited underneath attached P^+GC and suggests a role of Cav1 phosphorylation by the Src kinase during infection.

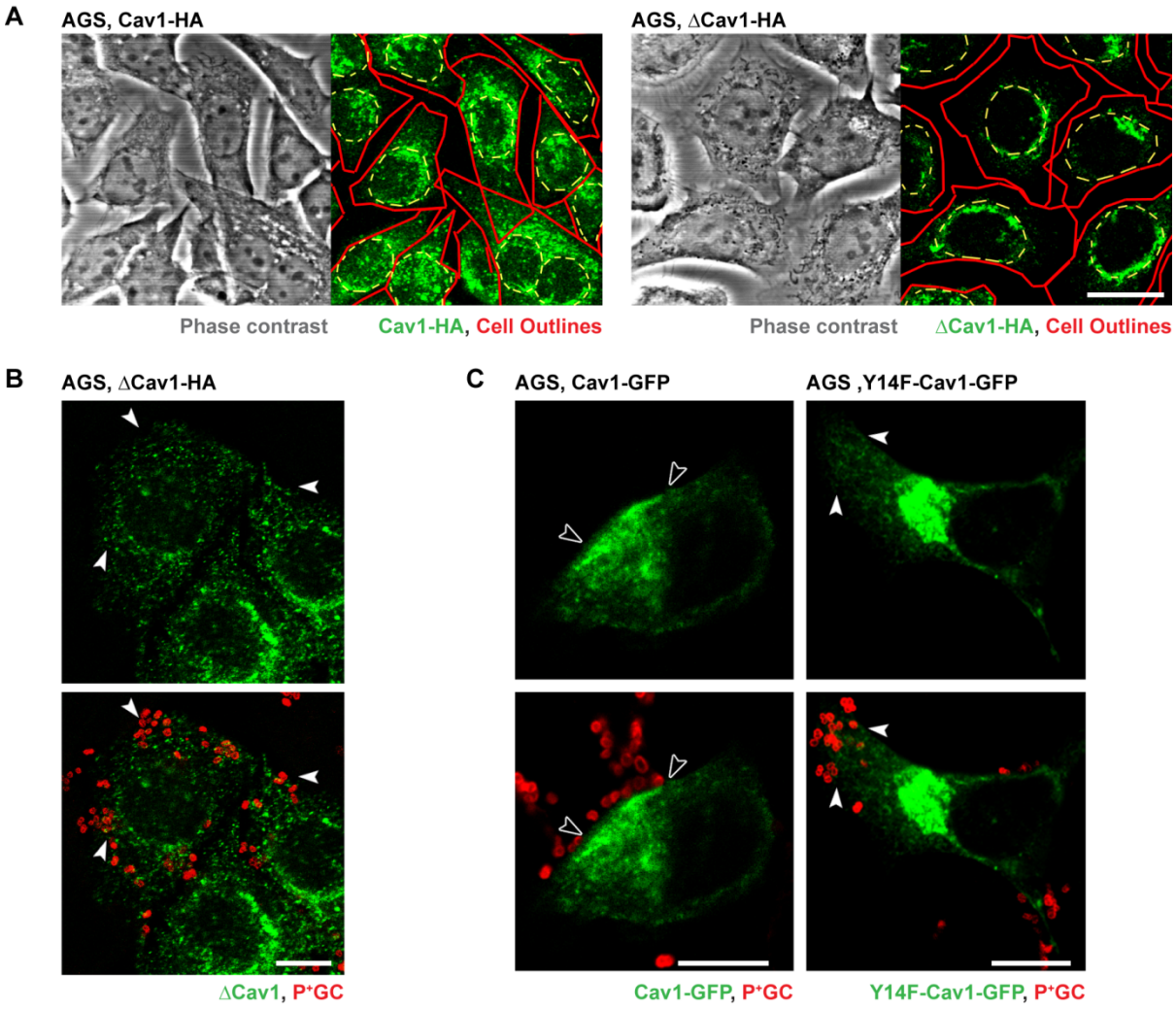

Figure 3-8. Recruitment of Cav1 during infection requires full-length, phosphorylatable Cav1. (A) Expressed ΔCav1-HA (green, right panel) shows a distinct expression pattern than expressed Cav1-HA (green, left panel). ΔCav1-HA is found in proximity of the nucleus (possibly remaining within the ER) whereas Cav1-HA localizes within the whole cell. Scale bar: 20 µm (B) ΔCav1-HA (green) is not recruited (white arrows) to attached P^+GC (red) after 2 h of infection. Scale bar: 10 µm (C) Expressed Cav1-GFP is recruited (black arrows) to attached P^+GC (red) after 2 h of infection (left panel). In contrast, non-phosphorylatable Y14F-Cav1-GFP is not recruited (white arrows) to attached P^+GC (red, right panel). Scale bars: 10 µm

To better understand the changes in the cellular localization of Cav1 and its recruitment during the infection process Cav1 mutants were generated and their ability to be recruited to the infection sites was analyzed. The functional importance of the Tyr14 phosphorylation site was investigated using a ΔCav1-HA construct that lacks the first 31 AA of wild type Cav1 and therefore does not comprise anymore the phosphorylatable Tyr14 site. In addition, the Tyr14 of wild type Cav1 was replaced with phenylalanine by site-directed mutagenesis, resulting in the constructs Y14F-Cav1-HA or Y14F-Cav1-GFP. Full-length constructs of Cav1 with either a C-terminal HA- or GFP-tag were used as control.

These Cav1 variants were then expressed in the human gastric carcinoma cell line AGS, which like many other malignant cell lines, does not contain detectable levels of Cav1 (*220*). Therefore this cell line was chosen as a system to study the behavior of the different Cav1 expression constructs during P^+GC infection.

Interestingly, ΔCav1-HA showed a different expression pattern than full-length Cav1-HA when expressed in AGS cells. In contrast to the wild type protein, which was distributed evenly in the cytoplasm and also in close vicinity to the plasma membrane, the majority of ΔCav1-HA was observed in proximity of the nucleus (Figure 3-8A). This localization indicates that ΔCav1-HA remains mainly in or at the endoplasmatic reticulum and cannot be mobilized to reach other cell compartments. P^+GC infection did not result in recruitment of the ΔCav1-HA construct (Figure 3-8B), which indicates that the first 31 amino acids of Cav1 are required for the correct localization of the protein as well as on the re-localization of Cav1 observed after P^+GC infection. To specifically investigate the Ty14 phosphorylation of Cav1, Cav1-GFP and Y14F-Cav1-GFP were expressed in the Cav1-negative AGS cells that were subsequently infected with P^+GC. In contrast to Cav1-GFP, Y14F-Cav1-GFP was not recruited to the sites of bacterial attachment (Figure 3-8C). Thus, Cav1 recruitment to the infection sites requires the Tyr14 residue and the deletion of the N-terminal part of the protein or exchange of this residue for another hydrophobic AA resulted in reduced mobilization and recruitment of the respective construct to P^+GC infection sites. This result shows the importance of Tyr14 of Cav1 during P^+GC infection and indicates a possible role of phospho-Tyr14-Cav1 signaling during infection.

To better understand the dynamics of Cav1 phosphorylation during infection with P^+GC, the phosphorylation state of Cav1 during a 2 h infection time course was monitored in serum starved ME-180 cells to synchronize the cells and suppress residual Src activity. Western blot analysis demonstrated that P^+GC infection stimulated Cav1 phosphorylation at Tyr14 (Figure 3-9) and the quantification of phospho-Tyr14-Cav1 in control-treated ME-180 cells showed that Cav1 phosphorylation levels were increased 1.5-fold after 5 min of infection. Cav1 Tyr14 phosphorylation levels remained constant until 30 min and then increased again to more than 3-fold after 90 min of infection. In accordance with previous reports (*147, 221*), this phosphorylation of Cav1 at Tyr14 depends on active Src- and Abl-kinases. Therefore, cells were treated with the Src family kinase inhibitor PP2 (*222*) and the

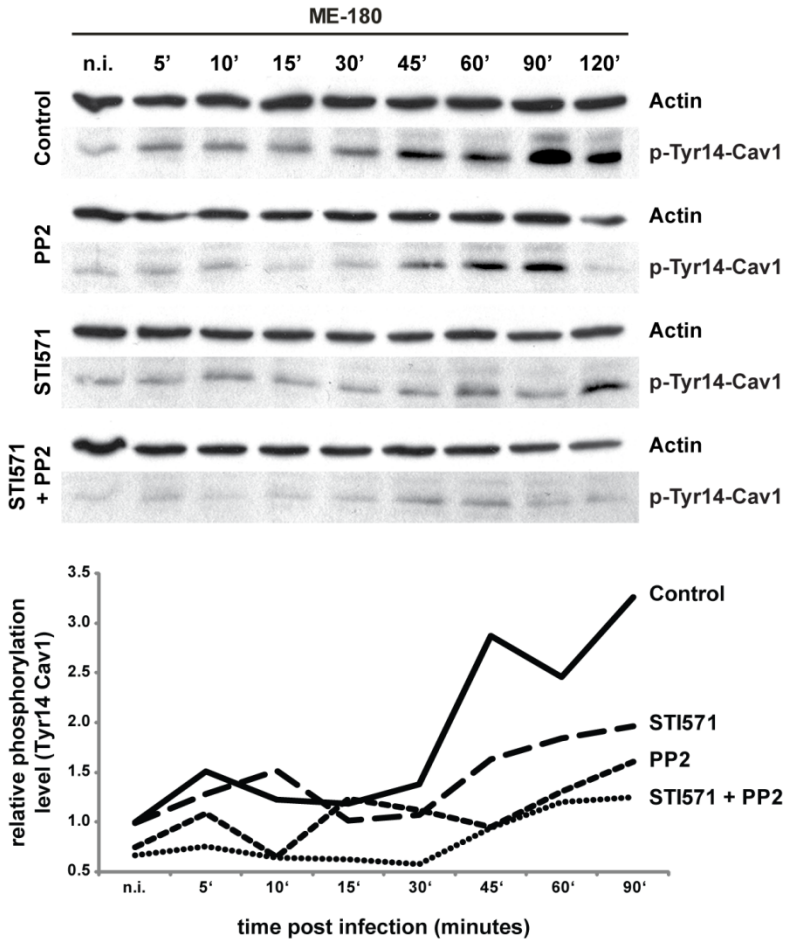

Figure 3-9. Cav1 phosphorylation during P^+GC infection depends on Abl and Src kinases. Western blot analysis of phospho-Tyr14-Cav1 levels (upper panels) and quantification of phosphorylation levels of three different experiments (lower panel) demonstrate elevated Cav1 phosphorylation starting 5 min post infection. Phosphorylation is increased by more than 3-fold in control-treated cells 90 min post infection. Stimulation of phosphorylation by P^+GC is strongly reduced in Src-inhibitor PP2 and Abl-inhibitor STI571-treated cells (both 10 µM) at all time points.

Abl tyrosine kinase inhibitor STI571/Imatinib (*223*) 1 h prior to infection to block Cav1 Tyr14 phosphorylation. In comparison to untreated control cells, stimulation of Cav1 phosphorylation by P^+GC in PP2- and STI571-treated cells was markedly reduced during the whole infection period. ME-180 cells treated simultaneously with both inhibitors exhibited minimal levels of Cav1 phosphorylation and stimulation by P^+GC was negligible.

Previous studies reported that Cav1 binds to proteins of the cytoskeleton such as the actin cross-linker filamin as well as to the intermediate filaments (*183, 224*). Moreover, Cav1 is relocated along cytoskeletal structures to the caveolae-free front of migrating cells, which requires phosphorylation of Tyr14 (*180*). To determine if the Cav1 association with the cytoskeleton (Figures 3-3B and 3-4) was dependent on the Tyr14 residue of Cav1, the

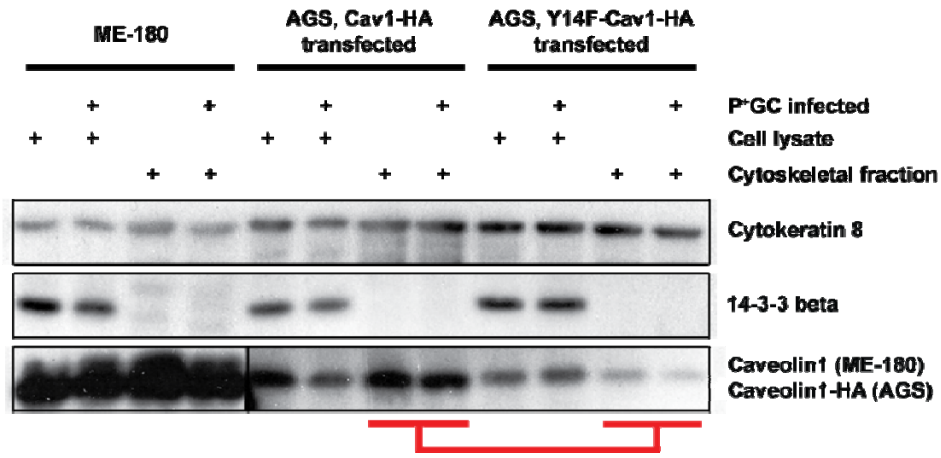

Figure 3-10. Interaction of Cav1 with cytoskeletal components depends on Cav1 phosphorylation but functions independently of P$^+$GC infection. Fractionation of transfected AGS cells reveals a strong association of wild-type Cav1 (Cav1-HA), but not the phosphorylation-deficient mutant (Y14F-Cav1-HA), with cytoskeletal components (lower panel, red marking). This was observed in P$^+$GC-infected as well as uninfected samples. Endogenous Cav1 likewise associates with cytoskeletal components in ME-180 cells independently of P$^+$GC-infection (lower panel). Cytokeratin 8 serves as a control for the correct localization of cytoskeleton-associated proteins into the cytoskeletal components fraction (upper panel). 14-3-3β serves as a control for complete removal of cytoplasm-associated proteins from the cytoskeletal components fraction (middle panel). Full lysate rows serve as loading and protein expression controls.

cytoskeletal fraction from AGS cells, which have been transfected either with Cav1-HA or with the phosphorylation-defective mutant Y14F-Cav1-HA, was purified. Similarly to the endogenous Cav1 in ME-180 cells, wild type Cav1-HA transfected into AGS cells was largely recovered from the cytoskeletal fraction, whereas Y14F-Cav1-HA showed a reduced association with the cytoskeleton as observed in P$^+$GC-infected as well as uninfected cells (Figure 3-10). Thus, phosphorylation of Cav1 on Tyr14 promotes its association with the cytoskeleton irrespective of P$^+$GC infection.

Since Cav1 recruitment to the infection sites blocks bacterial uptake, the requirement of Cav1 Tyr14 phosphorylation for impediment of P$^+$GC internalization was investigated. Therefore Cav1-HA and Y14F-Cav1-HA were expressed in Cav1-negative AGS cells, which were subsequently infected, fixed and immunostained using antibodies against Cav1 and P$^+$GC. Differential fluorescent staining of intracellular and extracellular bacteria revealed that, in contrast to wild-type Cav1, Y14F-Cav1 did not impede internalization (Figure 3-10). Thus, expression of wild-type Cav1 allowed the bacteria to colonize AGS cells completely extracellularly whereas expression of the phosphorylation-deficient Cav1 mutant lead to markedly increased bacterial uptake into the cells.

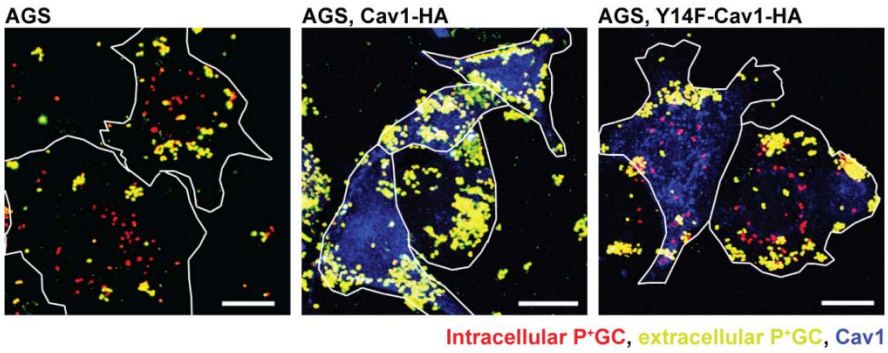

Figure 3-11. Bacterial uptake is observed in Cav1-negative, non-transfected AGS cells (left panel) but not in wild-type Cav1-transfected AGS cells (middle panel). In contrast, transfection of the phosphorylation-deficient mutant, Y14F Cav1, does not impede bacterial uptake by AGS cells (right panel). Intracellular bacteria appear in red, extracellular bacteria in yellow-green and Cav1 in blue. Cellular borders are represented as white outlines. Scale bars: 20 µm.

Taken together, these results indicate that Cav1 is phosphorylated on Tyr14 during P^+GC infection and that phospho-Tyr14-Cav1 is recruited to P^+GC infection sites. These data suggest that Cav1 phosphorylation at Tyr14 is required for P^+GC-induced Cav1 recruitment and Cav1-mediated prevention of bacterial uptake, as well as the tight association of Cav1 with the cytoskeleton. Cav1 phosphorylation most likely plays a role in signaling events that link Cav1 to a reorganization of the cytoskeleton.

3.3 RhoA GEF Vav2 is a novel, high affinity interaction partner of phospho-Tyr14-Cav1

Cav1 tyrosine phosphorylation plays a role in signal transduction, however only few interaction partners of phospho-Tyr14-Cav1 have been described so far. Large scale approaches have been undertaken to identify novel interaction partners; however, in a

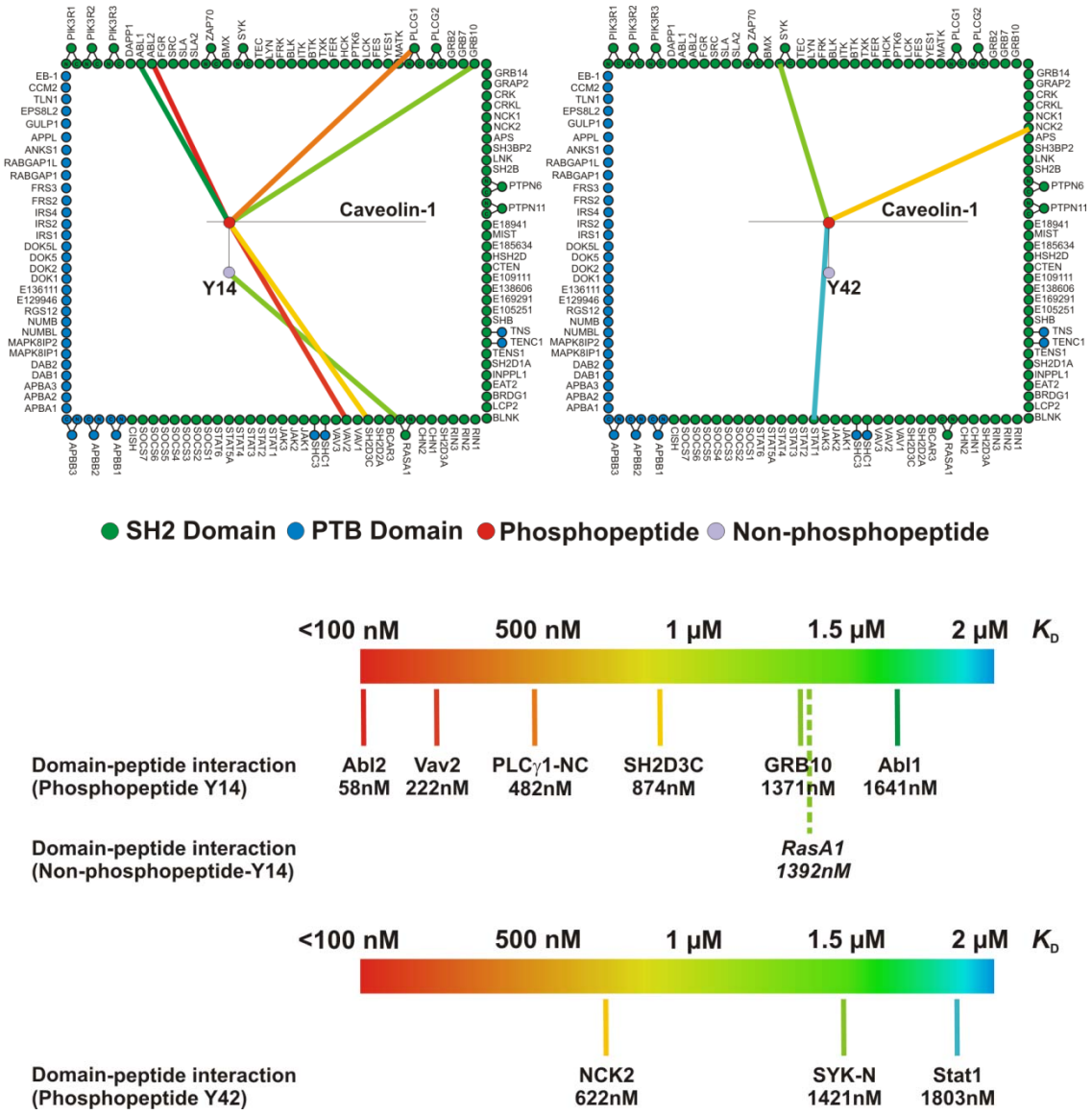

Figure 3-12*. A comprehensive, quantitative screen using microarrays of recombinant human SH2 and PTB domains reveals Tyr14-phosphorylation-dependent binding of Cav1 to several SH2-domain containing proteins. A Tyr14-Cav1 phosphopeptide, a Tyr42-Cav1 phosphopeptide and the respective non-phosphorylated peptide controls were probed with virtually all human SH2 and PTB domains. The RhoA GEF Vav2 shows a high-affinity interaction (KD of 222 nM) with the Tyr14-Cav1 phosphopeptide. The red circles represent the Cav1 phosphopeptides (18 amino acids); the purple circles represent the corresponding non-phosphorylated peptides; green and blue circles represent SH2 and PTB domains, respectively. Green or blue circles outside the rectangle represent tandem domains. The color of lines connecting peptides to domains indicates strength of observed interactions (see legend). KD values for each hit are provided on the figure.

* SH2-/PTB-domain screen was performed in the laboratory of Gavin MacBeath as previously described (215)

Gal4-based yeast two-hybrid screen only Csk was shown to bind to phospho-Tyr14-Cav1 (*182*).

To identify novel interaction partners of phospho-Tyr14-Cav1, two distinct experimental approaches were chosen: First, a large scale SH2-/PTB-domain protein array was screened for interactions with a Tyr14-Cav1 phosphopeptide. Second, a biotinylated Tyr14-Cav1 phosphopeptide was used as bait in a streptavidin pull-down, followed by identification of all precipitated proteins. Using these two independent approaches increased the probability of finding and verifying novel interaction partners of Ty14 phosphorylated Cav1.

In the SH2-/PTB-domain screening approach, two fluorescently labeled peptides with sequences corresponding to residues 5–22 of Cav1 were synthesized, one non-phosphorylated and the other phosphorylated on Tyr14. These peptides were then used to probe protein microarrays comprising virtually all Src homology 2 (SH2) and phosphotyrosine binding (PTB) domains encoded in the human genome, as previously described (*215*). In order to obtain quantitative information, the arrays were probed, in duplicate, with eight concentrations of each peptide, ranging from 10 nM to 5 μM. Then the resulting fluorescence data was fitted to an equation that describes saturation binding (*215*), giving the equilibrium dissociation constants (K_Ds) for the binding of each peptide to each recombinant domain (Figure 3-12). Previous studies with other phosphopeptides have shown that >90% of the SH2 and PTB domains on these arrays are active (*215*) and hence non-interactions should be viewed as reliable information as well.

In total, the arrays highlighted six SH2 domains that bound the Tyr14-Cav1 phosphopeptide with high affinity (K_D < 2 μM): Abl2 (K_D=58 nM), Vav2 (K_D=222 nM), Phospholipase Cγ1 (PLCγ1; K_D=482 nM), SH2D3C (K_D=874 nM), Grb10 (K_D=1371 nM) and Abl1 (K_D=1641 nM; Figure 3-12; Table 3-1). Strong interactions with the SH2 domain of Abl2 are frequently observed (this is a particularly promiscuous domain), therefore the high affinity interaction with the SH2 domain of RhoA GEF Vav2 (K_D=222 nM) was notable. Solely the GTPase-activating protein RasA1 was identified to bind to the non-phosphorylated Tyr14-Cav1 peptide (K_D=1392 nM) but not its phosphorylated form (Figure 3-12).

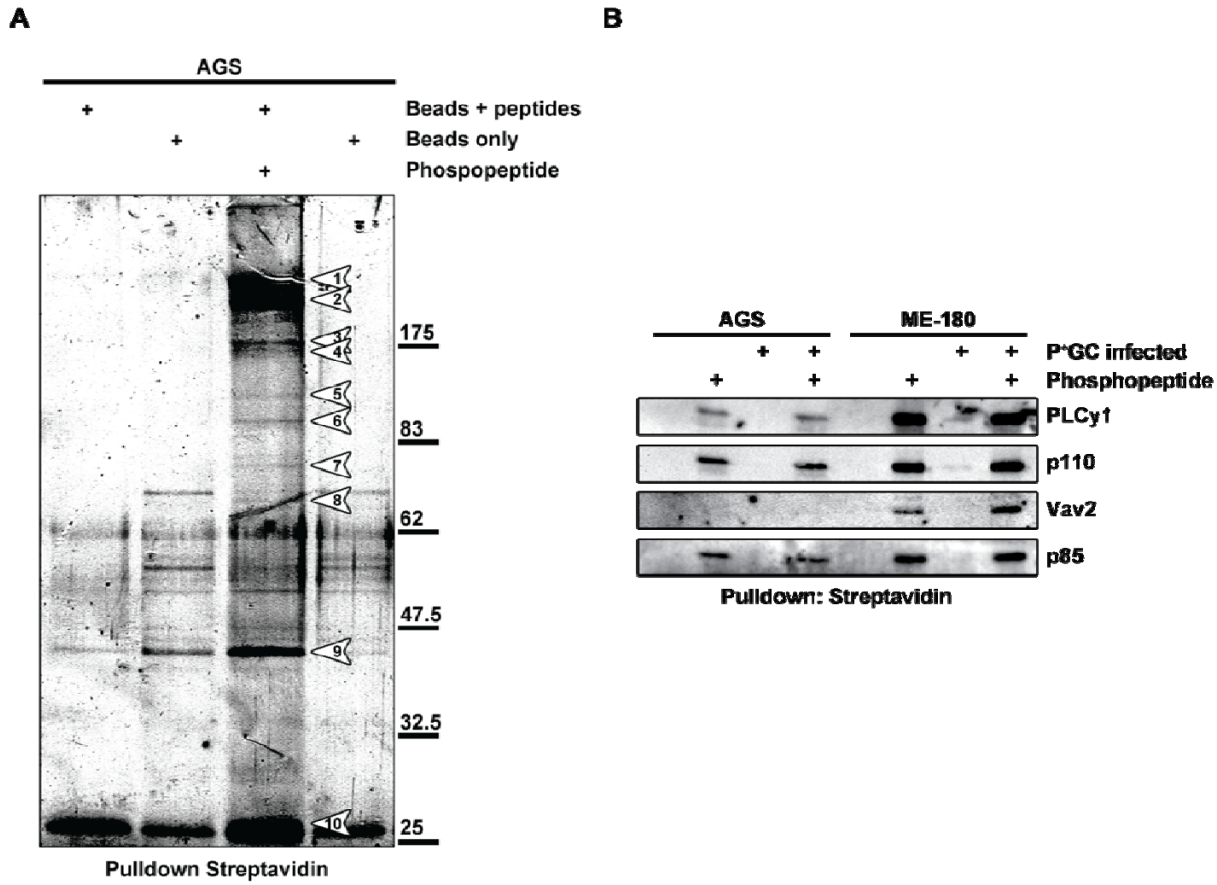

Figure 3-13. Precipitation of a biotinylated Tyr14-Cav1 phosphopeptide confirms Tyr14-phosphorylation-dependent binding of Cav1 to Vav2 and identifies further interaction partners. (A) Streptavidin-agarose pulldown assay using biotin-labeled phosphorylated and non-phosphorylated Tyr14-Cav1 peptides as baits was performed in AGS cells and precipitates were separated by SDS-PAGE. Phospho-specific bands on the SDS-Gel (numbered arrows) have been identified by Maldi-MS/MS (Table 1). Here, p85, regulatory subunit of phosphoinositide 3-kinase (PI3K), could be identified as an interaction partner of the Tyr14-Cav1 phosphopeptide (arrow No. 7). (B) Western blot analysis of streptavidin-precipitates of infected and uninfected AGS and ME-180 cells using biotin-labeled phosphorylated and non-phosphorylated Tyr14-Cav1 peptides as baits. Vav2, PLCγ1, p85 and p110, catalytic subunit of PI3K, are only detected in precipitates of the phosphorylated peptide. Levels of precipitated Vav2 increase upon infection with P^+GC in ME-180 cells.

To control for the Tyr14 specificity of the identified binding proteins, signaling proteins that could interact with Cav1 upon phosphorylation at Tyr42 were identified as well. Two fluorescently labeled peptides with sequences corresponding to residues 33–50 of Cav1 were synthesized, one phosphorylated on Tyr42 and the other non-phosphorylated. These peptides were then probed with identical protein microarrays. This experiment highlighted three SH2 domains that recognized the Tyr42-Cav1 phosphopeptide with high affinity: Nck2 (K_D=622 nM), Syk (K_D=1421 nM) and Stat1 (K_D=1803 nM; Figure 3-12; Table 3-2). Thus, none of the proteins identified to bind to the Tyr14-Cav1 phosphopeptide were as well identified to bind to the Tyr42-Cav1 phosphopeptide.

Next, a biochemical assay was developed to confirm the hits of the SH2/PTB-domain screen and also to identify novel phospho-Tyr14-Cav1 signaling partners. Therefore a pulldown assay using biotin-labeled, phosphorylated and non-phosphorylated Tyr14-Cav1 peptides comprising AA residues 7–21 of Cav1 as baits was performed in protein extracts of Cav1-negative AGS cells. Interacting proteins were precipitated using streptavidin-agarose, separated by SDS-PAGE and bands specific for the Tyr14 phosphorylated Cav1 peptide (Figure 3-13A; numbered arrows) were identified by Maldi-MS/MS (Table 3-3). Most interestingly, p85, the regulatory subunit of the phosphoinositide 3-kinase (PI3K), was identified as an additional novel interaction partner of the Tyr14-Cav1 phosphopeptide (Figure 3-13A arrow No. 7). Additionally, myosin IB, myosin ID, non muscle myosin heavy chain IIA, cytokeratin 1, beta-actin and splicing factor proline/glutamine rich (SFPQ/PSF) were identified as possible phospho-Tyr14-Cav1 binding partners (Figure 3-13A numbered arrows and Table 3-3).

The streptavidin-agarose pulldown assay was used to biochemically confirm the binding of the hits identified in the SH2-/PTB-domain screening. Therefore, the previously described biotin-labeled Tyr14-Cav1 peptides were incubated with cellular lysates derived from ME-180 and AGS cells. The peptides were subsequently precipitated with streptavidin-coated agarose beads, bound proteins were separated by SDS PAGE and the hits previously identified in the SH2-/PTB-domain screen were detected with corresponding antibodies by Western blot. Consistent with the microarray data, PLCγ1, p85 and also p110, the catalytic subunit of PI3K, showed a highly increased affinity to the phosphorylated Cav1 peptide compared to the non-phosphorylated peptide, independently of P^+GC infection (Figure 3-13B). Vav2 co-purified exclusively with the phosphorylated peptide in precipitates of ME-180 cells. In contrast to any other identified Tyr14-Cav1 phosphopeptide binding partners, 40% more Vav2 was recovered from infected cells than from uninfected cells when analyzing equal amounts of lysates (Figure 3-13B). PLCγ1, p85 and p110 were also exclusively detected in precipitates of the phosphorylated peptide from lysates of AGS cells, which also showed no difference in precipitation upon infection with P^+GC (Figure 3-13B).

To investigate the physiological relevance of the identified Tyr14-Cav1 phosphopeptide interaction partners, immunoprecipitation experiments with endogenous proteins as well as full length and truncated Vav2 constructs were performed next.

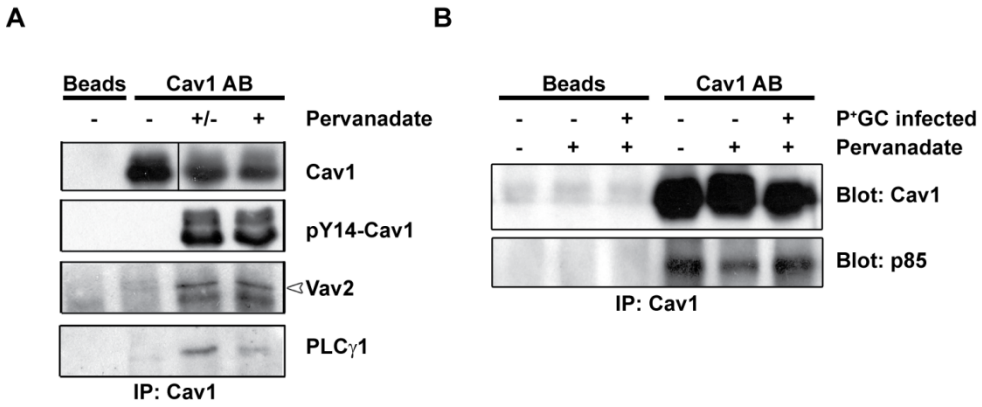

Figure 3-14. Co-immunoprecipitation confirms novel phospho-Tyr14-Cav1 interaction partners. (A) Co-immunoprecipitation demonstrates increased protein-protein interaction of Cav1 and Vav2 after cell treatment with the phosphatase inhibitor pervanadate. Western blot analysis of immunoprecipitates of ME-180 cells using full-length Cav1 protein as bait. Cav1 was immunoprecipitated from untreated cells (-), a 1:1 mixture of lysates derived from untreated and pervanadate-treated cells (+/-) and only pervanadate-treated cells (+). Precipitates were probed for Cav1, phospho-Tyr14-Cav1, Vav2 and PLCγ1. Tyrosine-phosphorylated Cav1 was precipitated exclusively from mixed and pervanadate-treated lysates. Levels of co-precipitated Vav2 and PLCγ1 were strongly increased in mixed and pervanadate-treated lysates. (B) Co-immunoprecipitation demonstrates protein-protein interaction of Cav1 and p85. Western blot analysis of immunoprecipitates of ME-180 cells using full-length Cav1 protein as bait. Precipitates were probed for Cav1 and p85. P85 could be co-precipitated independently of P^+GC-infection or pervanadate-treatment.

Endogenous Cav1 was immunoprecipitated from either untreated ME-180 cells or from cells that had been pretreated with the phosphatase-inhibitor pervanadate. Pervanadate treatment results in hyperphosphorylation not only of Cav1 but of all phospho-tyrosine proteins. Therefore Cav1 was also immunoprecipitated from a 1:1 mixture of lysates derived from untreated and pervanadate-treated cells, which revealed an interaction between phosphorylated Cav1 and non-phosphorylated Vav2 as shown by Western blot analysis (Figure 3-14A).

The effect of pervanadate treatment and P^+GC infection on the identified Cav1-p85 interaction was investigated similarly. Cav1 was immunoprecipitated from untreated, pervanadate-pretreated and additionally P^+GC infected ME-180 cells. Here, Western blot analysis demonstrated co-immunoprecipitation of p85 with full-length Cav1 in all samples (Figure 3-14B), however no difference could be detected here between untreated and pervanadate-treated cells. Furthermore, P^+GC infection did not impact significantly on the amount of co-immunoprecipitated p85.

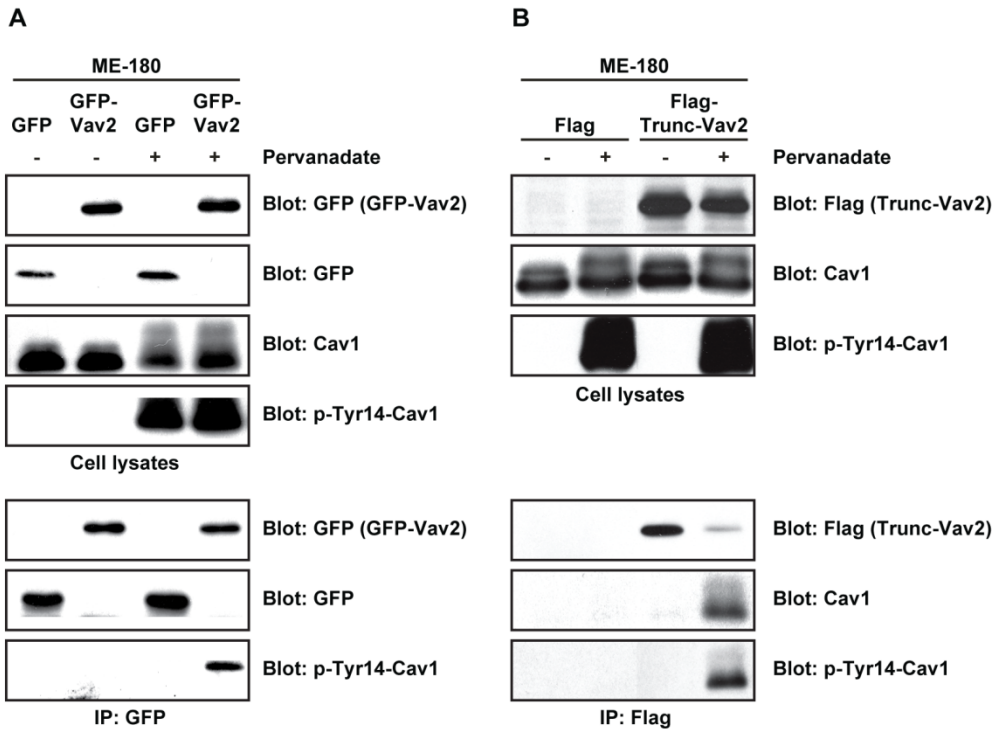

Figure 3-15. Co-immunoprecipitation confirms relevance of the SH2-domain of Vav2 for the reported phospho-Tyr14-Cav1-Vav2 interaction. (A) GFP-Vav2 and Cav1 interact exclusively after cell treatment with pervanadate. Western blot analysis of total cell lysates (upper panels) and immunoprecipitates (lower panels) using heterologously expressed GFP-Vav2 or GFP protein as baits. Lysates were probed for GFP, Cav1, and phospho-Tyr14-Cav1, respectively. GFP-Vav2 and GFP were immunoprecipitated from untreated (–) and pervanadate-treated cells (+) using a GFP antibody. Precipitates were probed for GFP and phospho-Tyr14-Cav1. Phosphorylated Cav1 was recovered exclusively from pervanadate-treated lysates of GFP-Vav2 expressing cells. (B) Truncated Vav2 and Cav1 interact exclusively after cell treatment with pervanadate. Western blot analysis of ME-180 cell lysates (upper panels) and immunoprecipitates (lower panels) using heterologously expressed truncated Vav2 or FLAG-tag peptide as baits. Truncated Vav2 only possesses the C-terminal SH3-SH2-SH3 domains of Vav2. Using a FLAG antibody, truncated Vav2 was immunoprecipitated from untreated (–) and pervanadate-treated cells (+). Phosphorylated Cav1 was recovered exclusively from lysates of truncated Vav2 expressing, pervanadate-treated cells.

To better understand the molecular mechanism of the observed specific phospho-Tyr14-Cav1–Vav2 interaction, different Vav2 constructs were expressed in ME-180 cells and immunoprecipitated using antibodies against the respective tags. To demonstrate the reciprocity of the observed Cav1-Vav2 protein-protein interaction, first, full-length Vav2 tagged with GFP was expressed in pervanadate- and control-treated cells. This allowed precipitating GFP-Vav2 and GFP alone using an anti-GFP antibody. Phospho-Tyr14-Cav1 co-precipitated exclusively from pervanadate-treated, GFP-Vav2 expressing cells (Figure 3-15A). This further demonstrated the phosphorylation-specificity of the phospho-Tyr14-Cav1–Vav2 protein-protein interaction.

Since only the SH2 domain of the Vav2 protein had been spotted on the protein microarray, it was legitimate to assume that the Vav2-Cav1 interaction was SH2-domain specific. To verify this, truncated, flag-tagged Vav2 that consists solely of the C-terminal SH3-SH2-SH3 domains of the protein was expressed in pervanadate- and control-treated cells. Similar to full-length Vav2, the truncated Vav2 could be precipitated from transfected cells using a FLAG antibody and again phospho-Tyr14-Cav1 co-precipitated exclusively with the truncated Vav2 from pervanadate-treated cells (Figure 3-15B). Thus the remaining domains of truncated Vav2 are relevant and sufficient for the observed phospho-Tyr14-Cav1–Vav2 interaction.

Taken together, these results identify a set of novel interaction partners of Tyr14 phosphorylated Cav1. These data suggest that the Rho family GEF Vav2 is an important signaling partner of Cav1 due to the high affinity and specificity of its phospho-Tyr14-Cav1 binding as well as the increase in binding upon $P^{+}GC$ infection.

Table 3-1: Phospho-Tyr14-Cav1 binding partners identified by screening of the SH2-/PTB-domain protein microarray.

K_D value (nM)	Identified protein:	NCBI Gene ID:	Confirmed by:
58	Abl2	27	
222	Vav2	7410	Cav1 peptide pulldown Cav1 Immunoprecipitation
482	PLCγ1	5335	Cav1 peptide pulldown Cav1 Immunoprecipitation
874	SH2D3C	10044	
1371	Grb10	2887	
1641	Abl1	25	

Table 3-2: Phospho-Tyr42-Cav1 binding partners identified by screening of the SH2-/PTB-domain protein microarray.

K_D value (nM)	Identified protein:	NCBI Gene ID:
622	Nck2	8440
1421	Syk	6850
1803	Stat1	6772

Table 3-3: Phospho-Tyr14-Cav1 binding partners identified by MALDI-TOF/TOF after streptavidin pulldown of biotin-labeled Tyr14-Cav1 peptides.

Band No.:	Identified protein:	NCBI Protein Database No.:	NCBI Gene ID:	Confirmed by:
1,2,3,4,5,7	non muscle myosin heavy chain IIA	12667788	4627	
5	myosin IB	44889481	4430	
6	splicing factor proline/glutamine rich (SFPQ/PSF)	23956214	6421	
6	myosin ID	119600629	4642	
7	PI3K, regulatory subunit p85α	32455248	5295	Cav1 peptide pulldown Cav1 Immunoprecipitation
8	cytokeratin 1	11935049	3848	
9	β-actin	15277503	60	
10	Chain A, Streptavidin Mutant	34811425	-	

3.4 Vav2 and RhoA act as downstream signaling partners of Cav1 during P$^+$GC infection and prevent internalization of P$^+$GC.

In the previous chapter, Vav2, PLCγ1, the p85 subunit of PI3K, Abl 1 and Abl 2, SH3D3C and the adaptor protein Grb10 were found to specifically bind to phospho-Tyr14-Cav1. As Cav1 was found to prevent P$^+$GC uptake, the possible role of the Rho family GEF Vav2 in this process was analyzed in detail as this protein can directly activate Rho/Rac leading to cytoskeletal reorganization. Therefore, the two phospho-Tyr14-Cav1 high affinity binders Vav2 and PLCγ1 were compared with regard to impede bacterial uptake to assess the importance of Vav2 and RhoA/Rac1 activation in P$^+$GC infection. However, the Abl family kinases and PI3K as well as the other discovered binding partners of Cav1 can have additional effects on cytoskeletal rearrangements which will be discussed later (chapter 4.2).

The role of Vav2 and PLCγ1 during P$^+$GC infection of ME-180 cells was analyzed by RNA interference. Confocal microscopy revealed that, as with Cav1, reducing Vav2 levels using siRNA resulted in efficient internalization of P$^+$GC by ME-180 cells (Figure 3-16).

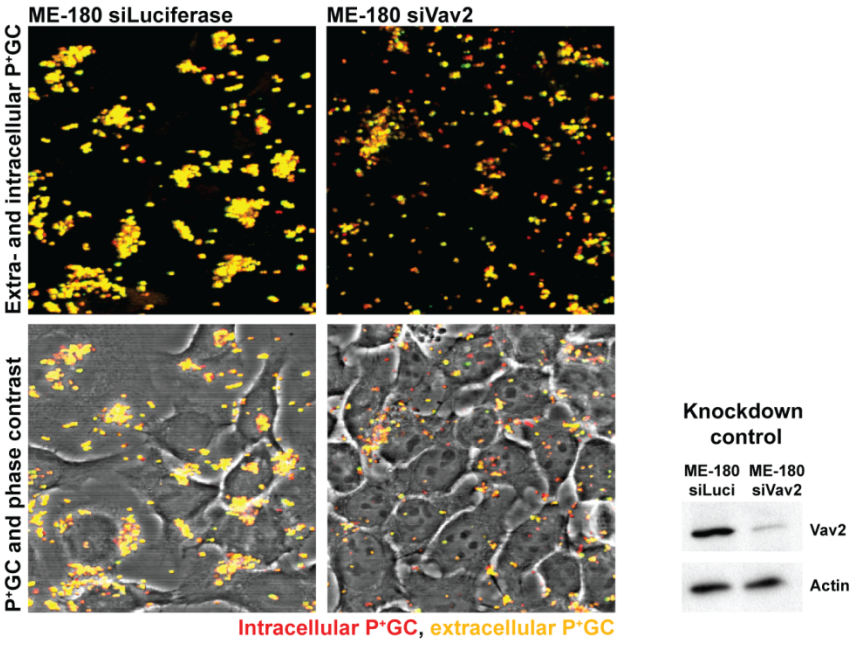

Figure 3-16. Knockdown of Vav2 levels in ME-180 cells using siRNA results in P$^+$GC internalization. Intracellular bacteria (red) are detected in siVav2-treated ME-180 cells (right panels), whereas only extracellular bacteria (yellow-green) are detected in siLuciferase-treated control cells (left panels). Efficiency of Vav2 knockdown in ME-180 cells after siRNA treatment (side panel). Scale bar: 20 µm.

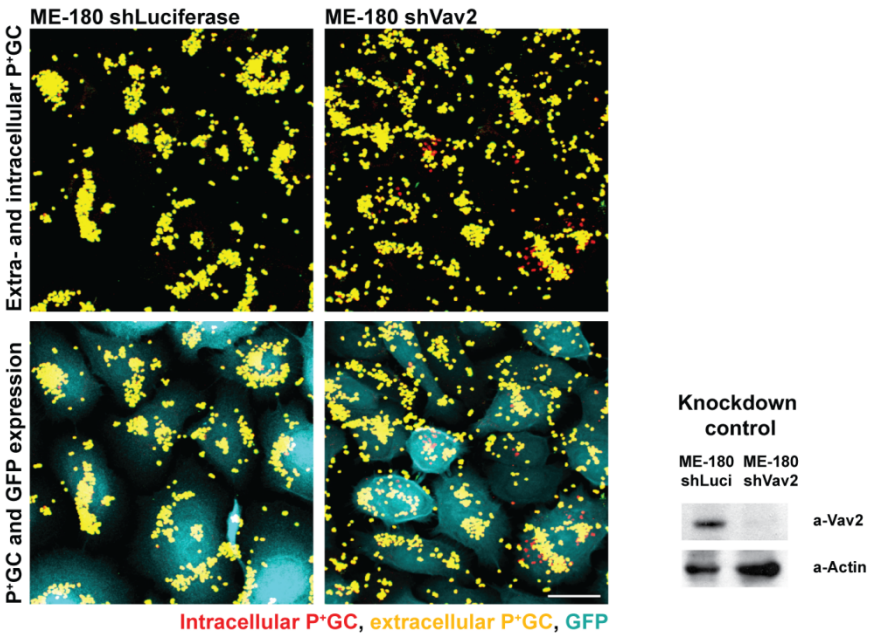

Figure 3-17. Knockdown of Vav2 levels in ME-180 cells using shRNA results in P$^+$GC internalization. Intracellular bacteria (red) are detected in ME-180 shVav2 cells (right panels) whereas only extracellular bacteria (yellow-green) are detected in ME-180 shLuciferase control cells (left panels). Efficiency of shRNA-mediated Vav2 knockdown in ME-180 cells after lentiviral transduction of shCav1 or control shLuciferase constructs (side panel). Scale bar: 20 µm.

Intracellular bacteria (red) were detected only in ME-180 cells treated with siRNA targeting Vav2 (Figure 3-16, right panels) whereas only extracellular bacteria (yellow-green) were detected in ME-180 cells treated with the control siLuciferase (Figure 3-16, left panels). The Vav2 knockdown efficiency was controlled by Western blot (Figure 3-16, side panel). To confirm this observation, Vav2 was downregulated by shRNA in ME-180 cells and P$^+$GC internalization was analyzed. The Vav2 knockdown efficiency by shRNA was controlled by Western blot and found to be comparable to the siRNA-mediated knockdown (Figure 3-17, side panel). Intracellular bacteria (red) were detected in ME-180 shVav2 cells (Figure 3-17, right panels) whereas only extracellular bacteria (yellow-green) were detected in shLuciferase-treated control cells (Figure 3-17, left panels). ShRNA-mediated downregulation of Vav2 led to a noticeable but less drastic P$^+$GC uptake than siRNA-mediated downregulation of the protein (Figure 3-17).

Taken together, these RNAi experiments demonstrate that bacterial uptake into host cells after downregulation of Cav1 or Vav2 is comparable, which suggests a close interplay of these interaction partners. By contrast, shRNA-mediated downregulation of PLCγ1 in ME-

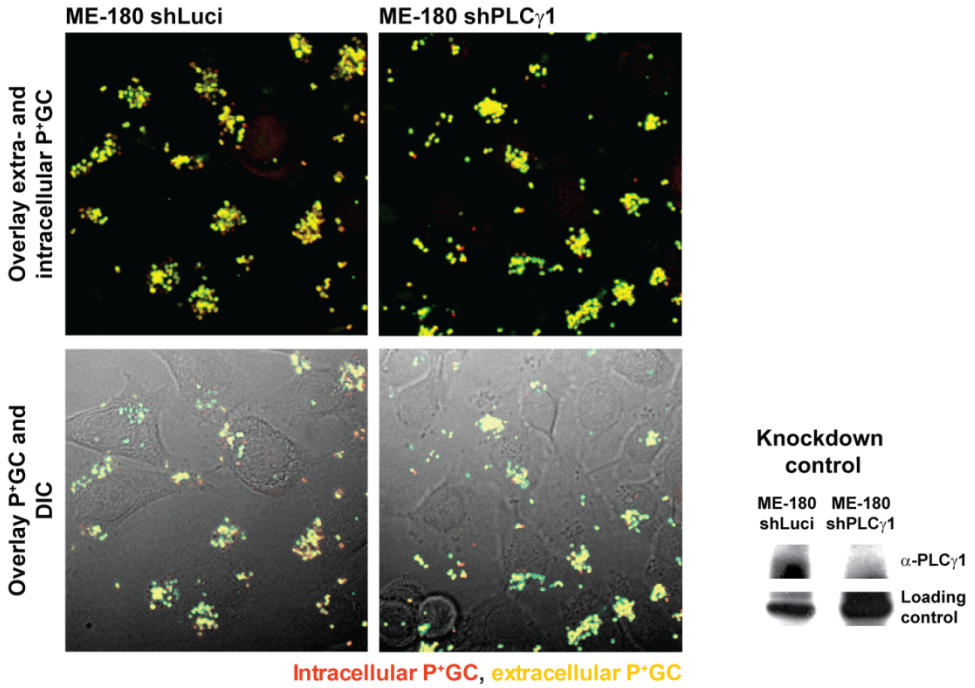

Figure 3-18. ShRNA-mediated downregulation of PLCγ1 in ME-180 cells does not result in P$^+$GC internalization. Only extracellular bacteria (yellow-green) are detected in ME-180 shPLCγ1 cells (upper right panels) and ME-180 shLuciferase control cells (upper left panels). Efficiency of PLCγ1 knockdown in ME-180 cells after lentiviral transduction of luciferase (control) or PLCγ1 shRNA constructs (lower panel). Scale bar:

180 cells did not result in P$^+$GC internalization (Figure 3-18) and no intracellular bacteria (red) but only extracellular bacteria (yellow-green) were detected in ME-180 shPLCγ1 cells or in shLuciferase treated control cells (Figure 3-18). This demonstrates that the interaction between phosho-Tyr14-Cav1 and PLCγ1 reported earlier is less important in impeding bacterial uptake.

Thus in contrast to PLCγ1, Vav2 plays a role in preventing bacterial internalization. Most likely it functions as a GEF for the Rho/Rac family of GTPases thereby promoting cytoskeletal reorganization after P$^+$GC infection. Alternatively, Vav2 could function in a manner independent of its GEF activity by physically linking signaling molecules to the actin cytoskeleton (*225*). To explain the underlying mechanism of Vav2 involvement, it was hypothesized that the small GTPases RhoA and/or Rac1 are involved.

To test for a possible involvement of RhoA in impeding bacterial internalization, ME-180 cells were treated with low concentrations of the Rho-specific inhibitor CT04, a cell permeable form of the C3 transferase from *Clostridium botulinum*, for 4 h. Subsequently the cells were infected with P$^+$GC. Interestingly, treatment with CT04 led to a strong uptake of

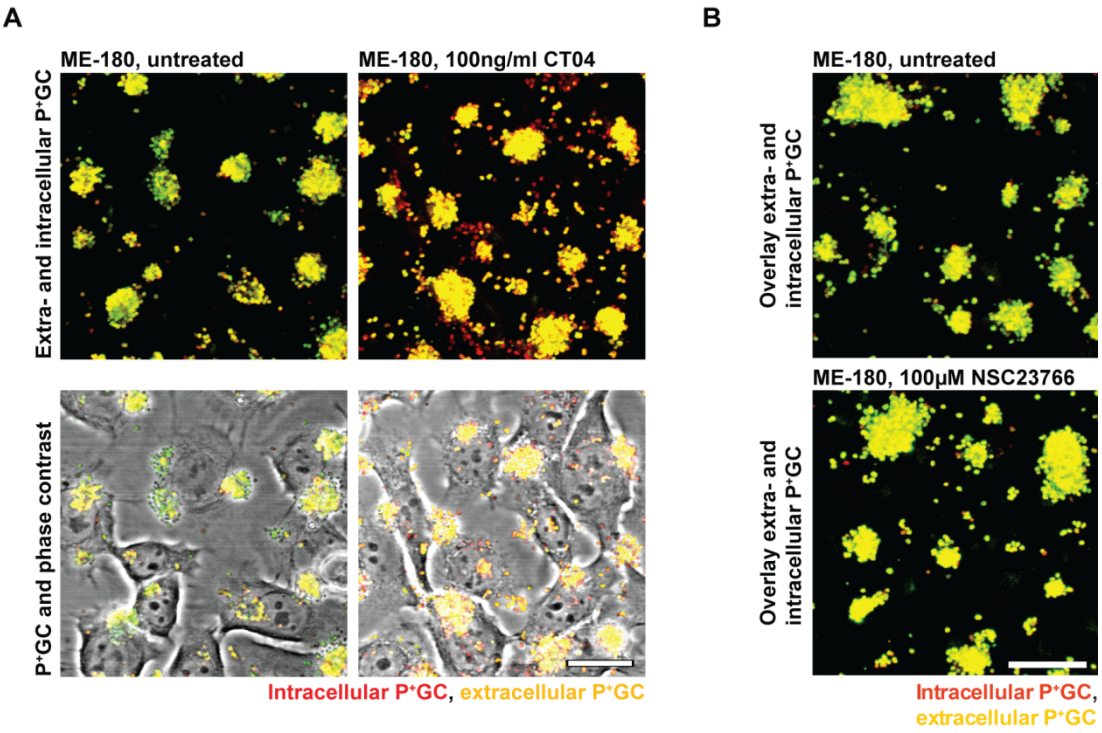

Figure 3-19. RhoA but not Rac1 is required for prevention of P$^+$GC uptake (A) Treatment of ME-180 cells with the membrane-permeable Rho inhibitor CT04 results in P$^+$GC internalization. Intracellular bacteria (red) are detected in CT04-treated ME-180 cells (right panels), whereas only extracellular bacteria (yellow-green) are detected in control-treated ME-180 cells (left panels). Scale bar: 20 µm. (B) Treatment of ME-180 cells with the Rac1 inhibitor NSC23766 does not result in P$^+$GC internalization. Only extracellular bacteria (yellow-green) are detected in 100 µM NSC23766-treated ME-180 cells (upper panel) and control-treated ME-180 cells (lower panel). Scale bar: 20 µm.

bacteria (Figure 3-19A). Confocal analysis detected many intracellular bacteria in CT04-treated ME-180 cells (Figure 3-19A, right panels) whereas only extracellular bacteria (yellow-green) could be detected in control-treated ME-180 cells (Figure 3-19A, left panels). The uptake was stronger than previously observed after downregulation of Cav1 or Vav2.

Since Vav2 is also known to activate Rac1 (*226*), the relevance of Rac1 for P$^+$GC internalization was also investigated. ME-180 cells were treated with the Rac1-specific chemical inhibitor NSC23766 (*227*) and subsequently infected with P$^+$GC. In contrast to Rho inhibition, treatment with NSC23766 did not affect bacterial uptake (Figure 3-19B); only extracellular bacteria (yellow-green) could be detected in NSC23766-treated as well as untreated ME-180 cells (Figure 3-19B). These data show that the small GTPase Rac1 does not play a role in the impediment of bacterial uptake and thus suggests a specific role of Rho for the reorganization of the cytoskeleton during infection.

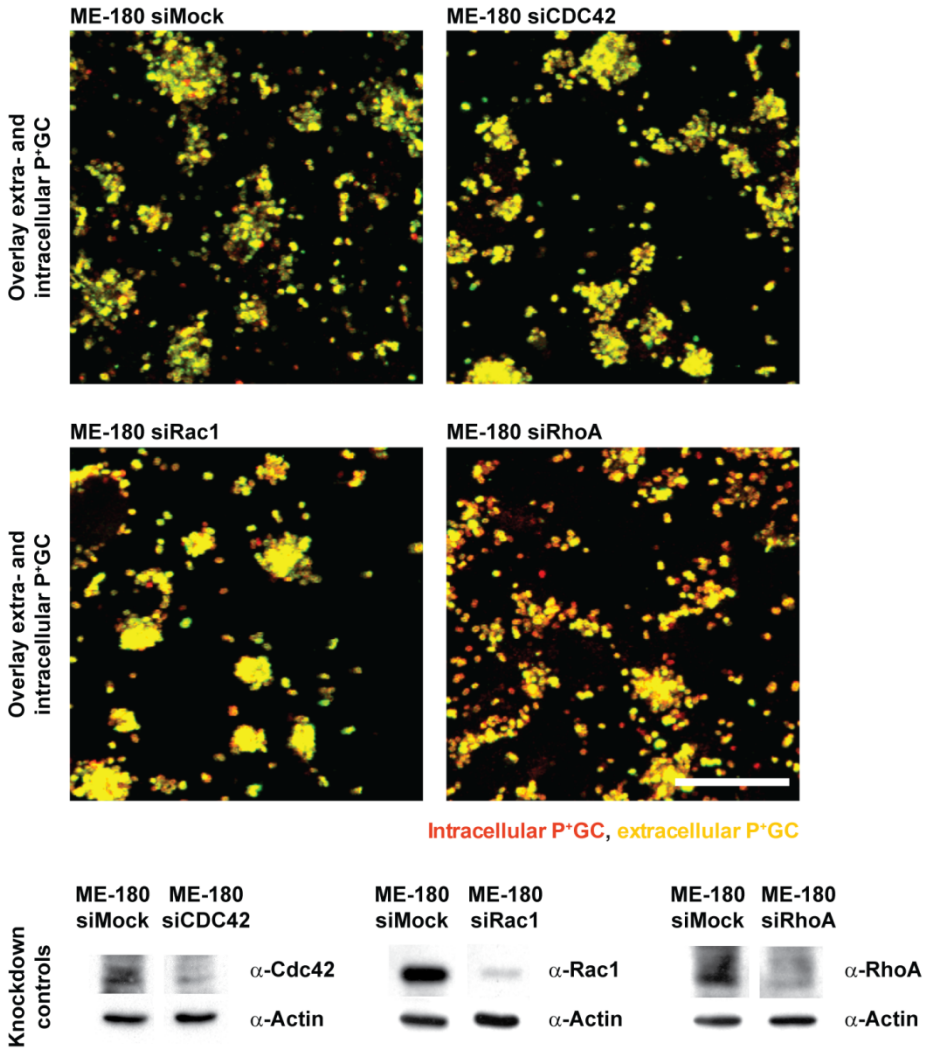

Figure 3-20. Knockdown of RhoA but not Rac1 or CDC42 in ME-180 results in P$^+$GC internalization. Intracellular bacteria (red) are detected in siRhoA-treated cells (upper panel, lower right image), whereas only extracellular bacteria (yellow-green) are detected in siCDC42-treated (upper right image), siRac1-treated (lower left image), and siMock-treated cells (upper left image). Knockdown efficiencies of CDC42, Rac1 and RhoA after siRNA treatment (lower panel). Scale bar: 20 µm.

To confirm this inhibitor-based data and to investigate the role of other small GTPases, RhoA, Rac1 and Cdc42 were downregulated using RNAi. The knockdown of these small GTPases, especially of RhoA and Cdc42, proved to be extremely difficult as siRNA-treated cells died readily, especially after the additional infection with P$^+$GC. However, a partial knockdown of RhoA further demonstrated the relevance of this small GTPase in impeding cellular uptake of P$^+$GC (Figure 3-20). Interestingly, downregulation of other small GTPases such as Cdc42 and Rac1 did not stimulate P$^+$GC internalization (Figure 3-20) and only extracellular bacteria (yellow-green) could be detected after the siRNA-mediated knockdown of Cdc42 in ME-180 cells. Rac1 siRNA-treated cells exhibited only minimal

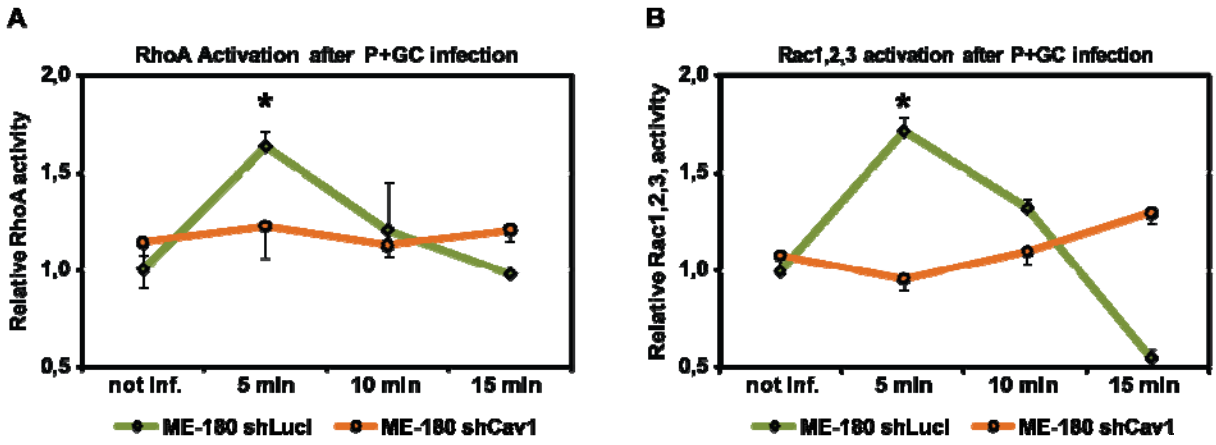

Figure 3-21. RhoA and Rac1 activation after P$^+$GC infection depends on Cav1 expression. Levels of the active, GTP-bound state of RhoA or Rac1 are compared between ME-180 shCav1 knockdown cells and ME-180 shLuciferase control cells during an infection time-course. At 5 min p.i. activity of these small GTPases is elevated in shLuciferase control cells but not in shCav1 knockdown cells. Data are mean ± standard deviation of triplicate wells after normalizing protein levels. All measured small GTPase activity was normalized to the respective small GTPase activity of uninfected ME-180 shLuciferase cells.

amounts of intracellular bacteria (red) in ME-180 cells, whereas the knockdown of RhoA resulted in high amounts of intracellular P$^+$GC.

These findings highlight the importance of the small GTPase RhoA in impeding bacterial uptake, probably by stimulating the formation of a cytoskeletal barrier beneath the bacteria. In total the presented results lead to the hypothesis that the observed phospho-Tyr14-Cav1-Vav2 interaction leads to an activation of RhoA, which consequently leads to cytoskeletal rearrangements and a block of internalization of bacteria into host cells. To test this hypothesis, the impact of Cav1 expression on RhoA activation after P$^+$GC infection was analyzed. RhoA and Rac1 activation was monitored in response to P$^+$GC infection of ME-180 shCav1 knockdown and shLuciferase control cells. The RhoA and Rac1 G-LISA™ activation assays (Cytoskeleton) were used to determine RhoA and Rac1 activity, respectively. Cav1 knockdown and control ME-180 cells were gradually serum-starved for 3 days and subsequently infected with P$^+$GC, lysed and immediately shock-frozen to preserve the activated, GTP-bound form of RhoA and Rac1. This was required as both small GTPases are quickly reverted to their inactive, GDP-bound form through GTP-hydrolysis. Equal amounts of protein of all analyzed time points were incubated in triplicates in RhoA- or Rac1-GTP affinity plates, which exclusively bind the activated form of the respective small GTPase. Finally, an ELISA-based readout allowed the detection of plate-bound RhoA- and Rac1-GTP. The infection was monitored for only 15 min.

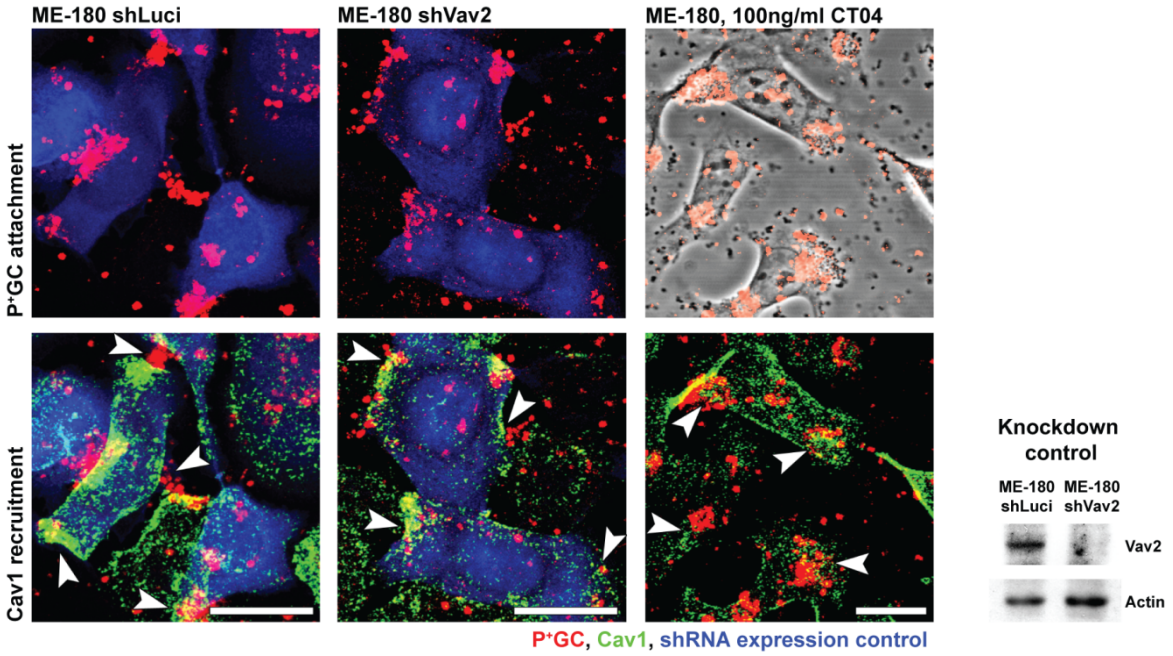

Figure 3-22. Cav1 recruitment does not depend on Vav2 expression or RhoA activation. Cav1 (green) recruitment to attached P$^+$GC (red) is observed in ME-180 shLuciferase control cells (blue, left panels), ME-180 shVav2 knockdown cells (blue, middle panels) and Rho inhibitor CT04-treated ME-180 cells (right panels). Recruited Cav1 is indicated by arrows. Efficiency of Vav2 knockdown in ME-180 cells after lentiviral transduction of luciferase (control) or Vav2 shRNA constructs (side panel). Scale bars: 20 µm.

ShLuciferase control cells showed a strong increase in the levels of the GTP-bound state of RhoA as well as Rac1 within the first five minutes of P$^+$GC infection, followed by a decline to basal levels over the next ten minutes. In contrast, RhoA was not activated throughout the early stages of infection in Cav1 knockdown cells ($p<0.05$, Figure 3-21). Also, levels of activated Rac1, but not RhoA, strongly decreased after 15 min of infection. In total these experiments show the impact of Cav1 expression on the activation of small GTPases after P$^+$GC infection and highlight the relevance of RhoA which plays an important role in the impediment of P$^+$GC internalization into host cells.

Taken together, these data suggest that Cav1, Vav2 and RhoA act in a signaling cascade, which inhibits the internalization of P$^+$GC by host cells. Finally, to delineate the sequence of the Cav1-Vav2-RhoA signaling cascade, both ME-180 shVav2 knockdown and Rho inhibitor CT04-treated ME-180 cells were infected with P$^+$GC and the recruitment of Cav1 was monitored by confocal microscopy (Figure 3-22). Cav1 was recruited to the infection sites in shLuciferase control cells (Figure 3-22, left panels), shVav2 knockdown cells (Figure 3-22, middle panels) as well as CT04-treated ME-180 cells (Figure 3-22, right panels), which indicates that Cav1 recruitment was not affected by either treatment. Thus Cav1

recruitment occurs upstream of Vav2 binding and RhoA activation in the proposed Cav1-Vav2-RhoA signaling cascade.

This data strongly suggests that $P^{+}GC$ infection induces a Cav1-Vav2-RhoA signaling cascade in the host cells. In response to the infection, Cav1 is recruited in a Tyr14 phosphorylation-dependent manner to the sites of the bacterial attachment, which induces the recruitment of Vav2 through direct interaction and the activation of RhoA. Bacterial internalization could subsequently be prevented via RhoA-dependent cytoskeletal rearrangements.

3.5 Phosphatidylinositol-4,5-bisphosphate and actin-binding protein filamin are recruited to P$^+$GC infection sites

Previously, it was shown that Cav1 binding to the actin cytoskeleton is mediated by the F-actin cross-linking protein filamin and depends on the N-terminal part of Cav1 (*183*). A single filamin molecule per actin filament is sufficient to induce gelation of an actin network, which increases its elasticity (*228, 229*). Therefore recruited Tyr14 phosphorylated Cav1 could interact with filamin and actin below the infection sites to reorganize the action cytoskeleton, triggering a gelation of the network to prevent bacterial uptake.

To better understand the interplay between Cav1, the actin cytoskeleton and the actin-binding protein filamin, it was analyzed if filamin is, similar to Cav1, recruited to P$^+$GC infection sites. Analogous to Cav1 and consistent with prior findings (*208*), infection of ME-

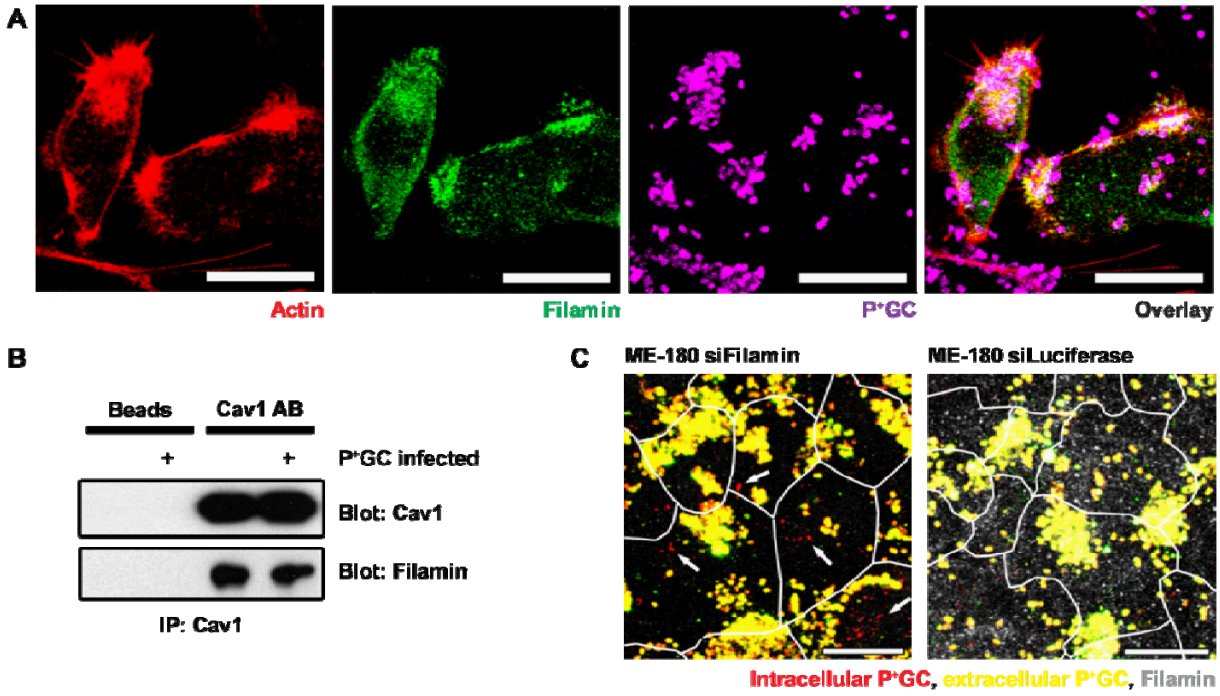

Figure 3-23. Actin-binding protein filamin is recruited to attached P$^+$GC and down-regulation of filamin in ME-180 cells results in P$^+$GC internalization (A) Recruitment of endogenous actin (red) and filamin (green) to attached P$^+$GC (purple) in ME-180 cells 2 h post infection. (B) Co-immunoprecipitation demonstrates protein-protein interaction of Cav1 and filamin. Western blot analysis of immunoprecipitates of ME-180 cells using full-length Cav1 protein as bait. Precipitates were probed for Cav1 and filamin. Filamin could be co-precipitated independently of P$^+$GC-infection. (C) Knockdown of filamin levels in ME-180 cells using siRNA results in P$^+$GC internalization. Intracellular bacteria (red) are detected in siFilamin-treated ME-180 cells (left panel), whereas only extracellular bacteria (yellow-green) are detected in siLuciferase-treated control cells (right panels). Efficiency of filamin knockdown is controlled by immunofluorescent detection of filamin (grey) in siLuciferase-treated control cells only. Cellular borders are represented as white outlines. Scale bar: 20 µm.

180 cells with P^+GC induced the accumulation of filamin at the sites of bacterial attachment where it co-localized with actin (Figure 3-23A).

To determine if P^+GC infection impacts on the previously described Cav1-filamin interaction (*183*), endogenous Cav1 protein was immunoprecipitated from either infected or uninfected ME-180 cells. Immunoprecipitates were probed for Cav1 and filamin in Western blot analysis, which showed that Filamin could be co-precipitated independently of P^+GC-infection, demonstrating that this protein-protein interaction is not inhibited by P^+GC infection (Figure 3-23A). Thus, filamin, recruited to P^+GC attachment sites, where it is likely to interact with the recruited Cav1 and also with F-actin.

To investigate the impact of filamin on bacterial internalization, P^+GC uptake was analyzed using confocal imaging after filamin knockdown. Few intracellular bacteria (red, arrows) could be detected in siFilamin-treated ME-180 cells (Figure 3-23C, left panel), whereas only extracellular bacteria (yellow-green) were detected in siLuciferase-treated control cells (Figure 3-23C, right panels). The filamin knockdown was confirmed by immunofluorescent detection of filamin (grey) and the protein could only be detected in siLuciferase-treated control cells. Thus, reduced filamin expression resulted in a breakdown of the bacterial entry barrier, similarly as observed after Cav1 and Vav2 downregulation as well as after RhoA blockage. A possible explanation for this impediment of bacterial uptake is that Cav1 and filamin are recruited to the bacterial attachment sites and enhanced cross-linking and gelation of the actin network. Thus, Cav1 and filamin are structural components of a physical barrier that prevents internalization of P^+GC. However, as demonstrated before, Cav1 in addition binds to Vav2 and activates RhoA via its phosphorylated Tyr14 residue, thereby also stimulating cytoskeletal rearrangements.

The p85 subunit of the PI3K is able to bind to phospho-Tyr14-Cav1, as demonstrated earlier in this study (Figure 3-13 and Figure 3-14B). Based on this finding it was hypothesized that during P^+GC infection pools of phosphatidylinositol-4,5-bisphosphate (PIP2) accumulate at bacterial attachment sites, which consequently are diminished due to conversion of PIP2 to phosphatidylinositol-3,4,5-trisphosphate (PIP3). Therefore the accumulation of PIP2, a main substrate of PI3K was analyzed. To monitor PIP2, the PIP2-sensing Phospholipase C delta pleckstrin homology domain coupled to GFP (PLCδ-PH-eGFP, green)

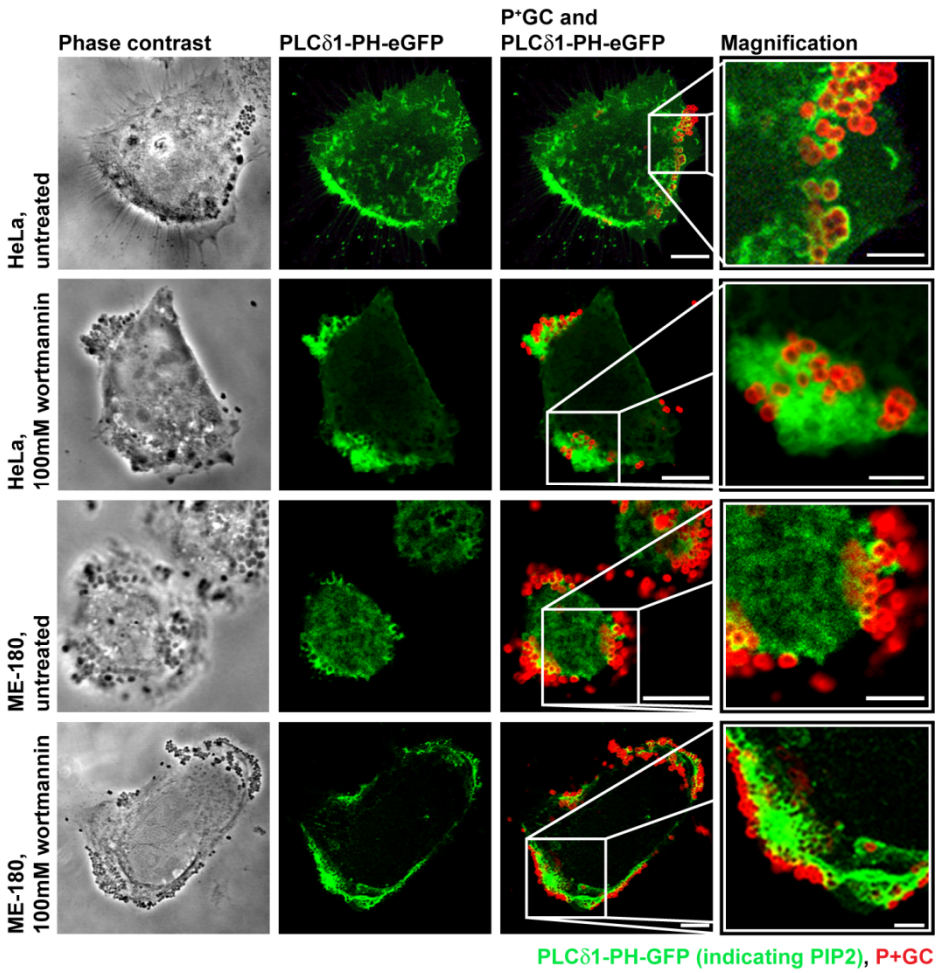

Figure 3-24. Phosphatidylinositol 4,5-bisphosphate (PIP2), a substrate for PI3K, is recruited to attached P$^+$GC. PIP2-sensing GFP-coupled Phospholipase C delta pleckstrin homology domain (PLCδ-PH-eGFP, green) was expressed in ME-180 and HeLa cells. Infection with P$^+$GC (red) for 2 h resulted in recruitment of PLCδ-PH-eGFP to the attached bacteria. Pretreatment of host cells with the PI3K-inhibitor wortmannin lead to increased PLCδ-PH-eGFP recruitment. Scale bars: 10 µm.

was expressed in ME-180 and HeLa cells, which were subsequently infected with P$^+$GC. To be able to determine the impact of PI3K activity on accumulated PIP2 pools, the cells were treated in addition with the specific PI3K inhibitor wortmannin. Confocal analysis revealed that PLCδ-PH-eGFP, representing PIP2, was accumulated at P$^+$GC infection sites in untreated ME-180 and HeLa cells 2 h post infection (Figure 3-24). PLCδ-PH-eGFP (green) co-localized with individual diplococci, appearing to closely envelop them. However, wortmannin treatment increased the accumulation of PLCδ-PH-eGFP drastically in both cell lines (Figure 3-24), resulting in large pools of recruited PLCδ-PH-eGFP underneath attached bacteria.

These data indicate that PIP2 is recruited to P$^+$GC infection sites where it is metabolized by PI3K to PIP3 as this process can be abrogated by inhibition with

wortmannin. The impact of Cav1 expression on this reaction has not been investigated here; however, as Cav1 directly binds to p85 of PI3K one could speculate it impacts on this reaction either by closely localizing the PI3K to PIP2 underneath $P^{+}GC$ and/or by exerting a negative or positive control by binding the regulatory subunit.

3.6 Tfp-producing EPEC induce Cav1 accumulation and prevent host cell entry.

To broaden the presented findings to other infection models, Cav1 recruitment in enteropathogenic *E. coli* (EPEC) infection of epithelial cells was investigated. EPEC, just like P^+GC, use Tfp, the type IV bundle-forming pili (BFP), for initial host cell adherence (*230*). To learn if EPEC infection triggers similar host cell responses as P^+GC infection, Cav1 recruitment to the attachment sites as well as bacterial uptake was analyzed. To avoid super-imposition with the actin-recruiting function of by the EPEC type III secretion system (TTSS; (*231*)) injected effectors, a TTSS deficient mutant that still expressed Bfp was

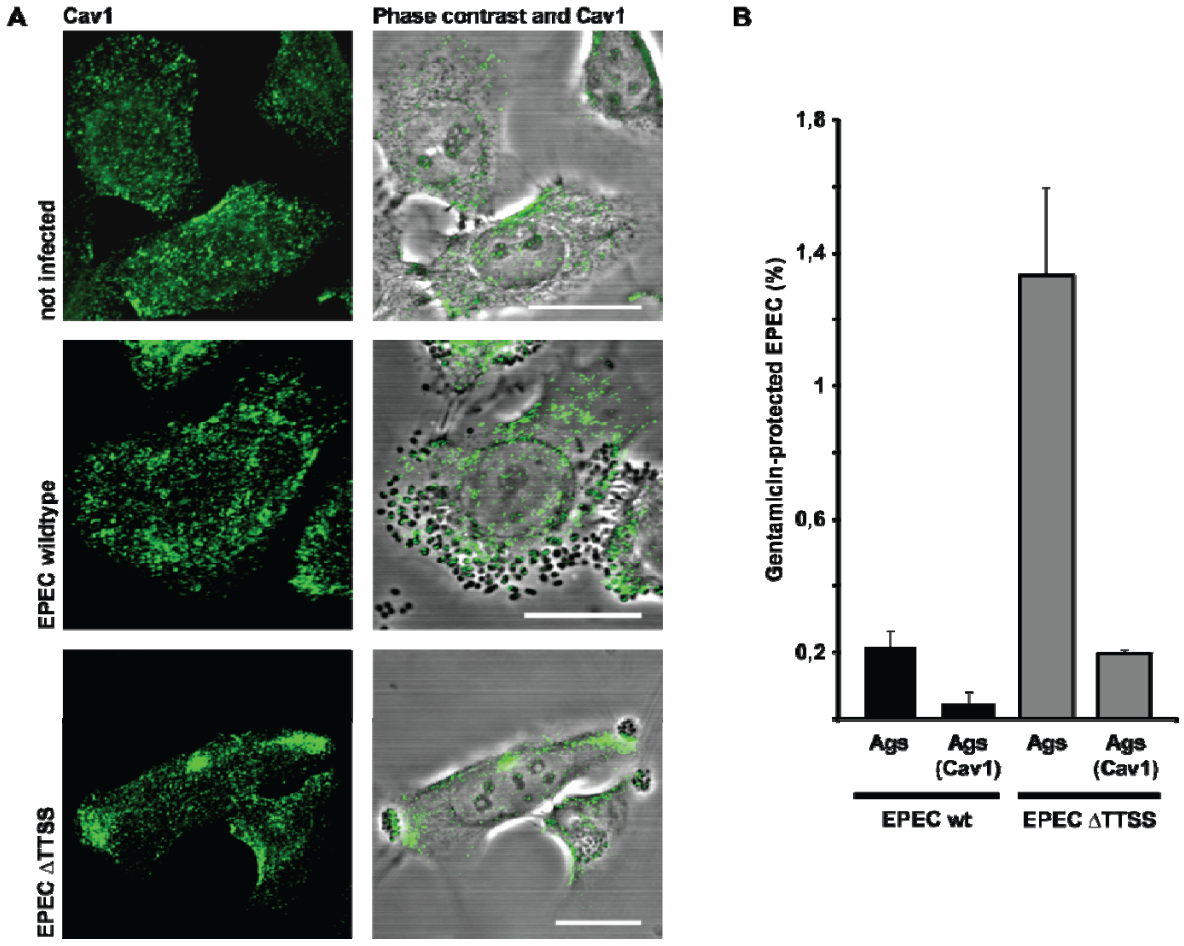

Figure 3-25. Tfp-producing EPEC induce Cav1 accumulation and prevent host cell entry. (A) ME-180 cells were infected with preactivated cultures of wild type EPEC strain E2348/69 and EPEC 2348/69 CVD452, a TTSS defective mutant (EPEC ΔTTSS), for 2 h. Endogenous Cav1 (green) is recruited to attachment sites of the MC-forming mutant whereas the TTSS-preactivated wild type adheres as individual bacteria and does not trigger as strong Cav1 recruitment. Scale bar: 20 µm (B) Expression of Cav1 in AGS cells inhibits EPEC ΔTTSS internalization. AGS cells and AGS (Cav1) cells were infected with EPEC wild type and EPEC ΔTTSS for 2 h. Intracellular Gentamicin protected bacteria were determined as a percentage of total cell associated bacteria. Error bars indicate mean ± standard error.

compared with wild type bacteria. Therefore, ME-180 cells were infected with preactivated cultures of either wild type EPEC strain E2348/69 or EPEC 2348/69 CVD452, a TTSS defective mutant (EPEC ΔTTSS), for 2 h. The mutant served as a model system to simulate an early state of the EPEC infection in which the TTSS is not yet expressed, thus preventing the TTSS-mediated intimate adherence and pedestal formation (*129, 230*). Interestingly, endogenous Cav1 (green) is recruited to attachment sites of the MC-forming EPEC ΔTTSS mutant. In contrast, the TTSS-preactivated wild type bacteria adhered as individual bacteria and did neither form MCs nor trigger a strong Cav1 recruitment. Taken together, these experiments show that, similar as observed during P^+GC infection, Bfp-mediated EPEC infection of epithelial cells is capable of inducing Cav1 accumulation beneath the bacteria, which can be overridden by expression of the TTSS (Figure 3-25A).

The impact of Cav1 expression on EPEC uptake into host cells was analyzed by gentamicin-protection assay. Host cells were infected with P^+GC and treated with gentamicin for 2 h to kill extracellular bacteria. Consequently intracellularly surviving bacteria were recovered and quantified by dilution plating. Bfp-producing EPEC entered Cav1-deficient AGS cells more rapidly compared to Cav1-expressing AGS cells (Figure 3-25B). This effect was also observed in the presence of the EPEC TTSS, thus emphasizing a generalized role of Cav1 in blocking cell entry of Bfp-producing bacteria. However, bacterial uptake into Cav1-negative cells was stronger in the absence of the TTSS. This data suggests that Cav1 accumulation is a general Tfp-specific and immediate cellular response to bacterial attachment that occurs throughout the early stages of infection.

3.7 P$^+$GC require participation of host cells to establish extracellular microcolonies during infection

The formation of extracellular MCs by *Neisseria* is a prerequisite of successful host infection and requires Tfp-expression and PilT-mediated pilus retraction (*49, 115-117*). Here it is hypothesized that host cells can impact on bacterial MC formation, possibly by modulation of bacterial behavior or cytoskeleton rearrangements.

To test this hypothesis, live-cell microscopy was utilized to study the dynamics of P$^+$GC motility on human epithelial cells. To compare the impact of possible host cell reactions on MC formation the bacterial behavior on living and fixed cells was investigated. ME-180 cells were first fixed using paraformaldehyde (PFA), which was subsequently rigorously removed. The fixed and living ME-180 cells were infected with P$^+$GC and the

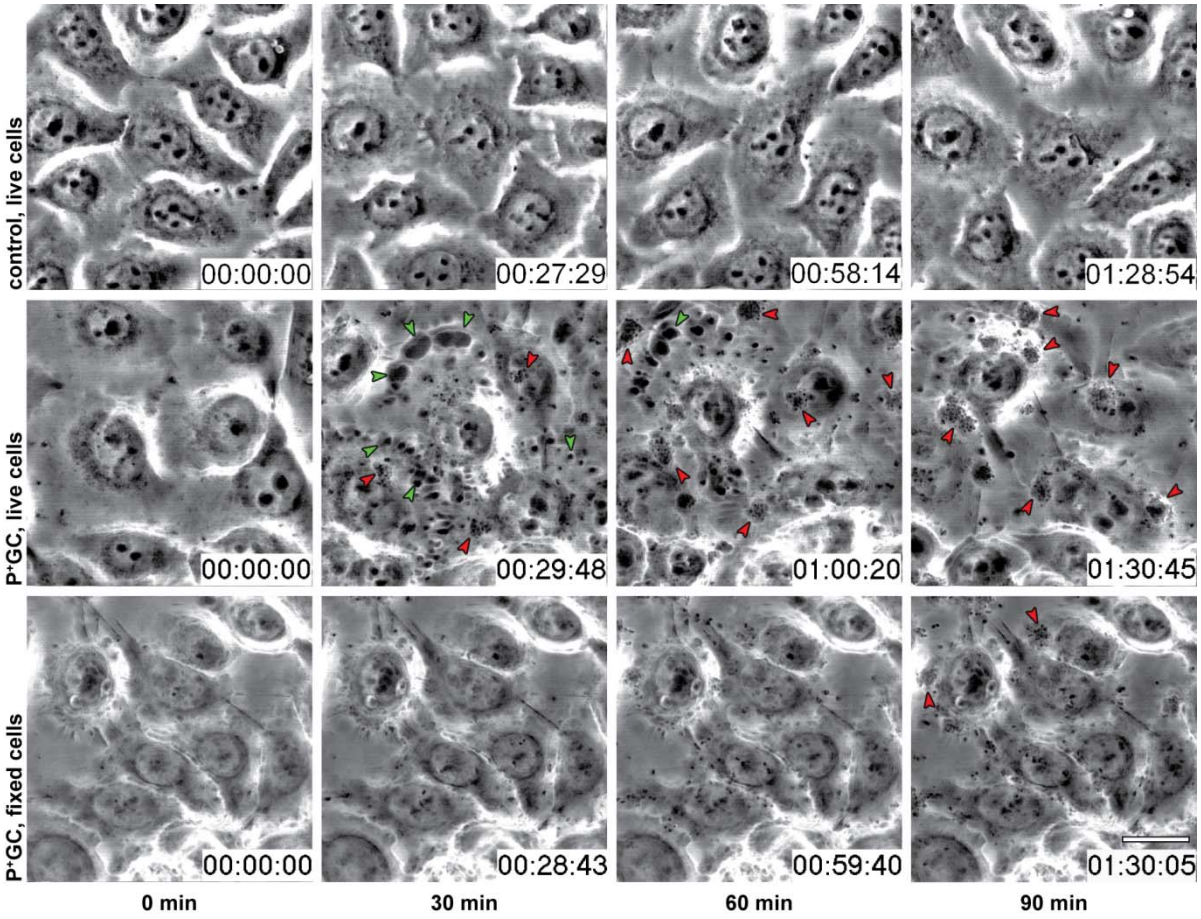

Figure 3-26. Excerpts from Movie 2: Infection of fixed cells results in reduced capacity of P$^+$GC to form MCs on host cells. During the monitored infection host cell ruffling (green arrows) starts at 8 min p.i. and peaks at 25 to 30 min p.i. P$^+$GC start to form MCs 30 min p.i. in living cells. 60 min p.i. MCs are observed extensively on living cells (red arrows) but not on fixed cells. 90 min p.i. MC-like bacterial aggregates are also observed on fixed cells. Scale bar: 20 µm

infection was monitored using live cell microscopy for 120 min (Figure 3-26 and Movie 2). As an additional control, uninfected cells were also recorded for 120 min. Images for the movies were acquired every 5 seconds. Infection led to massive formation of membrane ruffles on living host cells (Figure 3-26, green arrows and Movie 2, boxes), which could not be observed in uninfected cells. Ruffling started around 5-10 min and peaked at 25-30 min post infection. On living host cells, P^{+}GC started to form MCs around 30 min post infection and after 60 min of infection MCs were observed extensively (Figure 3-26, red arrows and Movie 2, white arrows). In contrast, on fixed cells MC-like bacterial aggregates could only be detected around 60 min post infection. After 90 min of infection numbers of bacterial aggregates on fixed cells were comparable to numbers of MCs observed on living cells at 60 min post infection, indicating a delay in MC formation on fixed cells. Furthermore, at later time points of infection, two or more MCs fused to larger colonies on living cells (Movie 2, black arrows). This process was not observed on fixed cells during the full 120 min of infection. Additionally, P^{+}GC appeared to move quicker and impetuously on fixed cells which could indicate an increased bacterial mobility.

Taken together, the observed P^{+}GC behavior differed drastically during infection of living and fixed host cells. This could be the result of either missing host cell feedback to the bacteria or of absence of by the bacteria exploited extracellular physical attributes of living cells, e.g. the observed membrane ruffles.

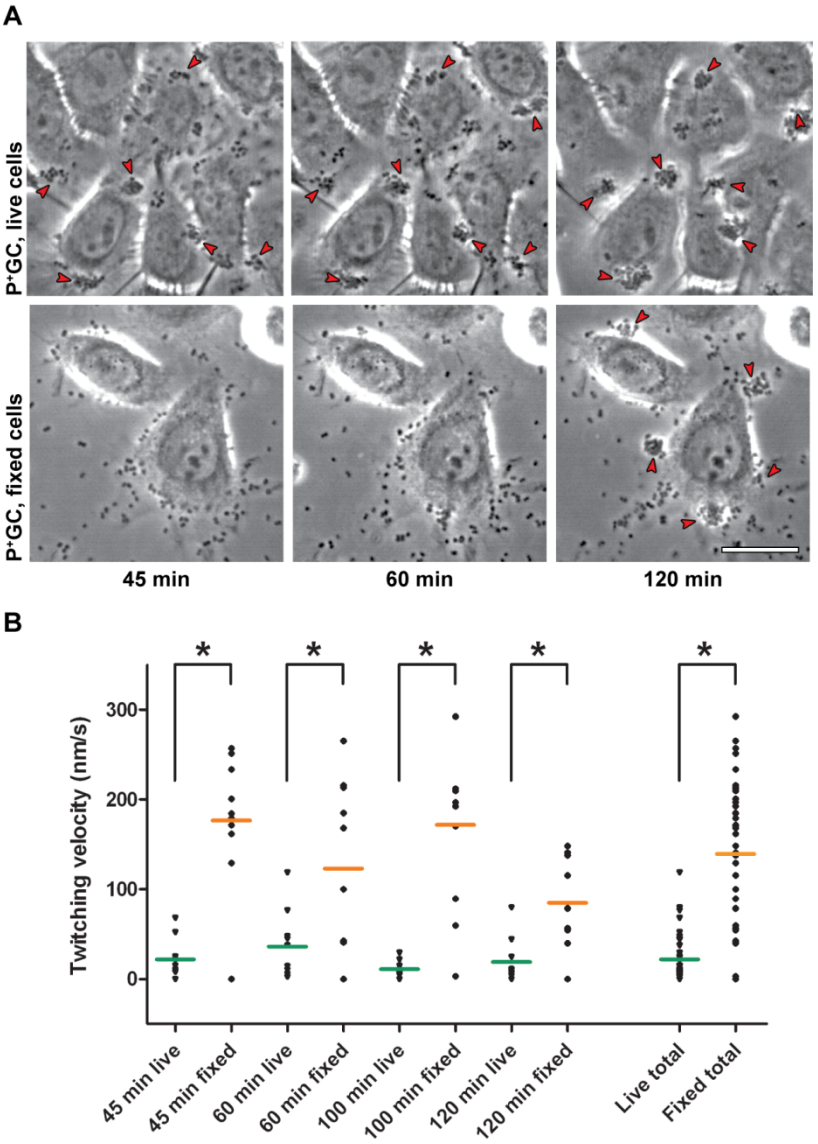

Figure 3-27. Excerpts from Movie 3: Infection of fixed cells results in reduced capacity of P$^+$GC to form MCs on host cells and in increased motility speeds of P$^+$GC over time. (A) P$^+$GC start to form MCs 30 min p.i. in living cells. 45 min and 60 min p.i. MCs are observed extensively on living cells (red arrows) but not on fixed cells. 120 min p.i. some MCs were fused to larger MCs on living host cells whereas MC-like bacterial aggregates can also be observed on fixed cells. Scale bar: 20 µm (B) Motility speeds of attached P$^+$GC vary during infection of fixed and live host cells. Live cell stream temporal resolution of 100 ms allows the determination of average P$^+$GC twitching motility speed within MCs on host cells over a time span of 10 s. P$^+$GC infecting fixed cells show a significantly faster twitching motility at all observed time points. In Movie 3 this is reflected in a flickering and impetuous movement of P$^+$GC on fixed cells compared to movement on living cells.

As movie 2 suggested that P$^+$GC exhibit a higher twitching motility on fixed cells, bacterial speeds were analyzed in more detail. Live-cell microscopy was applied again; however, pictures were taken now every 100 ms, yielding a temporal resolution which allowed determination of the average P$^+$GC twitching motility speed. To calculate the average motility speed, 10 individual diplococci infecting fixed or living cells and residing

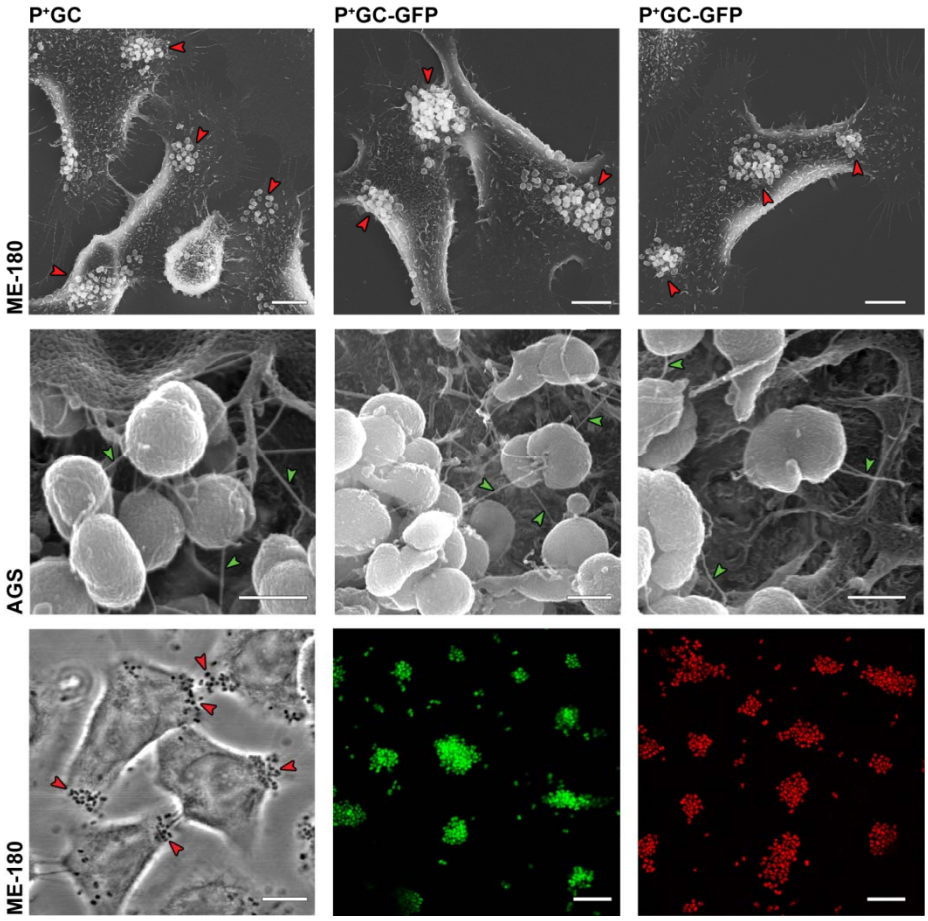

Figure 3-28. Generated P$^+$GC-GFP and P$^+$GC-RFP express pili and form MCs like wild type P$^+$GC. Transmission electron microscope analysis (TEM) reveals capacity of generated fluorescent P$^+$GC to express pili (middle panel, green arrowheads, Scale bars: 500 nm) and form MCs (upper panel, red arrowheads, Scale bars: 5 µm) equally to the wild type while emitting strong fluorescence signals as detected by confocal analysis (lower panel, Scale bars: 10 µm).

within or close to MCs were followed over 10 sec at different infection time points (45, 60, 100 and 120 min post infection). Together, n=40 bacteria were tracked for each cellular condition (Movie 3, white arrows). As observed before, MCs are formed extensively on living cells at 45 min and 60 min post infection whereas no MCs were detected on fixed cells at these time points (Figure 3-27A, red arrows and Movie 3). At 120 min post infection many MCs were fused to larger MCs on living host cells whereas MC-like bacterial aggregates were now also observed on fixed cells. As indicated before, twitching motility speed varied during infection of fixed and living host cells. Tracking of individual diplococci residing in or close to MCs (Movie 3, white arrows) revealed an average speed of 22.02 ± 4.2 nms^{-1} for P$^+$GC infecting living host cells. However, during infection of fixed cells, the bacteria moved at 139.2 ± 13.78 nms^{-1}. Thus, within MCs, over the time span of 10 sec bacteria moved about

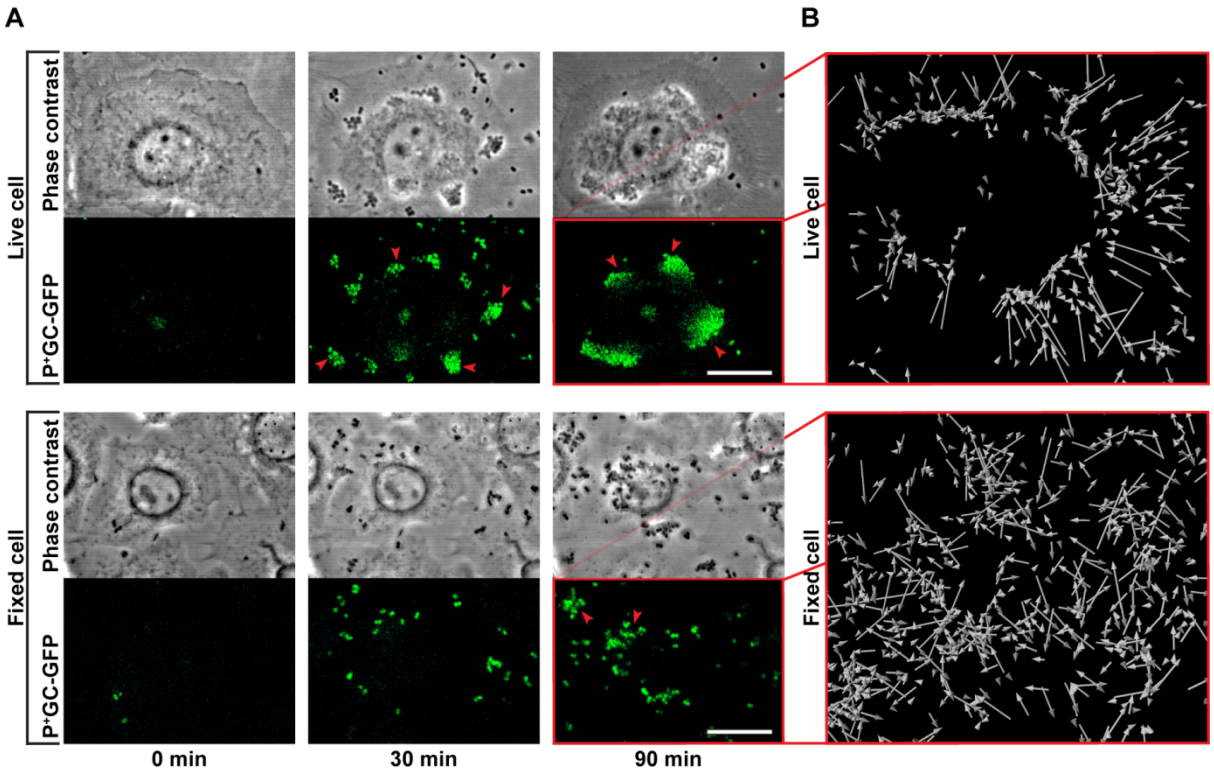

Figure 3-29. Excerpt from Movie 4. Tracking of P$^+$GC-GFP reveals the dependence of P$^+$GC on host cells to localize into MCs. P$^+$GC-GFP were monitored by live-cell imaging during infection of living and fixed host cells. (A) On living cells P$^+$GC-GFP attach and are moved by host cells into MCs (red arrows) whereas on fixed cells P$^+$GC-GFP attach, release and reattach. Scale bars: 20 µm (B) Fluorescent bacteria have been tracked throughout the infection course of 90 min. The resulting tracks have been analyzed for comprehensive directional movements of the bacteria, yielding corresponding vectors for the full infection course. On living cells most vectors point to MC formation points, indicating a straight move of the bacteria towards MCs. On fixed cells vectors point to random directions indicating erratic movement.

6 times faster during infection of fixed cells compared to the infection of living cells. Watching the movie it becomes apparent that this calculated difference in motility speed is not caused by an altered bacterial ability to twitch but the likeliness and frequency of the bacteria to release the host cell, relocate and adhere again. Together, this data demonstrates that infection of fixed cells resulted in reduced capacity of P$^+$GC to form MCs in time on host cells and in increased average motility speeds of P$^+$GC within MC-like aggregates on host cells. As MC formation is temporally delayed on fixed cells the dynamic of this process was analyzed in detail. To understand MC formation on the level of individual bacteria fluorescent gonococci were constructed. This was required as fluorescent signals permit automated tracking of bacteria on host cells. The stable expression of fluorescent proteins, mediated by a Hermes shuttle vector system, was successful in previously generated P$^+$GC strains N1081 (GFP) and N1082 (RFP) (*208*). To create fluorescent but still

piliated strains, the corresponding plasmids carrying the GFP/RFP Hermes shuttle vectors were transferred into P$^+$GC (strain N280) by conjugation. Resulting strains P$^+$GC-GFP (N1174) and P$^+$GC-RFP (N1175) were consequently checked for their capability to express pili, bind to host cells, form MCs and emit strong fluorescent signals. TEM revealed the capacity of generated fluorescent P$^+$GC to express pili (Figure 3-28, middle panel) and to form MCs similar to wild type P$^+$GC (Figure 3-28, upper panel). Confocal analysis further demonstrated that the newly generated strains were capable of emitting strong fluorescent signals (Figure 3-28, lower panel). Thus, P$^+$GC-GFP and P$^+$GC-RFP could now be used to further investigate dynamics of MC formation.

To better understand the dynamics of MC formation, ME-180 cells were infected with P$^+$GC-GFP and the infection was monitored by confocal live cell imaging for 90 min (Movie 4, Figure 3-29A). Similar to the wild type, P$^+$GC-GFP attached to host cells and then formed MCs on living cells (Figure 3-29A, red arrows) whereas on fixed cells P$^+$GC-GFP constantly attached to host cells, released them and reattached. This differential behaviour resulted in diminished numbers of MCs on fixed cells after 90 min of infection. Additionally, signals of individual fluorescent bacteria were tracked using Imaris imaging software (Bitplane) and resulting tracks were displayed as vectors (Movie 4, Figure 3-29B). Each vector represents the direction from the starting point to the end point of a recorded track which describes the way bacteria went after their initial contact with the host cell. Therefore the displayed vectors reveal comprehensive directional movements of the bacteria on host cells.

On living host cells the majority of calculated vectors pointed to defined positions on the host cells. Majority of vectors had the same vector direction, indicating a bacterial movement straight from the cell borders to positions closer to the centre of the cell. Finally, vectors congregate and overlap. At these points, MCs were formed as demonstrated by consequently shorter vectors and loss of identical vector direction. In contrast, on fixed cells no common direction of vectors could be observed. Vectors point in random directions, indicating erratic movements of the bacteria, and no congregating positions could be determined.

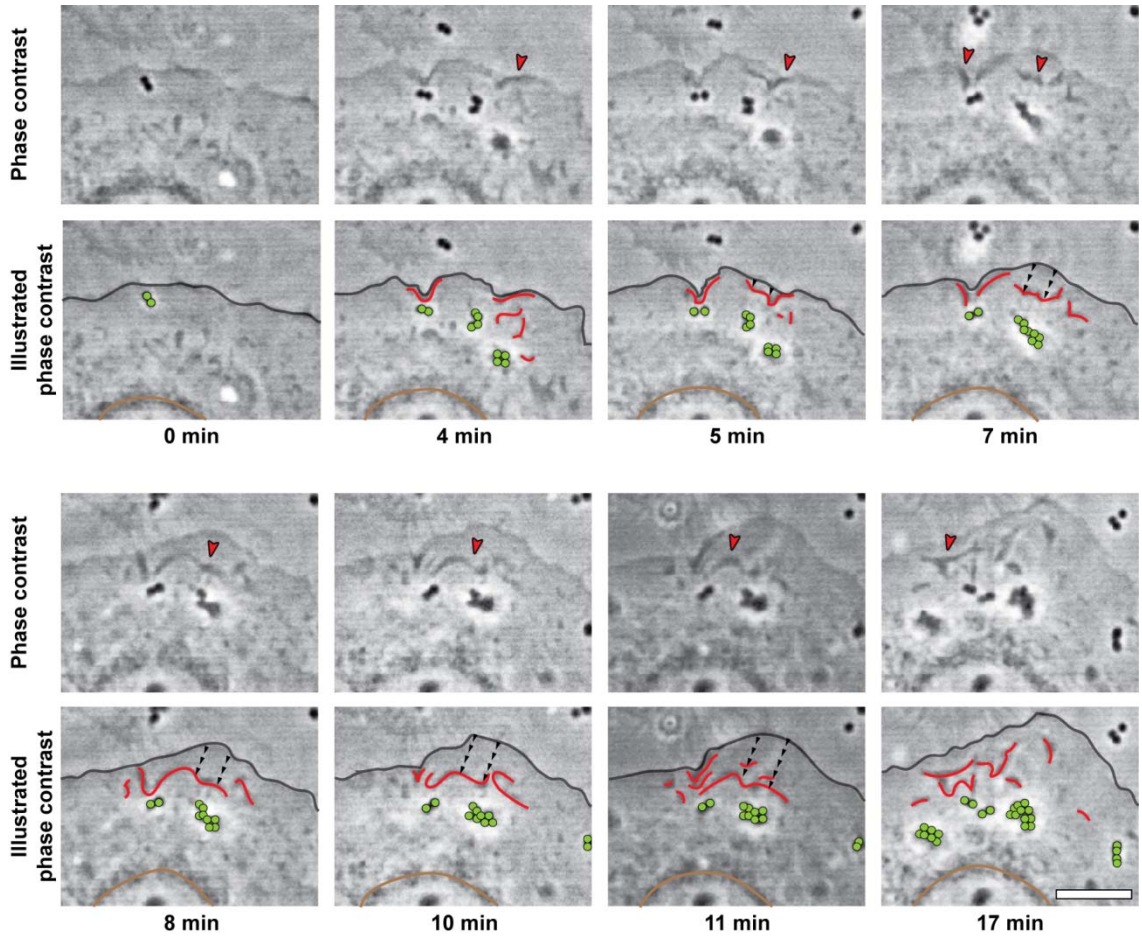

Figure 3-30. Excerpt from Movie 5. Live-cell microscopy demonstrates formation of membrane ruffles on host cells during P$^+$GC infection which move the bacteria towards the cell center. P$^+$GC infection of ME-180 cells was monitored by live-cell imaging. Membrane ruffles are detected by phase contrast microscopy (phase contrast panels, red arrows) after adherence of P$^+$GC. For better visualization, image details have been illustrated (illustrated panels). Membrane ruffles originate from the plasma membrane border and subsequently move towards the cell center within minutes (illustrated panels, black arrowheads). Membrane ruffling distances P$^+$GC from attachment sites and moves the bacteria towards the cell center. Color codes for the illustrated panels: black lines - host cell membranes; red lines - membrane ruffles; green dots – attached P$^+$GC; brown lines - nuclear envelopes; black arrowheads - distance of membrane ruffles from cell borders. Time points (in min) begin with the initial observation of attached P$^+$GC. Scale bar: 10 µm

These data demonstrate that fixed cells, in contrast to living cells, cannot contribute actively to MC formation, explaining the observed delayed formation of MCs on fixed cells. The reported directed movement of P$^+$GC along vectors on living cells could be caused by physical characteristics of living cells, which are elicited by P$^+$GC infection. The observed strong formation of membrane ruffles could enable the bacteria to group together and form MCs. In Movie 5 strong membrane movements can be observed as wave-like membrane ruffles pushing P$^+$GC from the cell poles to the cell centre (Movie 5 and Figure 3-30, red arrows). This indicates an active host cell dependent process pushing attached P$^+$GC. Thus,

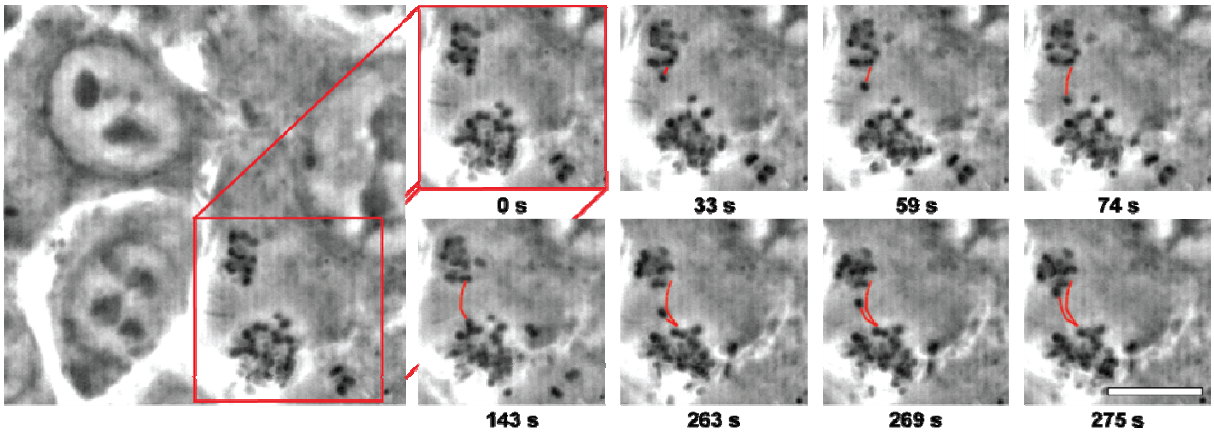

Figure 3-31. Excerpts from Movie 6: P$^+$GC are exchanged between close MCs. Individual bacteria can be observed to move back and forward between approaching MCs (red track). Time points (in s) begin with the initial observation of the alternating bacterium. Scale bar: 10 µm

attached P$^+$GC would be able to "membrane-surf" their host cells to reach preferred and suitable infection spots and form MCs.

The importance of bacterial Tfp- and PilT-expression for MC formation has been reported previously (*49*) and here it could be shown that MC formation requires also host-cell participation. Thus MC-formation is a two- or multi-component process. As it has been suggested before that P$^+$GC interbacterial communication takes place during MC fusion (*49*), this question was addressed next. To observe possible interbacterial communication fusing MCs were followed closely by live-cell imaging (Figure 3-31 and Movie 6). One can observe that while MCs were moved by host cells towards each other, there was also a massive exchange of bacteria between MCs (Movie 6). Individual diplococci moved from one MC towards the other, interacted there with other bacteria and finally twitched back to the first MC within 4:30 min (Figure 3-31). However, bacterial exchange took place only after the two MCs came into close proximity. Before this point was reached, bacteria did not leave any MC. Together, this data indicates that few bacteria twitch out of a microcolonial niche only if being close to another MC. As P$^+$GC can move between approaching MCs it is reasonable to hypothesize that this exchange of bacteria serves as means of communication. However, the importance of this bacterial communication during MC fusion remains to be clarified.

Here clear differences could be observed between P$^+$GC infection of living and fixed

cells. MCs were formed faster during infection of living cells compared to infection of fixed cells. Due to constant release of and reattachment to host cells, P^{+}GC move quicker on fixed cells compared to living cells. However, these increased bacterial movement speeds do not enhance MC formation. In contrast, living host cells actively participate in MC formation by directing bacteria along defined vectors. MCs are consequently formed at crossing points of these vectors. At later infection time points, MCs are moved by living host cells to fuse to massive colonies. Furthermore, interbacterial communication takes place during MC fusion, as observed by bacterial exchange between MCs. Together, this data indicates, that MC formation is a complex two or multi component process which depends on bacterial as well as host cell participation.

DISCUSSION

4 Discussion:

4.1 Pathogenic Tfp-expressing bacteria induce Cav1-Vav2-RhoA-mediated cytoskeletal rearrangements to prevent premature host cell uptake

Many bacterial pathogens, such as *Vibrio cholerae* (*34*), *Pseudomonas aeruginosa* (*36*), EPEC (*38*) and pathogenic *Neisseria* use Tfp to adhere to host cells. Much is known about pilus assembly, disassembly and involved pilus proteins (*232*); however, the importance of Tfp-mediated attachment for host cell signaling and cell cortex rearrangements still needs to be studied in detail. In this study, P^+GC are used as the main infection model to investigate host cell signaling and remodeling of the cytoskeleton elicited after Tfp-binding. P^+GC infection is initialized by Tfp-mediated attachment to host cells (*233*), followed by pili retraction in a force-generating depolymerization process (*234*) and MC formation on host epithelial cells (*33*). Cortical actin and various signal transducing proteins containing phosphotyrosine residues are recruited to the bacterial attachment sites (*235*). In addition, multiple signaling proteins that are recruited to P^+GC MCs have also been found to be associated with lipid rafts and caveolae, including CD44 (*236*), ICam-1 (*237*), EGFR (*238*) and Erb2 (*239, 240*), suggesting that caveolae or associated proteins play an essential role during the initial infection stages.

Kirchner et al. hypothesized that caveolae-associated proteins are localized to P^+GC infection sites and therefore monitored the subcellular localization of the major structural protein of plasma membrane caveolae, Cav1, following infection. Endogenous Cav1 was found to colocalize with P^+GC MCs after two hours of infection (*208*). Kirchner et al. also discovered that Cav1 expression and recruitment to the bacterial attachment sites is required to completely prevent the internalization of P^+GC into host cells in the early stages of infection (*208*). Down-regulation of Cav1 in ME-180 cells by siRNA lead to uptake of P^+GC into this cell line and Cav1-negative AGS cells showed an intrinsically high uptake rate of P^+GC. Bacterial uptake was found to be deleterious for the bacteria; the longer P^+GC remained intracellularly, the fewer bacteria could be recovered from lysed cells, indicating that P^+GC were killed inside the epithelial host cells. Thus, Tfp-mediated epithelial cell entry, stimulated by the absence of Cav1, is unfavorable since the viability of internalized bacteria decreased drastically with time. Stable expression of Cav1-HA in AGS cells efficiently

reduced the number of internalized bacteria, thus rescuing P^+GC from uptake and subsequent killing. Downregulation of Cav1 expression by siRNA in the Cav1-HA AGS cells again increased bacterial uptake restoring the original phenotype of the AGS cells. These results were confirmed here and extended to another experimental system by generating a stable Cav1 knockdown cell line. This shRNA Cav1 knockdown cell line also demonstrated an increased bacterial uptake in comparison to shLuciferase control cells. Furthermore, de Graaf reported that chemical inhibition of the protein kinase A (PKA) not only results in abrogation of Cav1 recruitment but also leads to a dosage-dependent increase of intracellular gonococci (*209*).

Therefore it was hypothesized here that bacterial attachment to the host cells triggers a Cav1-mediated signaling cascade that leads to a dynamic reorganization of the cytoskeleton at the sites of P^+GC infection. The interaction of the Tfp with the host receptors during the initial infection stages most likely not only mediates the attachment, but also triggers a series of signaling events within the host cells that leads to a reorganization of the actin cytoskeleton. The formation of a rigid cytoskeleton below the bacteria prevents the uptake of the pathogen into the host cells, which is essential for a successful infection as a premature uptake of the bacteria is deleterious for the pathogen. Thus, it was speculated here that P^+GC exploit host cell signaling mechanisms that lead to the formation of a rigid actin network below the infection sites to prevent the uptake of the bacteria.

This study extends on the findings by Kirchner et al. and used live-cell imaging to observe the reported accumulation of Cav1 at sites of P^+GC infection. Cav1-GFP was found to be continuously and substantially recruited to P^+GC attachment sites. Strikingly, Cav1-GFP recruitment turned out to be an immediate cellular reaction to P^+GC infection, as Cav1-GFP was recruited to infection sites within seconds. Furthermore, a microarray analysis performed by Kirchner and Churin failed to detect any increase in Cav1 mRNA expression after P^+GC infection (*209*). This finding indicates that Cav1 relocalizes from cytoplasmic pools or plasma membrane-located caveolae to the sites of bacterial attachment after P^+GC infection instead of a *de novo* synthesis of the protein. Other host proteins recruited to the sites of P^+GC infection, including actin, were found previously to comigrate with motile MCs (*49*). Likewise, Cav1-GFP recruited to single diplococci and MCs co-migrated with the extracellularly moving bacteria, indicating that Cav1 is a member of the reported protein

cluster forming underneath the attached bacteria. 3D reconstruction of confocal images and TEM identified recruited Cav1 to be located in the vicinity of the diplococci but not directly at the plasma membrane. To compare Cav1 localization with cytoskeletal proteins known to be recruited to P^+GC infection sites (*121*), F-actin and Cav1 recruitment was monitored simultaneously and actin was found to localize between the bacteria and Cav1. These data suggest that non-caveolar Cav1 is recruited from subcellular pools (probably after being phosphorylated) to P^+GC infection sites whereas plasma membrane-located caveolae are not involved here. Furthermore, recruited Cav1 localizes not only close to the bacteria but also in a defined position within a set of proteins, one of them being F-actin. This defined positioning suggests a function of Cav1 in mediating signaling events during cytoskeletal rearrangements.

Interestingly, Cav1 recruitment was a robust cellular answer to P^+GC infection as neither treatment with the RhoA inhibitor CT04 nor siRNA-mediated knockdown of the RhoA GEF Vav2 could impede Cav1 recruitment. However, treatment with the actin cytoskeleton-disrupting agent CytD prevented Cav1 accumulation below the infection sites. This suggests a Cav1-actin anchorage underneath P^+GC, possibly mediated by the F-actin cross-linking protein filamin, which was also recruited to P^+GC infection sites. Previously filamin was identified to bind to Cav1 (*183*) and this interaction was shown here to function irrespective of P^+GC-infection. Disruption of Cav1-F-actin-filamin anchorage underneath bacterial attachment sites by siRNA-mediated downregulation of filamin resulted in a minor uptake of P^+GC into host cells. Thus, filamin could account for a direct Cav1-actin interaction underneath P^+GC attachment sites and thus anchor Cav1 to the cytoskeleton. Interestingly, Kirchner and de Graaf showed that Cav1 recruitment to bacterial infection sites is abrogated by cholesterol depletion by MβCD (*208*), blockage of tyrosine phosphorylation through pervanadate treatment (*208*) and PKA inhibition by H89 treatment (*209*). How exactly these inhibitors impede Cav1 recruitment remains unclear, yet their activities have been linked previously to factors analyzed in this study. For example, filamin, which is recruited to P^+GC infection sites, is a substrate of PKA and its phosphorylation at serine 2152 increases its capability to cross-link actin filaments and bind to integrins (*241-244*). Furthermore, Cav1 binds cholesterol (*148*) and cholesterol depletion using MβCD results in the loss of the caveolar architecture (*147*). However, Cav1 tyrosine phosphorylation is increased after

MβCD treatment although Tyr14 is not part of the cholesterol-binding domain (*245*). Similarly, treatment with the phosphatase inhibitor pervanadate leads to hyper phosphorylation of Cav1, suggesting a role for tyrosine phosphorylation during P^+GC-induced Cav1 recruitment.

The observed subcellular localization of underneath P^+GC recruited Cav1 suggests a phosphorylation-dependent mobilization of the protein to non-caveolar regions as described before (*173, 246*). Together with the inhibitor-based experiments mentioned above, Cav1 Tyr14 phosphorylation is likely to play a role during P^+GC infection. Cav1 is a substrate for nonreceptor tyrosine kinases, including Src, Fyn, and Abl and is phosphorylated in response to a number of stimuli, including insulin, angiotensin II, osmotic shock, and oxidative stress (*176, 247*). To test for an involvement of Cav1 Tyr14 phosphorylation during P^+GC infection, the localization of phospho-Tyr14-Cav1 as well as its kinase Src was investigated following P^+GC infection. Phospho-Tyr14-Cav1 was recruited to P^+GC attachment sites and active Src kinase was recruited conjointly with Cav1 to infection sites. Furthermore, inhibition of phosphatases resulted in an increased accumulation of phospho-Tyr14-Cav1 at infections sites. These results are in line with previous reports detecting clustering of various tyrosine-phosphorylated proteins at P^+GC attachment sites (*121, 235, 248, 249*). As mobilization of Cav1 was described earlier to require its phosphorylation on Tyr14 (*173, 219*), it was hypothesized here that the Tyr14 residue is also essential for recruitment of Cav1 to the P^+GC infection sites. This hypothesis was confirmed as a ΔCav1-HA construct lacking the first 31 AA of wild type Cav1 and an Y14F-Cav1-GFP mutant demonstrated impaired recruitment to P^+GC attachment sites. Also, Src- and Abl-kinase dependent Cav1 Tyr14 phosphorylation after P^+GC infection was demonstrated in quantitative Western blot analysis. This experiment again highlighted an immediate cellular response to P^+GC infection, as Cav1 Tyr14 phosphorylation was detected already 5 min after infection and progressed throughout the infection. Also, Tyr14 phosphorylation of Cav1 was required to promote its association with the cytoskeleton independently of P^+GC infection, as demonstrated by fractionation experiments with Y14F- and wild type Cav1 expressing AGS cells. The observed Tyr14 phosphorylation, the mobility and subcellular localization of Cav1 recruited to P^+GC infection sites suggest a possible role of Cav1 signaling in cytoskeletal re-organization as reported earlier (*186, 219, 250*). Based on these results, it

was hypothesized here that Tyr14 phosphorylation plays a pivotal role during Cav1-mediated impediment of bacterial internalization thus underscoring the importance of Tyr14-phosphorylation of Cav1 for recruitment of the protein during P^+GC infection. This could be confirmed as, in contrast to wild-type Cav1, expression of the phosphorylation-deficient Cav1 mutant Y14F-Cav1 in Cav1-negative AGS cells did not impede internalization. These results highlight the importance of a functional Tyr14 residue for Cav1 recruitment. Considering the above-discussed inhibitor-based results it becomes apparent that Cav1 recruitment requires a distinct phosphorylation status of Cav1 and is abolished by either hyper-phosphorylation or phosphorylation deficiency. This functional ambivalence suggests of a role of Cav1 phosphorylation in Cav1 mobilization rather than in the local preservation of Cav1. Taken together, these data suggest that Cav1 Tyr14 phosphorylation plays a role in downstream signaling and/or by associating Cav1 with the cytoskeleton during infection.

Kirchner et al. reported that Tfp expression by P^+GC is required to elicit Cav1 recruitment to the infection sites as Tfp-negative Opa-positive bacteria failed to recruit Cav1 to the bacterial attachment sites (*208*). Interestingly, in that study Cav1 recruitment could even be stimulated only by treatment of host cells with beads coupled to purified PilC2 protein, the proposed Tfp adhesin (*11*). Based on these experiments it was hypothesized here that Cav1 recruitment to infection sites is a general cellular response after adherence of Tfp-producing bacteria. Therefore, Cav1 recruitment in host cells infected with a different Tfp expressing pathogen, enteropathogenic *E. coli* (EPEC), was analyzed. The MC-forming EPEC ΔTTSS mutant, in contrast to wild type bacteria, did trigger a strong Cav1 recruitment to the attachment sites. TTSS-expressing EPEC inject effector proteins, such as Tir, Map, EspF, EspG, EspH, EspZ, into the host cell (*128*), which causes actin-pedestal formation, cytoskeletal rearrangements and subsequently confers intimate attachment (*129*). Thus, it is possible that the observed Cav1 recruitment is a Tfp-dependent cellular answer observed in early phases of EPEC infection, which is subsequently overridden by TTSS-mediated translocation of bacterial effector proteins. Similarly, Opa protein expression and Opa-mediated invasion represents a subsequent step in *Neisseria* infection following initial Tfp-mediated adherence. Furthermore, it was hypothesized that Cav1 expression is also involved in blocking uptake of other Tfp-producing bacteria during early infection. This could be confirmed as Tfp-producing but TTSS-negative EPEC were found to enter Cav1 deficient

AGS cells more rapidly compared to cells producing Cav1, similarly as observed previously during P^+GC infection. This effect was also seen to a lesser extend in the presence of the EPEC TTSS, thus emphasizing a generalized role of Cav1 in blocking cell entry of Tfp-producing bacteria. These findings suggest a role for Cav1 recruitment exclusively during the early infection stages of Tfp-expressing bacteria. Thus, Cav1 recruitment is a Tfp-specific, immediate cellular response to bacterial attachment that occurs throughout the early stages of infection and requires phosphorylation of Cav1 at Tyr14. Together with Cav1, various surface proteins, such as CD44v3, CD44, CD46, EGFR and ICAM-1, as well as a subset of cytoskeleton-associates proteins, such as filamin, actin, cortactin and ezrin are recruited to P^+GC infection sites (*121, 248, 251*). The recruitment of Tyr14 phosphorylated Cav1 to the infection sites together with actin and actin-associated proteins (e.g. the actin cross-linking protein filamin) most likely leads to the formation of a rigid actin filaments below the bacterial attachment sites, which in turns prevents the uptake of the bacteria during the early stages of P^+GC infection. Interestingly, the recruitment of these factors seems to be also highly dynamic and readily reversible as the Cav1 recruitment sites exclusively co-localize with P^+GC MCs even as they move on the host cell surface. Thus the bacteria induce Cav1 recruitment only at their present localizations even during movement on the host cell, which requires a very rapid host signaling cascade mediated by Cav1 that leads to the formation of a rigid actin cytoskeleton below the bacteria, but also implies that the cytoskeleton quickly reverts to its original state after the bacteria move to a different area on the cell surface.

Cytoskeletal reorganization that prevents bacterial uptake seems to be mediated by Cav1, which is known induce cell signaling via its Caveolin scaffolding domain (CSD) or by phosphorylation of its Tyr14 residue. CSD interaction has only been shown to suppress the activation of binding partners, such as G-proteins, Src family kinases and eNOS (*246*), therefore the CSD signaling appears less likely to be involved in triggering cytoskeletal rearrangements. Furthermore, experimental data discussed above indicates a role of phospho-Tyr14-Cav1 signaling. Thus protein kinases, which phosphorylate Cav1 at Tyr14 are most likely also involved in the signaling events that lead to the actin reorganization after P^+GC infection. Until now, only two Src-homology 2 (SH2)-domain containing interaction partners of phospho-Tyr14-Cav1 could be identified, Grb7 (*175*) and C-terminal Src kinase

(Csk) (*182*). However, the links between these known interaction partners and factors mediating cytoskeletal rearrangements are rather weak and seem to function only indirectly: Grb7 is an adapter protein containing a Ras-associating domain (*252*) and binding of Grb7 to Tyr14-phosphorylated Cav1 was demonstrated to increase anchorage-independent growth and EGF-stimulated cell migration (*175*). Grande-García et al. suggested that phospho-Tyr14-Cav1 binding activates Csk, which in turn negatively regulates Src kinase by phosphorylation. Src kinase inactivation subsequently decreases activity of the p190 Rho GTPase-activating protein (p190RhoGAP) which results in increased levels of active GTP-bound RhoA, thus promoting RhoA signaling (*186*). Yang et al. reported that depletion of Cav1 sustained Src family kinase activity during a 6 h exposure to laminar shear stress and thereby blocked a decline of p190RhoGAP activity observed only at later time points of the experiment (*253*). Thus, this interesting and complex regulatory network seems to be of particular importance during long-term cellular stress. In contrast, P^{+}GC mediated Cav1 phosphorylation was already observed 5 min post infection, indicating an immediate cellular signaling response.

However, only very few binding partners of phospho-Tyr14-Cav1 have been reported so far and the observed immediate Cav1 recruitment to P^{+}GC attachment sites in infected cells allows the speculation that different, yet unknown phospho-Tyr14-Cav1 signaling partners are involved in P^{+}GC infection. Therefore, novel phospho-Tyr14-Cav1 interaction partners were identified in this study by two distinct experimental approaches. First, a large scale SH2-/PTB-domain protein array was screened for interactions with a Tyr14-Cav1 phosphopeptide. Second, a biotinylated Tyr14-Cav1 phosphopeptide was used as bait in a streptavidin pull-down and all co-precipitated proteins were subsequently identified. These two independent approaches were chosen to increase the probability of finding and verifying novel interaction partners of Ty14 phosphorylated Cav1. In total, 7 novel phospho-Tyr14-Cav1 binding proteins were identified here: Vav2, PLCγ1, the p85 subunit of PI3K, Abl 1 and Abl 2, SH3D3C and the adaptor protein Grb10. The importance of the identified phospho-Tyr14-Cav1 signaling partners for different cell biological aspects is discussed in greater detail in chapter 4.2. Importantly, the high affinity phospho-Tyr14-Cav1 binders Vav2 and PLCγ1 were confirmed by both approaches.

The ubiquitously expressed Vav2 protein, a member of the Vav protein family, is known to function as a guanine nucleotide exchange factors of the Rho GTPase family (Rho GEF) for RhoA, Rac1 and to a lesser extend Cdc42 (*225*). Importantly, the SH2-domain containing Vav2 can link cell surface receptors to their effectors functions, e.g. Rho GTPase family-mediated cytoskeletal rearrangements (*225, 254*). In this study, the two phospho-Tyr14-Cav1 high affinity binders Vav2 and PLCγ1 were compared with regard to impede bacterial uptake. In contrast to PLCγ1, knock-down of Vav2 resulted in bacterial uptake, indicating a possible role of this Rho family GEF during P^+GC infection. This result suggest that phospo-Tyr14-Cav1 and Vav2 interact during P^+GC infection at bacterial attachment sites and this interaction leads to an efficient impediment of bacterial uptake, possibly by activating RhoA or Rac1. Interestingly, the observed P^+GC internalization was more efficient after siRNA treatment in comparison to shRNA-mediated knock down of Vav2. This result can be explained by a possible shRNA off-target effect or an upregulation of a compensating factor in the shRNA knock down cell line (*255*). Vav2 has been associated previously with cytoskeletal rearrangements following infection, e.g. during TARP-mediated entry of the obligate intracellular pathogen *Chlamydia trachomatis* into host cells (*256, 257*) and invasin-stimulated internalization of the human pathogen *Yersinia pseudotuberculosis (258)*. In these studies, Vav2 was associated with facilitating bacterial invasion during infection. This contrasts the mechanism proposed in this study, which can be explained by the different infection courses exhibited by *Neisseria*, obligate intracellular *Chlamydia* and facultative intracellular *Yersinia.* As a result of effector translocation (e.g. TARP, invasin) and unique host-pathogen interplay, Vav2 might activate different Rho family GTPases during different infection courses. Importantly, during *Chlamydia trachomatis* entry, Vav2 was reported to be phosphorylated in response to Abl kinase activation (*256*). This finding is particularly interesting as Abl1 and Abl2 were also identified here as binding partners of phospho-Tyr14-Cav1, indicating a possible regulatory network in response to P^+GC infection.

Tfp fiber retraction generates mechanical forces of 50 to 100 pN and exerts physical stress on the host cell (*47, 259*). Thus, Tfp retraction induces stress kinase signaling and cytoskeletal rearrangements in the infected host cell (*33*). Activation of RhoA is known to induce the assembly of stress fibers and thereby induces cytoskeletal rearrangements (*260*). The actin rearrangements elicited by P^+GC infection are reminiscent of localized formation

of such dense stress fibers. This allows the interpretation that Src- and Abl-mediated Cav1 phosphorylation following P^+GC infection triggers a phospho-Tyr14-Cav1-Vav2-RhoA signaling cascade, which results in formation of stress fiber-like cytoskeletal rearrangements underneath P^+GC attachment sites. Interestingly, RhoA activation in response to mechanical cell stretching was demonstrated recently to be mediated by Vav2 and to require Src activity as well as Src-mediated Tyr14 phosphorylation of Cav1 (*219, 254*). These reports, involving all factors described in this study, allow the speculation that phospho-Tyr14-Cav1-Vav2-RhoA signaling cascade is also highly relevant for RhoA activation after different extracellular stimuli. Although Vav2 can function as a GEF for RhoA as well as for Rac1 and Cdc42, it was shown previously that Vav exchange activity towards each of these small GTPases differs depending on the activating stimulus and the cell type (*225, 254, 261*). Therefore, it was hypothesized here that Vav2 binding to phospho-Tyr14-Cav1 results in a specific signaling cascade possibly involving only one or two Rho family GTPases. To test this hypothesis, the involvement of RhoA, Rac1 and Cdc42 in impediment of P^+GC uptake was analyzed. Additionally, the activation of RhoA and Rac1 in response to P^+GC infection was tested in shRNA Cav1 knock down and control cells. Strikingly, inhibitor- and siRNA-based experiments demonstrated an involvement of RhoA but not Rac1 or Cdc42 in impediment of bacterial uptake during early infection. Additionally, significant Cav1-dependent RhoA activation was observed 5 min after P^+GC infection, indicating a phospho-Tyr14-Cav1-Vav2-RhoA signaling cascade during early P^+GC infection. Interestingly, Cav1-dependent Rac1 activation was also observed, however, Rac1 activation was of lesser importance during impediment of bacterial uptake. Thus, the function of a possible phospho-Tyr14-Cav1-Vav2-Rac1 signaling cascade during P^+GC infection needs to be addressed in future studies.

Together, data presented in this study reveal an immediate early anti-invasive activity of P^+GC, dependent on tyrosine-phosphorylated Cav1 host-cell signaling, that facilitates the establishment and maintenance of this pathogen's extracellular niche. This process, triggered by Vav2-mediated activation of RhoA, elicits cytoskeletal rearrangements that may function as a physical barrier to prevent internalization of attached bacteria. Cav1 is known to participate in protein trafficking (*160*), and a drastic, instantaneous, and RhoA-independent recruitment of Cav1 at sites of P^+GC attachment was observed. Furthermore, Cav1 recruited to P^+GC infection sites was found to be phosphorylated at Tyr14 and

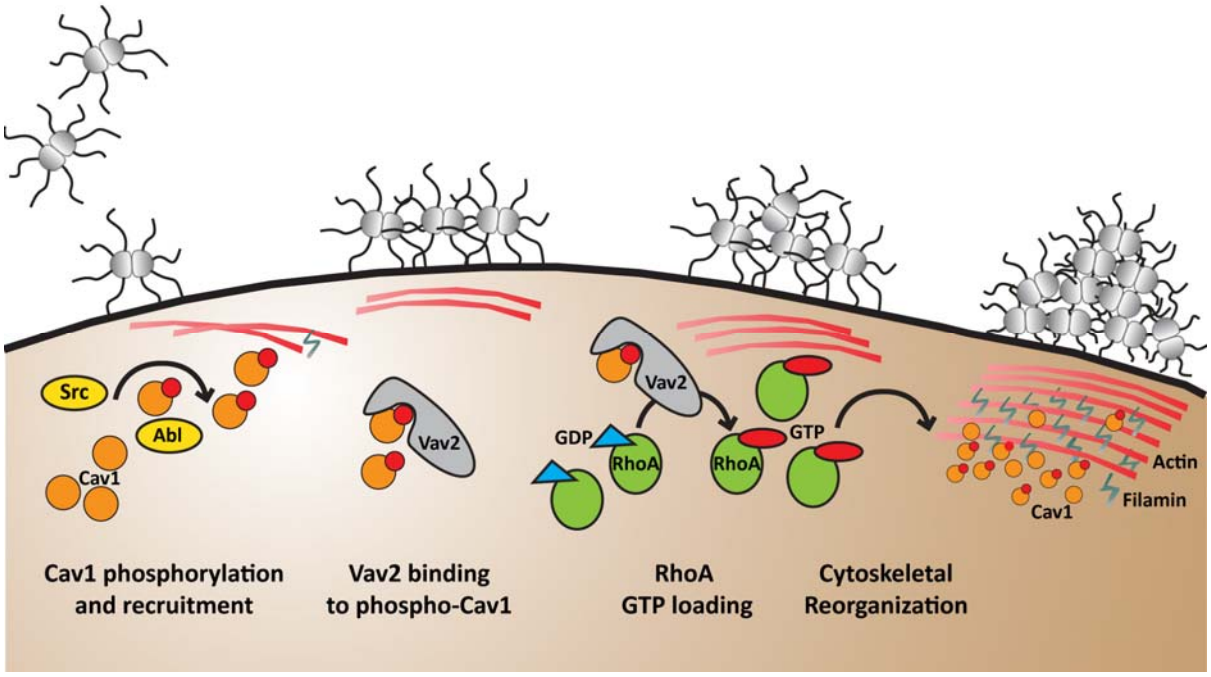

Figure 4-1. Model of Cav1-mediated host-cell signaling upon P$^+$GC infection. Tfp-mediated binding to host cells induces Cav1 recruitment and phosphorylation of Cav1 on Tyr14. Phospho-Tyr14-Cav1 directly interacts with the Rho family GEF Vav2 which in turn activates RhoA. RhoA activation induces the formation of cytoskeletal rearrangements underneath attached P$^+$GC functioning as a physical barrier to prevent internalization of bacteria.

phosphorylated Cav1 has been shown to recruit signaling proteins, providing a docking site for proteins possessing a SH2 domain (*175*). Thus, Cav1 is most likely the central element of the identified Cav1-Vav2-RhoA signaling cascade, playing a crucial role in the localization of its signaling partners to the site of infection. The identified Cav1-Vav2-RhoA signaling cascade prevents the premature uptake of P$^+$GC, which seems to be beneficial for these bacteria as they are rapidly killed inside host cells, as reported by Kirchner and de Graaf (*208, 209*). In contrast, Tfp exhibit an exquisite protection against extracellular humoral immune responses based on their vast antigenic variability with features including frequent intra-strain variation, post-translational modification and the release of soluble pilins (*262-266*). Thus, P$^+$GC, and probably other Tfp-producing bacteria including EPEC, could use this initial extracellular phase to adapt and prepare for the subsequent steps of infection. For example, GC later retract pili and employ variation of the Opa invasins to prepare individual bacteria for deliberate cell entry (*267*) and eventual transcytosis (*268*). EPEC, on the other hand, may use their Tfp as an immediate block to cell entry even before the TTSS is placed or used in delivering its anti-invasive effectors (*269*). Taken together, this Tfp-triggered mechanism extends our understanding of how P$^+$GC use pili to elicit cytoprotective effects

and modulate the host cell for their own benefit, as described previously (*270, 271*). By investigating P^+GC colonizing its host, these bacteria were exploited as a tool to identify an anti-invasive bacterial strategy as well as a novel Cav1-dependent signaling cascade leading to RhoA activation.

4.2 Novel signaling partners link Cav1 and caveolae to actin cytoskeleton remodeling

The findings of this study not only highlight a compelling anti-invasive bacterial infection strategy, but also uncover novel phosphotyrosine-Cav1 interaction partners and thus improve our understanding of Cav1-mediated cellular signaling. Cav1 is recognized today to be a highly versatile regulator of cell signaling as it can modulate signaling pathways through at least two different molecular mechanisms: (A) binding of interaction partners to the Cav1 scaffolding domain (CSD) results in inhibitory Cav1 signaling, whereas (B) phosphorylation of Cav1 on Tyr14 is associated with activation of downstream signaling partners (*272*). Generally, tyrosine phosphorylation allows binding to protein phosphotyrosine binding domains, particularly SH2 domains (*273*), which in turn activates downstream signaling cascades. Cav1 phosphorylation is known to play a role in very different cell biological processes, such as integrin-regulated caveolae internalization (*173*), Cav1 anterior polarization in transmigrating cells (*180*), focal adhesion kinase transposition between focal adhesions and cytosolic pools (*181*) and stretch-induced EGFR and Akt activation (*219*). Yet, only two SH2-domain containing interaction partners of phospho-Tyr14-Cav1 could be identified so far, Grb7 (*175*) and Csk (*182*). Thus, phosphorylation of Cav1 on Tyr14 is likely to be a step in signaling cascades within caveolae or at extra-caveolar pools of Cav1 (e.g. at focal adhesions). In addition, the importance of Tyr14 phosphorylation for mobilization and correct re-localization of Cav1 was reported before (*173, 246*) and could be confirmed in this study as only phosphorylated Cav1 was recruited to P^+GC infection sites, thus the correct subcellular localization of Cav1 after Tyr14 phosphorylation is a key factor controlling the elicited signaling.

The reports on the cell biological significance of phospho-Tyr14-Cav1 currently drastically outnumber the identified signaling partners. Furthermore, interactions of phospho-Tyr14-Cav1 with only Grb7 and Csk cannot fully account for all proposed cell

biological functions of phosphorylated Cav1. One can argue that not all functional phospho-Tyr14-Cav1 binding partners have been identified previously. However, it is critical to fully understand how Cav1 signaling leads to the remodeling of the actin cytoskeleton after $P^{+}GC$ infection and therefore novel interaction partners of phospho-Tyr14-Cav1 were identified in this study. Two competing and independent approaches were chosen to increase the probability of finding and verifying novel interaction partners of Ty14 phosphorylated Cav1. Importantly, next to unraveling how $P^{+}GC$ exploit host cell functions during the infection process, our general understanding of Cav1 cellular signaling can be improved through the identification of novel Cav1 binding proteins.

First, a large scale SH2-/PTB-domain protein array was screened for interactions with a Tyr14-Cav1 phosphopeptide with sequences corresponding to residues 5–22 of Cav1. Vav2, PLCγ1, SH2D3C, Grb10, and the non-receptor tyrosine kinases Abl1 and Abl2 were identified as possible interaction partners of tyrosine phosphorylated Cav1 by this approach, which suggests an even broader role of Cav1 in mediating cytoskeletal rearrangements through employment of a range of small GTPases. As discussed above, Vav2 functions as a Rho GEF for RhoA, Rac1 and to a lesser extend Cdc42 (*225*). Furthermore, Vav2 can function independently of its GEF activity by physically linking signaling molecules to the actin cytoskeleton (*225*). PLCγ1 not only hydrolyses phosphatidylinositol-4,5-bisphosphate to the second messenger molecules inositol-1,4,5-trisphosphate and diacylglycerol, which in turn activate protein kinase C and trigger intracellular calcium release. PLCγ1 also exhibits mitogenic activity by acting as a GEF for the small GTPase phosphatidylinositol-3-OH kinase PI3K enhancer (PIKE) (*274*) and is additionally capable of directly activating Rac1 (*275*). The putative phospho-Tyr14-Cav1 interaction partner SH2D3C is an integrin-associated signaling pathway component, proposed to regulate the actin cytoskeleton via its GEF-like domain, which binds Ras family GTPases and additionally forms a complex with the scaffolding protein Crk-associated substrate (Cas) (*276, 277*). Grb10, which putatively binds small GTPases of the Ras superfamily (*278*), was also identified as a possible phospho-Tyr14-Cav1 interactor. Finally, Abl 1 and abl2 kinases were identified to bind to phospho-Tyr14-Cav1. These kinases are known to link various cell surface receptors to signaling pathways involved in cytoskeletal reorganization and are also able to regulate the activation of Rac and Rho GTPases (*279, 280*). How exactly tyrosine phosphorylated Cav1 might influence

these various cellular processes, which lead to the concerted activation of diverse small GTPases and cytoskeletal rearrangements needs to be addressed in future studies. However, in case of Abl kinases, binding of tyrosine phosphorylated Cav1 to the SH2 domain likely disrupts the SH2–kinase-domain autoinhibitory interface, resulting in activation of the kinase (*281*) and consequent robust phosphorylation of Cav1 through a positive feedback loop as Cav1 itself is a target for Abl1 phosphorylation (*221*). Solely RasA1, a GTPase-activating protein, could be identified to bind to the non-phosphorylated Tyr14-Cav1 peptide but not to its phosphorylated form. This result contradicts the widely accepted paradigm that SH2-domains specifically bind to phosphorylated proteins and peptides (*273, 282*). Therefore RasA1 binding to the non-phosphorylated Cav1 peptide is probably an *in vitro* artifact.

Although Cav1 has not been reported to be phosphorylated at its Tyr42 residue, a Tyr14 phosphopeptide was additionally tested in the SH2-/PTB-domain protein array. This experiment was performed as a control for the Tyr14 specificity of the binding proteins of the Tyr14 phosphopeptide identified earlier. It was also hypothesized that Tyr42 phosphorylation might control additional yet unidentified Cav1 signaling functions, which might have a similar importance for cell signaling as signaling mediated by Tyr14 phosphorylation. None of the proteins identified to bind to the Tyr14-Cav1 phosphopeptide screen bound to the Tyr42-Cav1 phosphopeptide, which demonstrates a high specificity of the detected interactions. The adaptor protein Nck2, Spleen tyrosine kinase (Syk) and STAT1 were identified to bind to phosphorylated Tyr42 of Cav1. The three SH3 domains and one SH2 domain-containing protein Nck2 was found to be a potent Wiskott-Aldrich syndrome protein (WASP) activator *in vitro*, a protein which regulates the actin cytoskeleton via the Arp2/3 complex (*283*). The STAT1 transcription factor has previously been reported to associate with lipid rafts and caveolae (*284*). The identified STAT1 binding to phospho-Tyr42-Cav1 could therefore serve to anchor interferon-gamma/JAK/STAT-signaling to caveolae. Most interestingly, Syk, an important signaling mediator, is activated by dual binding of its tandem SH2 domains to two phosphorylated tyrosine residues of transmembrane adaptors, as present in Cav1 homo-oligomers in caveolae. Activated Syk subsequently recruits and directly binds to five signaling partners: members of the Vav and PLCγ families, the p85α subunit of the PI3K, as well as the adaptor proteins leukocyte

protein 65 and 76. The compelling overlap between reported Syk signaling partners and the phospho-Tyr14-Cav1 interaction partners found in this study (Vav2, PLCγ1 and p85α) suggests possible dual and/or compensating roles of Tyr14/Tyr42 phosphorylation in Cav1 signaling. Thus, the identified Tyr42 binding partners are interesting and might be of physiological relevance. However, as Tyr42 phosphorylation of Cav1 was neither in this study nor previously demonstrated, a Cav1 Tyr42 signaling platform remains a tentative but highly speculative hypothesis.

In the second approach chosen to identify binding partners of Ty14 phosphorylated Cav1, a biotinylated Tyr14-Cav1 phosphopeptide was used as bait in a streptavidin pull-down, followed by identification of all precipitated proteins. This experiment was conducted in Cav1-negative AGS cells to exclude possible competition between the added Cav1 peptides and endogenous Cav1. The regulatory subunit p85α of the PI3K, myosin IB, myosin ID, non-muscle myosin heavy chain IIA, cytokeratin 1, beta-actin and splicing factor proline/glutamine rich (SFPQ/PSF) were identified with this approach as possible phospho-Tyr14-Cav1 binding partners. SFPQ/PSF is a main component of paraspeckles, a new class of ribonucleoprotein bodies located in the interchromatin space of mammalian cell nuclei (*285*). Thus, the binding identified *in vitro* between phospho-Tyr14-Cav1 and SFPQ/PSF is most likely unphysiological, since the proteins have very different subcellular localizations and functions. In contrast, the identified phospho-Tyr14-Cav1 interaction with myosins, cytokeratins and beta-actin again underscores a close association of Tyr14 phosphorylated Cav1 with cytoskeletal components. Myosin 1B and 1D are class 1 myosins, which are small motor proteins with the ability to simultaneously bind to cellular membranes and actin filaments (*286*). Non muscle myosin heavy chain IIA was reported to mediate cross-talk of the actomyosin system with microtubules and thus is important for cellular contractility, focal adhesions formation and actin stress fiber organization (*287*). Cytokeratin 1, an intermediate filament keratin, was proposed to be an integrin-binding protein in a multi-protein receptor complex (*288*). However, none of these proteins possess an SH2-domain and the observed enhanced association with phospho-Tyr14-Cav1 could result from secondary binding and/or complex formation, as a direct interaction with phospho-Tyr14-Cav1 seems unlikely. The selected approach to identify phospho-Tyr14-Cav1 interaction partners by Maldi-MS/MS after precipitation is likely to identify only those proteins that

bind strongly and in higher abundance to the bait and can also co-precipitate large protein complexes. Nevertheless, the numerous association of the phospho-Tyr14-peptide with cytoskeletal components is striking. These results strengthen the cell fractionation experiments presented previously in this study that demonstrate Tyr14 expression to be required for a strong association of Cav1 with cytoskeletal components.

Most importantly, the SH2-domain containing regulatory subunit of the PI3K, p85α, was identified as an additional phospho-Tyr14-Cav1 binding protein. This finding is particularly interesting, as several groups previously reported an impact of Cav1 expression and Cav1 Tyr14 phosphorylation on the activity of the PI3K/Akt pathway. Two independent studies demonstrated that Cav1 sensitizes fibroblasts and epithelial cells to cytotoxic insults, such as TNFα, staurosporine, H_2O_2 and arsenite via activation of the PI3K/Akt pathway (*289, 290*). Cav1-overexpression directly activated the PI3K/Akt pathway in these studies and Sedding et al. demonstrated that Cav1 is required for the integrin-mediated activation of PI3K/Akt (*291*). In line with these findings and the results presented here, Src-mediated Tyr14 phosphorylation of Cav1 was demonstrated to be required for stretch-induced PI3K-mediated Akt activation in mesanglial cells (*219*). The catalytic subunit p85 of the heterodimeric PI3K is maintained in a low-activity state by the catalytic subunit p110 (*292*). This inhibition is abrogated when the regulatory subunit interacts with phosphotyrosine residues such as the phosphorylated Tyr14 in Cav1 (*292*). Thus, the direct p85α interaction with phospho-Tyr14-Cav1 can functionally explain the previous findings and strongly suggests that phospho-Tyr14-Cav1 interaction with p85α stimulates PI3K/Akt activation after different extracellular stimuli.

The streptavidin-agarose pulldown approach allowed to biochemically confirm the identified hits of the SH2-/PTB-domain screening. Western blot analysis revealed that Vav2, PLCγ1, p85 and p110 (the catalytic subunit of PI3K) demonstrated a highly increased binding affinity to the phosphorylated Cav1 peptide compared to the non-phosphorylated peptide in ME-180 and AGS cells. Thus, all tested hits of the SH2-/PTB-domain screening were identified reciprocally in the streptavidin-agarose pulldown approach. Interestingly, p110 could also be identified to specifically interact with phospho-Tyr14-Cav1; however, this interaction most likely represents the formation of a complex between phospho-Tyr14-Cav1, p85 and p110 and supports the hypothesis of a phospho-Tyr14-Cav1-mediated

activation of the PI3K as discussed above. The hits Vav2, PLCγ1 and p85 were further confirmed by immunoprecipitation of strongly phosphorylated Cav1. Vav2 and PLCγ1 again demonstrated exclusive phosphorylation-dependent binding to Cav1. Interestingly, a truncated Vav2 that consists solely of the C-terminal SH3-SH2-SH3 domains was able to bind to phospho-Tyr14-Cav1, again indicating a specific SH2-domain/phosphotyrosine interaction between Vav2 and Cav1. In contrast, p85 co-precipitated with both, phosphorylated and non-phosphorylated Cav1. This result contradicts the specific binding of p85 to the phospho-Tyr14-Cav1-peptide; however, it allows hypothesizing that a secondary interaction between p85 and Cav1 can take place after the initial SH2-domain/phosphotyrosine binding. This interaction might be mediated by the caveolin scaffolding domain (CSD), which is not present in the phospho-Tyr14-Cav1-peptide.

The specificity of phospho-Tyr14-Cav1 binding to Vav2 and PLCγ1 as well as the previously reported reliability of the SH2-/PTB-domain protein array (*215*) again underscores the relevance of all in this screening identified novel Cav1 binding partners. Previous studies using other phosphopeptides demonstrated that >90% of the SH2 and PTB domains on the protein microarrays are active, however a small rest was found to be inactive (*215*). Grb7 and Csk, in previous studies identified phospho-Tyr14-Cav1 binding partners (*175, 182*), as well as p85 could not be identified in the SH2-/PTB-domain protein array, which might indicate that the respective spotted domains are inactive. However, the SH2-domains of Grb7 and Grb10 are approximately 70% identical (*293*) and crystallization studies revealed conserved phosphotyrosine-binding residues present in the SH2-domains of the Grb7 and Grb10 but not in other SH2 domains (*294*). Lee et al. identified Grb7 with an immunoprecipitation-based approach (*175*). However, given the reported homology of Grb7 and Grb10, antibody cross-reaction might have resulted in false identification of Grb7 instead of Grb10 in that study; especially as Grb10 binding to phospho-Tyr14-Cav1 was not separately tested.

In recent studies, Cav1 was reported to interact directly with both RhoA and the Rho-associated protein kinase (ROCK) (*184, 187*) and Tyr14 phosphorylated Cav1 was repeatedly associated with RhoA activation (*186, 188, 295-297*). MβCD-induced stress fiber formation was demonstrated to require Cav1 expression and Src family kinase activity, suggesting that Cav1 phosphorylation is obligatory for RhoA-mediated stress fiber formation (*295*).

Furthermore, phosho-Tyr14-Cav1 was found to localize at the ends of actin stress fibers (*298*). Importantly, TGFβ-induced RhoA activation was demonstrated to be absent in mesanglial cells lacking Cav1 (*296*). In contrast to expression of a non-phosphorylatable Cav1 mutant, re-expression of Cav1 restored RhoA activation in that study (*296*). Additionally, two independent studies demonstrated that Src kinase-dependent Tyr14 phosphorylation of Cav1 promotes RhoA activation during cell migration (*186, 188*). All studies are in line with the findings presented here, as RhoA activation after P^+GC infection was demonstrated to depend on Cav1 expression. Until now, phospho-Tyr14-Cav1-mediated activation of RhoA was hypothesized to function indirectly through recruiting of Csk and thus inhibiting the Src–p190RhoGAP pathway (*186, 297*). However, the novel phospho-Tyr14-Cav1 interaction partners identified in this study could provide a direct explanation for the reported Cav1-mediated RhoA activation after different stimuli. A direct link between RhoA activation and tyrosine phosphorylated Cav1 is reported, mediated via Vav2. The status of tyrosine phosphorylation of Cav1 may thus serve as a crucial switch between the activated and inactivated state of RhoA. Thus, the direct interaction of tyrosine-phosphorylated Cav1 with Vav2 might support increased activation of RhoA in cell compartments where tyrosine phosphorylated Cav1 accumulates, such as focal adhesions or underneath P^+GC attachment sites.

Given the number of small GTPases-activating proteins among the identified novel phospho-Tyr14-Cav1 interaction partners, it is tempting to speculate that some of them might have additional relevance for cytoskeleton rearrangements. However, the role of PLCγ1, the PI3K, Abl 1, Abl 2, SH3D3C and Grb10 during phospho-Tyr14-Cav1 signaling is not well defined yet and requires future studies. A tempting speculation is that different phospho-Tyr14-Cav1 interaction partners together mediate Cav1 signalling. Vav2 activity is known to be stimulated by binding to phosphatidylinositol-3,4,5-trisphosphate (PIP3) whereas binding to phosphatidylinositol-4,5-bisphosphate (PIP2) was found to be inhibitory (*299*). Thus, phosphorylation of PIP2 to PIP3 by the PI3K increases Vav2-mediated activation of RhoA, and a synergetic effect of the phospho-Tyr14-Cav1 interaction partners Vav2 and PI3K could be possible. In this study, PIP2 was recruited to P^+GC infection sites where it was metabolized by the PI3K to PIP3 as this process could be abrogated by inhibition with wortmannin. Thus, PIP2 and PIP3 might regulate Vav2 activity during P^+GC infection.

Taken together, the novel phospho-Tyr14-Cav1 interaction partners presented in this study strongly increase knowledge of Cav1/caveolae-mediated signaling. However, additional studies are required to identify the signaling pathways underlying the diverse phospo-Tyr14-Cav1-dependent cellular functions.

4.3 Host cells impact on extracellular P^+GC microcolony formation

MC formation is recognized today as an important step of *Neisseria* pathogenesis as MCs have repeatedly been detected in patient biopsies (*115-117*). Extracellular MCs serve *Neisseria* in different ways as MCs confer resistance to shear stress (*117*) and shield bacteria from antibiotics and the host immune system (*118*). However, the complex process of MC formation still needs to be clarified in detail. During the first hours of infection MCs of approximately 10–100 bacteria are formed, which depends on the expression of the bacterial Type-IV-pili (Tfp). Tfp are required for bacterial aggregation and twitching motility and thus Tfp-negative *Neisseria* do not form MCs (*33*). In the cell culture infection model MCs appear as round dome-shaped three-dimensional bacterial clusters and this morphology depends on the expression of the pilus retraction ATPase PilT which mediates the pilus twitching motility (*50, 259*). Importantly, meningococci were found to induce a strong reorganization of the host cell plasma membrane during MC formation resulting in microvilli-like cellular projections which penetrate bacterial MCs and thereby confer resistance to shear stress (*300*). The formation of cellular projections, which reach into MCs was triggered by the bacterial minor pilin PilV and requires intact host lipid microdomains. Using live-cell microscopy Higashi et al. discovered that gonococcal MCs are motile on host cell membranes and fuse to form progressively larger structures, which induce massive rearrangements of the host microvillus architecture that result in a PilT-dependent formation of a MC-host cell microvilli lattice (*49, 301*). Interestingly, host cell components recruited underneath MCs, such as actin, ezrin and cortactin, were demonstrated to comigrate with motile MCs. These findings were confirmed in this study as recruited Cav1-GFP was found to comigrate with MCs during a P^+GC infection course. Thus, only Tfp and the pilus-associated protein PilT have been identified to be required for MC formation and host cell microvilli and PilV have been described to promote the three-dimensional stability of

MCs.

Therefore it was hypothesized here that host cell factors can also impact on MC formation during the infection process. This hypothesis was tested in an infection model of P^+GC with living and fixed ME-180 cells in which the infection process was carefully monitored by live-cell imaging. Various striking differences could be observed: (A) MCs were formed faster during infection of living cells compared to infection of fixed cells; (B) MCs only fuse on living cells to larger structures; (C) Living host cells participate in MC formation by directing bacteria along defined vectors; (D) P^+GC move quicker during infection of fixed cells compared to living cells.

Live–cell imaging proved to be an excellent tool to temporally resolve the P^+GC infection process in greater detail. During a 2 h infection time course, strong host cell membrane ruffling already started after 5-10 min, peaked around 30 min and continued in individual cells throughout the infection. These findings are in line with the study of Edwards et al. which reports the formation of membrane ruffles in primary cell systems 30 and 90 min post infection (*120*). Similarly, membrane ruffling was reported to occur during *Salmonella* infection and function independently of *Salmonella* host-cell invasion (*302*). However, the membrane ruffling elicited by P^+GC seems to be a strong cellular response to infection, which not only affects membrane sections directly surrounding the attached P^+GC but the whole cell. The strong membrane movements suggest a physical effect (e.g. by pushing) on attached bacteria. Careful visualization and illustration of membrane ruffles allowed directional observation of the wave-like ruffles which move along the plasma membrane from the cell border towards the cell center within a few minutes. The elicited wave-like ruffles phenotypically resemble previously reported circular dorsal ruffles or “dorsal waves” (*303, 304*). Dorsal waves are formed in response to receptor tyrosine kinase stimulation by different growth factors (*305*) and this process depends on dynamin, cortactin, components of the Arp2/3 complex and requires the remodeling of a dynamic actin cytoskeleton (*306*). P^+GC were found in this study be moved along common definite vectors after binding to living host cells. After Tfp-mediated binding to the host cells, many bacteria were found to be moved towards the cell center where individual vectors overlapped, indicating bacterial aggregation and formation of MCs. In contrast, P^+GC infecting fixed cells did not share common directions and movements were more erratic. In

line with these findings, MC formation was delayed by 30-60 minutes during infection of ME-180 fixed cells compared with infection of living ME-180 host cells. These data allow the speculation that the observed strong membrane ruffling or dorsal waves push attached bacteria along specific routes, which are defined by the actual plasma membrane movement. However, the importance of the dorsal wave-associated cytoskeletal proteins mentioned above for MC formation has not been investigated here and this question requires future studies to investigate the link between plasma membrane dorsal waves and MC formation. Together, the observations permit the hypothesis that attached P^+GC "membrane-surf" on their host cells until they reach other bacteria, aggregate and form a MC.

As reported before, MCs were observed here to fuse to larger structures starting around 60 min post infection (*49*). Importantly, fusion of MCs was not observed during infection of fixed cells compared to infection of living cells. This indicates that MC fusion also depends on host cell processes and contradicts the earlier notion that MC fusion is solely a result of MC crawling across the host cell membrane (*49*). One can hypothesize that proteins recruited underneath MCs, the three-dimensional shape of the host cell and the lipid composition and fluidity of the membrane affects MC motion. In contrast, active crawling of bacterial MCs would require coordinated retraction of pili by hundreds of bacteria within the MC, which seems unlikely. However, interbacterial communication might take place during MC fusion, as observed by bacterial movements between close MCs. Importantly, bacterial aggregates forming on fixed cells additionally demonstrate a less compact and three-dimensional morphology compared to MCs on living cells. This finding can be explained with the absence of stabilizing microvilli within the bacterial aggregates on fixed cells as reported previously (*300, 301*).

Next to the differences during MC formation and fusion, P^+GC exhibited altered motility during infection of fixed cells compared with infection of living cells. P^+GC appeared to move quicker and impetuously on fixed cells. P^+GC infecting living host cells and residing in or close to MCs moved at an average speed of 22 ± 4 $nm*s^{-1}$ over the time span of 10 sec compared to 139 ± 14 $nm*s^{-1}$ for P^+GC infecting fixed host cells. Holz et al. demonstrated that P^+GC twitching motility speeds depends on the fluidity of the membrane and twitching motility speed of non-adherent P^+GC was determined to be 570 ± 30 $nm*s^{-1}$ on fluid charged

membranes, which mimic plasma membranes (*307*). The differences between motility speeds on artificial fluid charged membranes, living and PFA-fixed host cell membranes therefore could result from lipid modifications by the fixing agent. However, PFA does not chemically alter lipids or affect the lipid content of cell membranes (*308, 309*). Importantly, bacterial motility was monitored in this study over a time span of 10 sec, thus immobile bacteria bound to the host cell membrane reduced the recorded average speeds. Thus, the monitored movement speeds represent also the likeliness and frequency of the bacteria to release the host cell, relocate and adhere again and do not directly indicate an altered twitching motility. Further differences between P^{+}GC infecting fixed and living host cells could be elucidated by monitoring gene regulation after infection using a *Neisseria* microarray as reported previously (*310*). In conclusion, the observed difference in bacterial motility and speed could indicate a behavioral discrepancy, such as the preference of the bacteria to closely stick to living cells and not remain on fixed cells to seek a better infection niche.

Taken together, these data clearly demonstrate that host cells do impact on bacterial MC formation. Thus, MC formation is a complex multi step process, which requires bacterial as well as host cell participation.

4.4 Conclusion and Outlook

This study improves our understanding of the importance of functional host cell signaling for different aspects of bacterial pathogenesis. An immediate and apparently anti-invasive strategy utilized by *N. gonorrhoeae* and other Tfp-expressing bacteria during infection is proposed, which requires reorganization of the actin cytoskeleton. Cav1 is recruited to P^{+}GC attachment sites where it was found to be phosphorylated and to prevent internalization of the bacteria. Vav2 and its substrate, the small GTPase RhoA, were found to play a direct role in the Cav1-mediated prevention of bacterial uptake. As enteropathogenic *E. coli* was also found to recruit Cav1, these findings highlight how Tfp-producing bacteria avoid host cell uptake, uncover Vav2 as an important novel Cav1 signaling partner, and suggest ways in which tyrosine-phosphorylated-Cav1 could mediate cytoskeletal rearrangements. Furthermore, protein microarrays and pulldown assays

highlighted six novel SH2-domain containing interaction partners of tyrosine phosphorylated Cav1, all of which have been implicated in modulating the cytoskeleton. Furthermore, evidence is provided that host cell participation is required for formation of extracellular microcolonies during *Neisseria* infection. $P^{+}GC$ infecting fixed host cells show altered motility and MC formation and MC fusion is impaired compared to living host cells, indicating host-pathogen interactions during these multi step processes.

Overall a more accurate picture of early $P^{+}GC$ infection-mediated cell signaling was obtained. However, some questions still remain in the bigger picture of pathogen-induced signaling during infection. Are there other ways to activate RhoA during infection, maybe at later infection time points involving different virulence factors? Which other recruited factors can mediate cytoskeletal rearrangements during $P^{+}GC$ infection? Which factors and signaling pathways are essential for successful microcolony formation? These important questions may be addressed in future studies using broader analyses. Importantly, data presented in this study establish a mechanistic link between Cav1 phosphorylation and pathogen-induced cytoskeleton reorganization, and advance our understanding of caveolin function. The knowledge of phospho-Tyr14-Cav1 binding partners identified in this study would be crucial for future research on cellular Cav1 signaling.

REFERENCES

5 References

1. Parton,R.G. & Simons,K. The multiple faces of caveolae. *Nat. Rev. Mol. Cell Biol.* **8**, 185-194 (2007).

2. Meyer,T.F., Pohlner,J., & van Putten,J.P. Biology of the pathogenic Neisseriae. *Curr. Top. Microbiol. Immunol.* **192**, 283-317 (1994).

3. Spisni,E., Tomasi,V., Cestaro,A., & Tosatto,S.C. Structural insights into the function of human caveolin 1. *Biochem. Biophys. Res. Commun.* **338**, 1383-1390 (2005).

4. Beachey,E.H. Bacterial adherence: adhesin-receptor interactions mediating the attachment of bacteria to mucosal surface. *J. Infect. Dis.* **143**, 325-345 (1981).

5. Finlay,B.B. & Cossart,P. Exploitation of mammalian host cell functions by bacterial pathogens. *Science* **276**, 718-725 (1997).

6. Kline,K.A., Falker,S., Dahlberg,S., Normark,S., & Henriques-Normark,B. Bacterial adhesins in host-microbe interactions. *Cell Host. Microbe* **5**, 580-592 (2009).

7. Telford,J.L., Barocchi,M.A., Margarit,I., Rappuoli,R., & Grandi,G. Pili in gram-positive pathogens. *Nat. Rev. Microbiol.* **4**, 509-519 (2006).

8. Hacker,J. Role of fimbrial adhesins in the pathogenesis of Escherichia coli infections. *Can. J. Microbiol.* **38**, 720-727 (1992).

9. Hahn,H.P. The type-4 pilus is the major virulence-associated adhesin of Pseudomonas aeruginosa--a review. *Gene* **192**, 99-108 (1997).

10. Pizarro-Cerda,J. & Cossart,P. Bacterial adhesion and entry into host cells. *Cell* **124**, 715-727 (2006).

11. Rudel,T., Scheurerpflug,I., & Meyer,T.F. Neisseria PilC protein identified as type-4 pilus tip-located adhesin. *Nature* **373**, 357-359 (1995).

12. Dehio,C., Gray-Owen,S.D., & Meyer,T.F. The role of neisserial Opa proteins in interactions with host cells. *Trends Microbiol.* **6**, 489-495 (1998).

13. Abdelrahman,Y.M. & Belland,R.J. The chlamydial developmental cycle. *FEMS Microbiol. Rev.* **29**, 949-959 (2005).

14. Walker,T.S. Rickettsial interactions with human endothelial cells in vitro: adherence and entry. *Infect. Immun.* **44**, 205-210 (1984).

15. Isberg,R.R., Voorhis,D.L., & Falkow,S. Identification of invasin: a protein that allows enteric bacteria to penetrate cultured mammalian cells. *Cell* **50**, 769-778 (1987).

16. Isberg,R.R. & Leong,J.M. Multiple beta 1 chain integrins are receptors for invasin, a protein that promotes bacterial penetration into mammalian cells. *Cell* **60**, 861-871 (1990).

17. Alrutz,M.A. & Isberg,R.R. Involvement of focal adhesion kinase in invasin-mediated uptake. *Proc. Natl. Acad. Sci. U. S. A* **95**, 13658-13663 (1998).

18. Bruce-Staskal,P.J., Weidow,C.L., Gibson,J.J., & Bouton,A.H. Cas, Fak and Pyk2 function in diverse signaling cascades to promote Yersinia uptake. *J. Cell Sci.* **115**, 2689-2700 (2002).

19. Apicella,M.A. Neisseria meningitidis in *Principles and practice of infectious diseases* (eds. Mandell,G.L., Bennet,J.E. & Dolin,R.) 1896-1909 (Churchill Livingstone, New York, 1995).

20. Handsfield,H.H. & Sparling,P.F. Neisseria gonorrhoeae in *Principles and practice of infectious diseases* (eds. Mandell,G.L., Bennet,J.E. & Dolin,R.) 1909-1926 (Churchill Livingstone, New York, 1995).

21. Johnson,A.P. The pathogenic potential of commensal species of Neisseria. *J. Clin. Pathol.* **36**, 213-223 (1983).

22. Caugant,D.A. & Maiden,M.C. Meningococcal carriage and disease--population biology and evolution. *Vaccine* **27 Suppl 2**, B64-B70 (2009).

23. Booy,R. & Kroll,J.S. Bacterial meningitis and meningococcal infection. *Curr. Opin. Pediatr.* **10**, 13-18 (1998).

24. Stephens,D.S., Greenwood,B., & Brandtzaeg,P. Epidemic meningitis, meningococcaemia, and Neisseria meningitidis. *Lancet* **369**, 2196-2210 (2007).

25. Pollard,A.J., Nadel,S., Ninis,N., Faust,S.N., & Levin,M. Emergency management of meningococcal disease: eight years on. *Arch. Dis. Child* **92**, 283-286 (2007).

26. WHO. Global Prevalence and Incidence of Selected Curable Sexually Transmitted Infections - Overview and Estimates. 2001. Geneva, WHO.

27. Casey,S.G., Shafer,W.M., & Spitznagel,J.K. Neisseria gonorrhoeae survive intraleukocytic oxygen-independent antimicrobial capacities of anaerobic and aerobic granulocytes in the presence of pyocin lethal for extracellular gonococci. *Infect. Immun.* **52**, 384-389 (1986).

28. Simons,M.P., Nauseef,W.M., & Apicella,M.A. Interactions of Neisseria gonorrhoeae with adherent polymorphonuclear leukocytes. *Infect. Immun.* **73**, 1971-1977 (2005).

29. McCormack,W.M., Stumacher,R.J., Johnson,K., & Donner,A. Clinical spectrum of gonococcal infection in women. *Lancet* **1**, 1182-1185 (1977).

30. Sayeed,Z.A., Bhaduri,U., Howell,E., & Meyers,H.L., Jr. Gonococcal meningitis. A review. *JAMA* **219**, 1730-1731 (1972).

31. Masi,A.T. & Eisenstein,B.I. Disseminated gonococcal infection (DGI) and gonococcal arthritis (GCA): II. Clinical manifestations, diagnosis, complications, treatment, and prevention. *Semin. Arthritis Rheum.* **10**, 173-197 (1981).

32. Kerle,K.K., Mascola,J.R., & Miller,T.A. Disseminated gonococcal infection. *Am. Fam. Physician* **45**, 209-214 (1992).

33. Merz,A.J. & So,M. Interactions of pathogenic neisseriae with epithelial cell membranes. *Annu. Rev. Cell Dev. Biol.* **16**, 423-457 (2000).

34. Taylor,R.K., Miller,V.L., Furlong,D.B., & Mekalanos,J.J. Use of phoA gene fusions to identify a pilus colonization factor coordinately regulated with cholera toxin. *Proc. Natl. Acad. Sci. U. S. A* **84**, 2833-2837 (1987).

35. Zhang,X.L. *et al.* Salmonella enterica serovar typhi uses type IVB pili to enter human intestinal epithelial cells. *Infect. Immun.* **68**, 3067-3073 (2000).

36. Pasloske,B.L., Finlay,B.B., & Paranchych,W. Cloning and sequencing of the Pseudomonas aeruginosa PAK pilin gene. *FEBS Lett.* **183**, 408-412 (1985).

37. Marrs,C.F. *et al.* Cloning and sequencing of a Moraxella bovis pilin gene. *J. Bacteriol.* **163**, 132-139 (1985).

38. Giron,J.A., Ho,A.S., & Schoolnik,G.K. An inducible bundle-forming pilus of enteropathogenic Escherichia coli. *Science* **254**, 710-713 (1991).

39. Kellogg,D.S.J., Peacock,W.L.J., Deacon,W., Brown,l., & Pirkle,D. Neisseria gonorrhoeae. I. Virulence genetically linked to clonal variation. *J. Bacteriol.* **85**, 1274-1279 (1963).

40. Swanson,J. *et al.* Gonococcal pilin variants in experimental gonorrhea. *J. Exp. Med.* **165**, 1344-1357 (1987).

41. Strom,M.S., Nunn,D.N., & Lory,S. A single bifunctional enzyme, PilD, catalyzes cleavage and N-methylation of proteins belonging to the type IV pilin family. *Proc. Natl. Acad. Sci. U. S. A* **90**, 2404-2408 (1993).

42. Freitag,N.E., Seifert,H.S., & Koomey,M. Characterization of the pilF-pilD pilus-assembly locus of Neisseria gonorrhoeae. *Mol. Microbiol.* **16**, 575-586 (1995).

43. Forest,K.T. & Tainer,J.A. Type-4 pilus-structure: outside to inside and top to bottom--a minireview. *Gene* **192**, 165-169 (1997).

44. Parge,H.E. *et al.* Structure of the fibre-forming protein pilin at 2.6 A resolution. *Nature* **378**, 32-38 (1995).

45. Wolfgang,M., van Putten,J.P., Hayes,S.F., Dorward,D., & Koomey,M. Components and dynamics of fiber formation define a ubiquitous biogenesis pathway for bacterial pili. *EMBO J.* **19**, 6408-6418 (2000).

46. Whitchurch,C.B., Hobbs,M., Livingston,S.P., Krishnapillai,V., & Mattick,J.S. Characterisation of a Pseudomonas aeruginosa twitching motility gene and evidence for a specialised protein export system widespread in eubacteria. *Gene* **101**, 33-44 (1991).

47. Maier,B. *et al.* Single pilus motor forces exceed 100 pN. *Proc. Natl. Acad. Sci. U. S. A* **99**, 16012-16017 (2002).

48. Wolfgang,M. *et al.* PilT mutations lead to simultaneous defects in competence for natural transformation and twitching motility in piliated Neisseria gonorrhoeae. *Mol. Microbiol.* **29**, 321-330 (1998).

49. Higashi,D.L. *et al.* Dynamics of Neisseria gonorrhoeae attachment: microcolony development, cortical plaque formation, and cytoprotection. *Infect. Immun.* **75**, 4743-4753 (2007).

50. Wolfgang,M., Park,H.S., Hayes,S.F., van Putten,J.P., & Koomey,M. Suppression of an absolute defect in type IV pilus biogenesis by loss-of-function mutations in pilT, a twitching motility gene in Neisseria gonorrhoeae. *Proc. Natl. Acad. Sci. U. S. A* **95**, 14973-14978 (1998).

51. Morand,P.C. *et al.* Type IV pilus retraction in pathogenic Neisseria is regulated by the PilC proteins. *EMBO J.* **23**, 2009-2017 (2004).

52. Jonsson,A.B., Nyberg,G., & Normark,S. Phase variation of gonococcal pili by frameshift mutation in pilC, a novel gene for pilus assembly. *EMBO J.* **10**, 477-488 (1991).

53. Rahman,M., Kallstrom,H., Normark,S., & Jonsson,A.B. PilC of pathogenic Neisseria is associated with the bacterial cell surface. *Mol. Microbiol.* **25**, 11-25 (1997).

54. Winther-Larsen,H.C. *et al.* Neisseria gonorrhoeae PilV, a type IV pilus-associated protein essential to human epithelial cell adherence. *Proc. Natl. Acad. Sci. U. S. A* **98**, 15276-15281 (2001).

55. Park,H.S., Wolfgang,M., & Koomey,M. Modification of type IV pilus-associated epithelial cell adherence and multicellular behavior by the PilU protein of Neisseria gonorrhoeae. *Infect. Immun.* **70**, 3891-3903 (2002).

56. Haas,R. & Meyer,T.F. The repertoire of silent pilus genes in Neisseria gonorrhoeae: evidence for gene conversion. *Cell* **44**, 107-115 (1986).

57. Swanson,J. *et al.* Gene conversion involving the pilin structural gene correlates with pilus+ in equilibrium with pilus- changes in Neisseria gonorrhoeae. *Cell* **47**, 267-276 (1986).

58. Koomey,M., Gotschlich,E.C., Robbins,K., Bergstrom,S., & Swanson,J. Effects of recA mutations on pilus antigenic variation and phase transitions in Neisseria gonorrhoeae. *Genetics* **117**, 391-398 (1987).

59. Kallstrom,H., Liszewski,M.K., Atkinson,J.P., & Jonsson,A.B. Membrane cofactor protein (MCP or CD46) is a cellular pilus receptor for pathogenic Neisseria. *Mol. Microbiol.* **25**, 639-647 (1997).

60. Edwards,J.L. *et al.* A co-operative interaction between Neisseria gonorrhoeae and complement receptor 3 mediates infection of primary cervical epithelial cells. *Cell Microbiol.* **4**, 571-584 (2002).

61. Kirchner,M., Heuer,D., & Meyer,T.F. CD46-independent binding of neisserial type IV pili and the major pilus adhesin, PilC, to human epithelial cells. *Infect. Immun.* **73**, 3072-3082 (2005).

62. Edwards,J.L. & Apicella,M.A. I-domain-containing integrins serve as pilus receptors for Neisseria gonorrhoeae adherence to human epithelial cells. *Cell Microbiol.* **7**, 1197-1211 (2005).

63. Dehio,C., Gray-Owen,S.D., & Meyer,T.F. The role of neisserial Opa proteins in interactions with host cells. *Trends Microbiol.* **6**, 489-495 (1998).

64. Swanson,J. Studies on gonococcus infection. XII. Colony color and opacity varienats of gonococci. *Infect. Immun.* **19**, 320-331 (1978).

65. Bhat,K.S. *et al.* The opacity proteins of Neisseria gonorrhoeae strain MS11 are encoded by a family of 11 complete genes. *Mol. Microbiol.* **5**, 1889-1901 (1991).

66. Stern,A. & Meyer,T.F. Common mechanism controlling phase and antigenic variation in pathogenic neisseriae. *Mol. Microbiol.* **1**, 5-12 (1987).

67. Stern,A., Brown,M., Nickel,P., & Meyer,T.F. Opacity genes in Neisseria gonorrhoeae: control of phase and antigenic variation. *Cell* **47**, 61-71 (1986).

68. Murphy,G.L., Connell,T.D., Barritt,D.S., Koomey,M., & Cannon,J.G. Phase variation of gonococcal protein II: regulation of gene expression by slipped-strand mispairing of a repetitive DNA sequence. *Cell* **56**, 539-547 (1989).

69. Kupsch,E.M., Knepper,B., Kuroki,T., Heuer,I., & Meyer,T.F. Variable opacity (Opa) outer membrane proteins account for the cell tropisms displayed by Neisseria gonorrhoeae for human leukocytes and epithelial cells. *EMBO J.* **12**, 641-650 (1993).

70. Chen,T., Belland,R.J., Wilson,J., & Swanson,J. Adherence of pilus- Opa+ gonococci to epithelial cells in vitro involves heparan sulfate. *J. Exp. Med.* **182**, 511-517 (1995).

71. van Putten,J.P. & Paul,S.M. Binding of syndecan-like cell surface proteoglycan receptors is required for Neisseria gonorrhoeae entry into human mucosal cells. *EMBO J.* **14**, 2144-2154 (1995).

72. Grassme,H. *et al.* Acidic sphingomyelinase mediates entry of N. gonorrhoeae into nonphagocytic cells. *Cell* **91**, 605-615 (1997).

73. Gomez-Duarte,O.G. *et al.* Binding of vitronectin to opa-expressing Neisseria gonorrhoeae mediates invasion of HeLa cells. *Infect. Immun.* **65**, 3857-3866 (1997).

74. Bos,M.P., Grunert,F., & Belland,R.J. Differential recognition of members of the carcinoembryonic antigen family by Opa variants of Neisseria gonorrhoeae. *Infect. Immun.* **65**, 2353-2361 (1997).

75. Chen,T., Grunert,F., Medina-Marino,A., & Gotschlich,E.C. Several carcinoembryonic antigens (CD66) serve as receptors for gonococcal opacity proteins. *J. Exp. Med.* **185**, 1557-1564 (1997).

76. Gray-Owen,S.D., Lorenzen,D.R., Haude,A., Meyer,T.F., & Dehio,C. Differential Opa specificities for CD66 receptors influence tissue interactions and cellular response to Neisseria gonorrhoeae. *Mol. Microbiol.* **26**, 971-980 (1997).

77. Bates,P.A., Luo,J., & Sternberg,M.J. A predicted three-dimensional structure for the carcinoembryonic antigen (CEA). *FEBS Lett.* **301**, 207-214 (1992).

78. Virji,M. *et al.* Critical determinants of host receptor targeting by Neisseria meningitidis and Neisseria gonorrhoeae: identification of Opa adhesiotopes on the N-domain of CD66 molecules. *Mol. Microbiol.* **34**, 538-551 (1999).

79. Heumann,D., Glauser,M.P., & Calandra,T. Molecular basis of host-pathogen interaction in septic shock. *Curr. Opin. Microbiol.* **1**, 49-55 (1998).

80. Danaher,R.J. *et al.* Genetic basis of Neisseria gonorrhoeae lipooligosaccharide antigenic variation. *J. Bacteriol.* **177**, 7275-7279 (1995).

81. Porat,N., Apicella,M.A., & Blake,M.S. Neisseria gonorrhoeae utilizes and enhances the biosynthesis of the asialoglycoprotein receptor expressed on the surface of the hepatic HepG2 cell line. *Infect. Immun.* **63**, 1498-1506 (1995).

82. Song,W., Ma,L., Chen,R., & Stein,D.C. Role of lipooligosaccharide in Opa-independent invasion of Neisseria gonorrhoeae into human epithelial cells. *J. Exp. Med.* **191**, 949-960 (2000).

83. Johnston,K.H., Holmes,K.K., & Gotschlich,E.C. The serological classification of Neisseria gonorrhoeae. I. Isolation of the outer membrane complex responsible for serotypic specificity. *J. Exp. Med.* **143**, 741-758 (1976).

84. van der,L.P., Heckels,J.E., Virji,M., Hoogerhout,P., & Poolman,J.T. Topology of outer membrane porins in pathogenic Neisseria spp. *Infect. Immun.* **59**, 2963-2971 (1991).

85. Cannon,J.G., Buchanan,T.M., & Sparling,P.F. Confirmation of association of protein I serotype of Neisseria gonorrhoeae with ability to cause disseminated infection. *Infect. Immun.* **40**, 816-819 (1983).

86. Sandstrom,E.G. *et al.* Serogrouping of Neisseria gonorrhoeae: correlation of serogroup with disseminated gonococcal infection. *Sex Transm. Dis.* **11**, 77-80 (1984).

87. Morello,J.A. & Bohnhoff,M. Serovars and serum resistance of Neisseria gonorrhoeae from disseminated and uncomplicated infections. *J. Infect. Dis.* **160**, 1012-1017 (1989).

88. Rudel,T. *et al.* Modulation of Neisseria porin (PorB) by cytosolic ATP/GTP of target cells: parallels between pathogen accommodation and mitochondrial endosymbiosis. *Cell* **85**, 391-402 (1996).

89. Muller,A. *et al.* Neisserial porin (PorB) causes rapid calcium influx in target cells and induces apoptosis by the activation of cysteine proteases. *EMBO J.* **18**, 339-352 (1999).

90. Muller,A. *et al.* Targeting of the pro-apoptotic VDAC-like porin (PorB) of Neisseria gonorrhoeae to mitochondria of infected cells. *EMBO J.* **19**, 5332-5343 (2000).

91. Muller,A. *et al.* VDAC and the bacterial porin PorB of Neisseria gonorrhoeae share mitochondrial import pathways. *EMBO J.* **21**, 1916-1929 (2002).

92. Binnicker,M.J., Williams,R.D., & Apicella,M.A. Gonococcal porin IB activates NF-kappaB in human urethral epithelium and increases the expression of host antiapoptotic factors. *Infect. Immun.* **72**, 6408-6417 (2004).

93. Massari,P., Ho,Y., & Wetzler,L.M. Neisseria meningitidis porin PorB interacts with mitochondria and protects cells from apoptosis. *Proc. Natl. Acad. Sci. U. S. A* **97**, 9070-9075 (2000).

94. Massari,P., King,C.A., Ho,A.Y., & Wetzler,L.M. Neisserial PorB is translocated to the mitochondria of HeLa cells infected with Neisseria meningitidis and protects cells from apoptosis. *Cell Microbiol.* **5**, 99-109 (2003).

95. Bauer,F.J., Rudel,T., Stein,M., & Meyer,T.F. Mutagenesis of the Neisseria gonorrhoeae porin reduces invasion in epithelial cells and enhances phagocyte responsiveness. *Mol. Microbiol.* **31**, 903-913 (1999).

96. van Putten,J.P., Duensing,T.D., & Carlson,J. Gonococcal invasion of epithelial cells driven by P.IA, a bacterial ion channel with GTP binding properties. *J. Exp. Med.* **188**, 941-952 (1998).

97. Rechner,C., Kuhlewein,C., Muller,A., Schild,H., & Rudel,T. Host glycoprotein Gp96 and scavenger receptor SREC interact with PorB of disseminating Neisseria gonorrhoeae in an epithelial invasion pathway. *Cell Host. Microbe* **2**, 393-403 (2007).

98. Plaut,A.G., Gilbert,J.V., Artenstein,M.S., & Capra,J.D. Neisseria gonorrhoeae and neisseria meningitidis: extracellular enzyme cleaves human immunoglobulin A. *Science* **190**, 1103-1105 (1975).

99. Pohlner,J., Halter,R., Beyreuther,K., & Meyer,T.F. Gene structure and extracellular secretion of Neisseria gonorrhoeae IgA protease. *Nature* **325**, 458-462 (1987).

100. Brandtzaeg,P. The role of humoral mucosal immunity in the induction and maintenance of chronic airway infections. *Am. J. Respir. Crit Care Med.* **151**, 2081-2086 (1995).

101. Hauck,C.R. & Meyer,T.F. The lysosomal/phagosomal membrane protein h-lamp-1 is a target of the IgA1 protease of Neisseria gonorrhoeae. *FEBS Lett.* **405**, 86-90 (1997).

102. Lin,L. *et al.* The Neisseria type 2 IgA1 protease cleaves LAMP1 and promotes survival of bacteria within epithelial cells. *Mol. Microbiol.* **24**, 1083-1094 (1997).

103. Hopper,S. *et al.* Effects of the immunoglobulin A1 protease on Neisseria gonorrhoeae trafficking across polarized T84 epithelial monolayers. *Infect. Immun.* **68**, 906-911 (2000).

104. Seiler,A., Reinhardt,R., Sarkari,J., Caugant,D.A., & Achtman,M. Allelic polymorphism and site-specific recombination in the opc locus of Neisseria meningitidis. *Mol. Microbiol.* **19**, 841-856 (1996).

105. Zhu,P., Morelli,G., & Achtman,M. The opcA and (psi)opcB regions in Neisseria: genes, pseudogenes, deletions, insertion elements and DNA islands. *Mol. Microbiol.* **33**, 635-650 (1999).

106. Virji,M. *et al.* Expression of the Opc protein correlates with invasion of epithelial and endothelial cells by Neisseria meningitidis. *Mol. Microbiol.* **6**, 2785-2795 (1992).

107. Virji,M., Makepeace,K., & Moxon,E.R. Distinct mechanisms of interactions of Opc-expressing meningococci at apical and basolateral surfaces of human endothelial cells; the role of integrins in apical interactions. *Mol. Microbiol.* **14**, 173-184 (1994).

108. van,D.M., Brandtzaeg,P., & van der Meer,J.W. Update on meningococcal disease with emphasis on pathogenesis and clinical management. *Clin. Microbiol. Rev.* **13**, 144-66, table (2000).

109. Geoffroy,M.C., Floquet,S., Metais,A., Nassif,X., & Pelicic,V. Large-scale analysis of the meningococcus genome by gene disruption: resistance to complement-mediated lysis. *Genome Res.* **13**, 391-398 (2003).

110. Kugelberg,E., Gollan,B., & Tang,C.M. Mechanisms in Neisseria meningitidis for resistance against complement-mediated killing. *Vaccine* **26 Suppl 8**, I34-I39 (2008).

111. Jarvis,G.A. & Vedros,N.A. Sialic acid of group B Neisseria meningitidis regulates alternative complement pathway activation. *Infect. Immun.* **55**, 174-180 (1987).

112. Hammerschmidt,S. *et al.* Capsule phase variation in Neisseria meningitidis serogroup B by slipped-strand mispairing in the polysialyltransferase gene (siaD): correlation with bacterial invasion and the outbreak of meningococcal disease. *Mol. Microbiol.* **20**, 1211-1220 (1996).

113. Pace,D., Pollard,A.J., & Messonier,N.E. Quadrivalent meningococcal conjugate vaccines. *Vaccine* **27 Suppl 2**, B30-B41 (2009).

114. Pujol,C., Eugene,E., de Saint,M.L., & Nassif,X. Interaction of Neisseria meningitidis with a polarized monolayer of epithelial cells. *Infect. Immun.* **65**, 4836-4842 (1997).

115. Sim,R.J., Harrison,M.M., Moxon,E.R., & Tang,C.M. Underestimation of meningococci in tonsillar tissue by nasopharyngeal swabbing. *Lancet* **356**, 1653-1654 (2000).

116. Harrison,O.B. *et al.* Analysis of pathogen-host cell interactions in purpura fulminans: expression of capsule, type IV pili, and PorA by Neisseria meningitidis in vivo. *Infect. Immun.* **70**, 5193-5201 (2002).

117. Mairey,E. *et al.* Cerebral microcirculation shear stress levels determine Neisseria meningitidis attachment sites along the blood-brain barrier. *J. Exp. Med.* **203**, 1939-1950 (2006).

118. Neil,R.B. & Apicella,M.A. Clinical and laboratory evidence for Neisseria meningitidis biofilms. *Future. Microbiol.* **4**, 555-563 (2009).

119. Anderson,G.G. & O'Toole,G.A. Innate and induced resistance mechanisms of bacterial biofilms. *Curr. Top. Microbiol. Immunol.* **322**, 85-105 (2008).

120. Edwards,J.L., Shao,J.Q., Ault,K.A., & Apicella,M.A. Neisseria gonorrhoeae elicits membrane ruffling and cytoskeletal rearrangements upon infection of primary human endocervical and ectocervical cells. *Infect. Immun.* **68**, 5354-5363 (2000).

121. Merz,A.J., Enns,C.A., & So,M. Type IV pili of pathogenic Neisseriae elicit cortical plaque formation in epithelial cells. *Mol. Microbiol.* **32**, 1316-1332 (1999).

122. Ochoa,T.J., Salazar-Lindo,E., & Cleary,T.G. Management of children with infection-associated persistent diarrhea. *Semin. Pediatr. Infect. Dis.* **15**, 229-236 (2004).

123. Ochoa,T.J., Barletta,F., Contreras,C., & Mercado,E. New insights into the epidemiology of enteropathogenic Escherichia coli infection. *Trans. R. Soc. Trop. Med. Hyg.* **102**, 852-856 (2008).

124. Chen,H.D. & Frankel,G. Enteropathogenic Escherichia coli: unravelling pathogenesis. *FEMS Microbiol. Rev.* **29**, 83-98 (2005).

125. Garmendia,J., Frankel,G., & Crepin,V.F. Enteropathogenic and enterohemorrhagic Escherichia coli infections: translocation, translocation, translocation. *Infect. Immun.* **73**, 2573-2585 (2005).

126. Levine,M.M. *et al.* The diarrheal response of humans to some classic serotypes of enteropathogenic Escherichia coli is dependent on a plasmid encoding an enteroadhesiveness factor. *J. Infect. Dis.* **152**, 550-559 (1985).

127. Vallance,B.A. & Finlay,B.B. Exploitation of host cells by enteropathogenic Escherichia coli. *Proc. Natl. Acad. Sci. U. S. A* **97**, 8799-8806 (2000).

128. Dean,P. & Kenny,B. The effector repertoire of enteropathogenic E. coli: ganging up on the host cell. *Curr. Opin. Microbiol.* **12**, 101-109 (2009).

129. Kenny,B. *et al.* Enteropathogenic E. coli (EPEC) transfers its receptor for intimate adherence into mammalian cells. *Cell* **91**, 511-520 (1997).

130. Lee,S.H. & Dominguez,R. Regulation of actin cytoskeleton dynamics in cells. *Mol. Cells* **29**, 311-325 (2010).

131. Bailly,M. & Condeelis,J. Cell motility: insights from the backstage. *Nat. Cell Biol.* **4**, E292-E294 (2002).

132. Burridge,K. & Wennerberg,K. Rho and Rac take center stage. *Cell* **116**, 167-179 (2004).

133. Raftopoulou,M. & Hall,A. Cell migration: Rho GTPases lead the way. *Dev. Biol.* **265**, 23-32 (2004).

134. Huveneers,S. & Danen,E.H. Adhesion signaling - crosstalk between integrins, Src and Rho. *J. Cell Sci.* **122**, 1059-1069 (2009).

135. Galan,J.E. & Wolf-Watz,H. Protein delivery into eukaryotic cells by type III secretion machines. *Nature* **444**, 567-573 (2006).

136. Patel,J.C. & Galan,J.E. Manipulation of the host actin cytoskeleton by Salmonella--all in the name of entry. *Curr. Opin. Microbiol.* **8**, 10-15 (2005).

137. Munter,S., Way,M., & Frischknecht,F. Signaling during pathogen infection. *Sci. STKE.* **2006**, re5 (2006).

138. Hayward,R.D. & Koronakis,V. Pathogens reWritE Rho's rules. *Cell* **124**, 15-17 (2006).

139. Belyi,Y. & Aktories,K. Bacterial toxin and effector glycosyltransferases. *Biochim. Biophys. Acta* **1800**, 134-143 (2010).

140. Lemonnier,M., Landraud,L., & Lemichez,E. Rho GTPase-activating bacterial toxins: from bacterial virulence regulation to eukaryotic cell biology. *FEMS Microbiol. Rev.* **31**, 515-534 (2007).

141. Vogelsgesang,M., Pautsch,A., & Aktories,K. C3 exoenzymes, novel insights into structure and action of Rho-ADP-ribosylating toxins. *Naunyn Schmiedebergs Arch. Pharmacol.* **374**, 347-360 (2007).

142. Billker,O. *et al.* Distinct mechanisms of internalization of Neisseria gonorrhoeae by members of the CEACAM receptor family involving Rac1- and Cdc42-dependent and -independent pathways. *EMBO J.* **21**, 560-571 (2002).

143. Simons,K. & Ikonen,E. Functional rafts in cell membranes. *Nature* **387**, 569-572 (1997).

144. Simons,K. & Toomre,D. Lipid rafts and signal transduction. *Nat. Rev. Mol. Cell Biol.* **1**, 31-39 (2000).

145. Schuck,S. & Simons,K. Polarized sorting in epithelial cells: raft clustering and the biogenesis of the apical membrane. *J. Cell Sci.* **117**, 5955-5964 (2004).

146. YAMADA,E. The fine structure of the gall bladder epithelium of the mouse. *J. Biophys. Biochem. Cytol.* **1**, 445-458 (1955).

147. Rothberg,K.G. *et al.* Caveolin, a protein component of caveolae membrane coats. *Cell* **68**, 673-682 (1992).

148. Murata,M. *et al.* VIP21/caveolin is a cholesterol-binding protein. *Proc. Natl. Acad. Sci. U. S. A* **92**, 10339-10343 (1995).

149. Way,M. & Parton,R.G. M-caveolin, a muscle-specific caveolin-related protein. *FEBS Lett.* **376**, 108-112 (1995).

150. Razani,B. *et al.* Caveolin-2-deficient mice show evidence of severe pulmonary dysfunction without disruption of caveolae. *Mol. Cell Biol.* **22**, 2329-2344 (2002).

151. Sowa,G., Pypaert,M., Fulton,D., & Sessa,W.C. The phosphorylation of caveolin-2 on serines 23 and 36 modulates caveolin-1-dependent caveolae formation. *Proc. Natl. Acad. Sci. U. S. A* **100**, 6511-6516 (2003).

152. Scherer,P.E. *et al.* Caveolin isoforms differ in their N-terminal protein sequence and subcellular distribution. Identification and epitope mapping of an isoform-specific monoclonal antibody probe. *J. Biol. Chem.* **270**, 16395-16401 (1995).

153. Fujimoto,T., Kogo,H., Nomura,R., & Une,T. Isoforms of caveolin-1 and caveolar structure. *J. Cell Sci.* **113 Pt 19**, 3509-3517 (2000).

154. Dietzen,D.J., Hastings,W.R., & Lublin,D.M. Caveolin is palmitoylated on multiple cysteine residues. Palmitoylation is not necessary for localization of caveolin to caveolae. *J. Biol. Chem.* **270**, 6838-6842 (1995).

155. Glenney,J.R., Jr. & Zokas,L. Novel tyrosine kinase substrates from Rous sarcoma virus-transformed cells are present in the membrane skeleton. *J. Cell Biol.* **108**, 2401-2408 (1989).

156. Li,S., Seitz,R., & Lisanti,M.P. Phosphorylation of caveolin by src tyrosine kinases. The alpha-isoform of caveolin is selectively phosphorylated by v-Src in vivo. *J. Biol. Chem.* **271**, 3863-3868 (1996).

157. Li,S., Couet,J., & Lisanti,M.P. Src tyrosine kinases, Galpha subunits, and H-Ras share a common membrane-anchored scaffolding protein, caveolin. Caveolin binding negatively regulates the auto-activation of Src tyrosine kinases. *J. Biol. Chem.* **271**, 29182-29190 (1996).

158. Ostrom,R.S. & Insel,P.A. The evolving role of lipid rafts and caveolae in G protein-coupled receptor signaling: implications for molecular pharmacology. *Br. J. Pharmacol.* **143**, 235-245 (2004).

159. Oh,P. & Schnitzer,J.E. Segregation of heterotrimeric G proteins in cell surface microdomains. G(q) binds caveolin to concentrate in caveolae, whereas G(i) and G(s) target lipid rafts by default. *Mol. Biol. Cell* **12**, 685-698 (2001).

160. Pelkmans,L., Burli,T., Zerial,M., & Helenius,A. Caveolin-stabilized membrane domains as multifunctional transport and sorting devices in endocytic membrane traffic. *Cell* **118**, 767-780 (2004).

161. Bush,W.S., Ihrke,G., Robinson,J.M., & Kenworthy,A.K. Antibody-specific detection of caveolin-1 in subapical compartments of MDCK cells. *Histochem. Cell Biol.* **126**, 27-34 (2006).

162. White,M.A. & Anderson,R.G. Signaling networks in living cells. *Annu. Rev. Pharmacol. Toxicol.* **45**, 587-603 (2005).

163. Couet,J., Li,S., Okamoto,T., Ikezu,T., & Lisanti,M.P. Identification of peptide and protein ligands for the caveolin-scaffolding domain. Implications for the interaction of caveolin with caveolae-associated proteins. *J. Biol. Chem.* **272**, 6525-6533 (1997).

164. Bucci,M. *et al.* In vivo delivery of the caveolin-1 scaffolding domain inhibits nitric oxide synthesis and reduces inflammation. *Nat. Med.* **6**, 1362-1367 (2000).

165. Okamoto,T., Schlegel,A., Scherer,P.E., & Lisanti,M.P. Caveolins, a family of scaffolding proteins for organizing "preassembled signaling complexes" at the plasma membrane. *J. Biol. Chem.* **273**, 5419-5422 (1998).

166. Henley,J.R., Krueger,E.W., Oswald,B.J., & McNiven,M.A. Dynamin-mediated internalization of caveolae. *J. Cell Biol.* **141**, 85-99 (1998).

167. Schnitzer,J.E., Oh,P., & McIntosh,D.P. Role of GTP hydrolysis in fission of caveolae directly from plasma membranes. *Science* **274**, 239-242 (1996).

168. Pelkmans,L., Puntener,D., & Helenius,A. Local actin polymerization and dynamin recruitment in SV40-induced internalization of caveolae. *Science* **296**, 535-539 (2002).

169. Anderson,R.G., Kamen,B.A., Rothberg,K.G., & Lacey,S.W. Potocytosis: sequestration and transport of small molecules by caveolae. *Science* **255**, 410-411 (1992).

170. Tuma,P.L. & Hubbard,A.L. Transcytosis: crossing cellular barriers. *Physiol Rev.* **83**, 871-932 (2003).

171. Del Pozo,M.A. *et al.* Integrins regulate Rac targeting by internalization of membrane domains. *Science* **303**, 839-842 (2004).

172. Echarri,A. & Del Pozo,M.A. Caveolae internalization regulates integrin-dependent signaling pathways. *Cell Cycle* **5**, 2179-2182 (2006).

173. Del Pozo,M.A. *et al.* Phospho-caveolin-1 mediates integrin-regulated membrane domain internalization. *Nat. Cell Biol.* **7**, 901-908 (2005).

174. Labrecque,L. *et al.* Regulation of vascular endothelial growth factor receptor-2 activity by caveolin-1 and plasma membrane cholesterol. *Mol. Biol. Cell* **14**, 334-347 (2003).

175. Lee,H. *et al.* Constitutive and growth factor-regulated phosphorylation of caveolin-1 occurs at the same site (Tyr-14) in vivo: identification of a c-Src/Cav-1/Grb7 signaling cassette. *Mol. Endocrinol.* **14**, 1750-1775 (2000).

176. Mastick,C.C., Brady,M.J., & Saltiel,A.R. Insulin stimulates the tyrosine phosphorylation of caveolin. *J. Cell Biol.* **129**, 1523-1531 (1995).

177. Parat,M.O., Stachowicz,R.Z., & Fox,P.L. Oxidative stress inhibits caveolin-1 palmitoylation and trafficking in endothelial cells. *Biochem. J.* **361**, 681-688 (2002).

178. Volonte,D., Galbiati,F., Pestell,R.G., & Lisanti,M.P. Cellular stress induces the tyrosine phosphorylation of caveolin-1 (Tyr(14)) via activation of p38 mitogen-activated protein kinase and c-Src kinase. Evidence for caveolae, the actin cytoskeleton, and focal adhesions as mechanical sensors of osmotic stress. *J. Biol. Chem.* **276**, 8094-8103 (2001).

179. Sanguinetti,A.R., Cao,H., & Corley,M.C. Fyn is required for oxidative- and hyperosmotic-stress-induced tyrosine phosphorylation of caveolin-1. *Biochem. J.* **376**, 159-168 (2003).

180. Parat,M.O., nand-Apte,B., & Fox,P.L. Differential caveolin-1 polarization in endothelial cells during migration in two and three dimensions. *Mol. Biol. Cell* **14**, 3156-3168 (2003).

181. Goetz,J.G. *et al.* Concerted regulation of focal adhesion dynamics by galectin-3 and tyrosine-phosphorylated caveolin-1. *J. Cell Biol.* **180**, 1261-1275 (2008).

182. Cao,H., Courchesne,W.E., & Mastick,C.C. A phosphotyrosine-dependent protein interaction screen reveals a role for phosphorylation of caveolin-1 on tyrosine 14: recruitment of C-terminal Src kinase. *J. Biol. Chem.* **277**, 8771-8774 (2002).

183. Stahlhut,M. & van,D.B. Identification of filamin as a novel ligand for caveolin-1: evidence for the organization of caveolin-1-associated membrane domains by the actin cytoskeleton. *Mol. Biol. Cell* **11**, 325-337 (2000).

184. Rashid-Doubell,F. *et al.* Caveolin-1 and lipid rafts in confluent BeWo trophoblasts: evidence for Rock-1 association with caveolin-1. *Placenta* **28**, 139-151 (2007).

185. Gingras,D., Gauthier,F., Lamy,S., Desrosiers,R.R., & Beliveau,R. Localization of RhoA GTPase to endothelial caveolae-enriched membrane domains. *Biochem. Biophys. Res. Commun.* **247**, 888-893 (1998).

186. Grande-Garcia,A. *et al.* Caveolin-1 regulates cell polarization and directional migration through Src kinase and Rho GTPases. *J. Cell Biol.* **177**, 683-694 (2007).

187. Dubroca,C. *et al.* RhoA activation and interaction with Caveolin-1 are critical for pressure-induced myogenic tone in rat mesenteric resistance arteries. *Cardiovasc. Res.* **73**, 190-197 (2007).

188. Joshi,B. *et al.* Phosphorylated caveolin-1 regulates Rho/ROCK-dependent focal adhesion dynamics and tumor cell migration and invasion. *Cancer Res.* **68**, 8210-8220 (2008).

189. Gonzalez,E., Nagiel,A., Lin,A.J., Golan,D.E., & Michel,T. Small interfering RNA-mediated down-regulation of caveolin-1 differentially modulates signaling pathways in endothelial cells. *J. Biol. Chem.* **279**, 40659-40669 (2004).

190. Nevins,A.K. & Thurmond,D.C. Caveolin-1 functions as a novel Cdc42 guanine nucleotide dissociation inhibitor in pancreatic beta-cells. *J. Biol. Chem.* **281**, 18961-18972 (2006).

191. Nethe,M. *et al.* Focal-adhesion targeting links caveolin-1 to a Rac1-degradation pathway. *J. Cell Sci.* **123**, 1948-1958 (2010).

192. Servitja,J.M., Marinissen,M.J., Sodhi,A., Bustelo,X.R., & Gutkind,J.S. Rac1 function is required for Src-induced transformation. Evidence of a role for Tiam1 and Vav2 in Rac activation by Src. *J. Biol. Chem.* **278**, 34339-34346 (2003).

193. Kawakatsu,T. *et al.* Vav2 as a Rac-GDP/GTP exchange factor responsible for the nectin-induced, c-Src- and Cdc42-mediated activation of Rac. *J. Biol. Chem.* **280**, 4940-4947 (2005).

194. Miyamoto,Y., Yamauchi,J., & Itoh,H. Src kinase regulates the activation of a novel FGD-1-related Cdc42 guanine nucleotide exchange factor in the signaling pathway from the endothelin A receptor to JNK. *J. Biol. Chem.* **278**, 29890-29900 (2003).

195. Tu,S., Wu,W.J., Wang,J., & Cerione,R.A. Epidermal growth factor-dependent regulation of Cdc42 is mediated by the Src tyrosine kinase. *J. Biol. Chem.* **278**, 49293-49300 (2003).

196. Fukuyama,T. *et al.* Involvement of the c-Src-Crk-C3G-Rap1 signaling in the nectin-induced activation of Cdc42 and formation of adherens junctions. *J. Biol. Chem.* **280**, 815-825 (2005).

197. Shin,J.S. & Abraham,S.N. Co-option of endocytic functions of cellular caveolae by pathogens. *Immunology* **102**, 2-7 (2001).

198. Lafont,F., Tran Van,N.G., Hanada,K., Sansonetti,P., & van der Goot,F.G. Initial steps of Shigella infection depend on the cholesterol/sphingolipid raft-mediated CD44-IpaB interaction. *EMBO J.* **21**, 4449-4457 (2002).

199. Shin,J.S., Gao,Z., & Abraham,S.N. Involvement of cellular caveolae in bacterial entry into mast cells. *Science* **289**, 785-788 (2000).

200. Wooldridge,K.G., Williams,P.H., & Ketley,J.M. Host signal transduction and endocytosis of Campylobacter jejuni. *Microb. Pathog.* **21**, 299-305 (1996).

201. Norkin,L.C., Wolfrom,S.A., & Stuart,E.S. Association of caveolin with Chlamydia trachomatis inclusions at early and late stages of infection. *Exp. Cell Res.* **266**, 229-238 (2001).

202. Stuart,E.S., Webley,W.C., & Norkin,L.C. Lipid rafts, caveolae, caveolin-1, and entry by Chlamydiae into host cells. *Exp. Cell Res.* **287**, 67-78 (2003).

203. Vieira,F.S., Correa,G., Einicker-Lamas,M., & Coutinho-Silva,R. Host-cell lipid rafts: a safe door for micro-organisms? *Biol. Cell* **102**, 391-407 (2010).

204. Lafont,F. & van der Goot,F.G. Bacterial invasion via lipid rafts. *Cell Microbiol.* **7**, 613-620 (2005).

205. Orlandi,P.A. & Fishman,P.H. Filipin-dependent inhibition of cholera toxin: evidence for toxin internalization and activation through caveolae-like domains. *J. Cell Biol.* **141**, 905-915 (1998).

206. Coconnier,M.H., Lorrot,M., Barbat,A., Laboisse,C., & Servin,A.L. Listeriolysin O-induced stimulation of mucin exocytosis in polarized intestinal mucin-secreting cells: evidence for toxin recognition of membrane-associated lipids and subsequent toxin internalization through caveolae. *Cell Microbiol.* **2**, 487-504 (2000).

207. Abrami,L., Liu,S., Cosson,P., Leppla,S.H., & van der Goot,F.G. Anthrax toxin triggers endocytosis of its receptor via a lipid raft-mediated clathrin-dependent process. *J. Cell Biol.* **160**, 321-328 (2003).

208. Kirchner,M. Interaktion pathogener Neisserien mit humanen Epithelzellen. Dissertation, Eberhard Karls Universität Tübingen, 2004.

209. de Graaf,D. Adherence to and invasion of epithelial cells by Neisseria gonorrhoeae. Dissertation, Freie Universität Berlin, 2009.

210. Meyer,T.F., Billyard,E., Haas,R., Storzbach,S., & So,M. Pilus genes of Neisseria gonorrheae: chromosomal organization and DNA sequence. *Proc. Natl. Acad. Sci. U. S. A* **81**, 6110-6114 (1984).

211. Jarvis,K.G. *et al.* Enteropathogenic Escherichia coli contains a putative type III secretion system necessary for the export of proteins involved in attaching and effacing lesion formation. *Proc. Natl. Acad. Sci. U. S. A* **92**, 7996-8000 (1995).

212. Broome,M.A. & Hunter,T. Requirement for c-Src catalytic activity and the SH3 domain in platelet-derived growth factor BB and epidermal growth factor mitogenic signaling. *J. Biol. Chem.* **271**, 16798-16806 (1996).

213. Friedberg,D., Umanski,T., Fang,Y., & Rosenshine,I. Hierarchy in the expression of the locus of enterocyte effacement genes of enteropathogenic *Escherichia coli*. *Mol. Microbiol* **34**, 941-952 (1999).

214. Vuopio-Varkila,J. & Schoolnik,G.K. Localized adherence by enteropathogenic Escherichia coli is an inducible phenotype associated with the expression of new outer membrane proteins. *J. Exp. Med.* **174**, 1167-1177 (1991).

215. Jones,R.B., Gordus,A., Krall,J.A., & MacBeath,G. A quantitative protein interaction network for the ErbB receptors using protein microarrays. *Nature* **439**, 168-174 (2006).

216. Kaushansky,A. *et al.* System-wide investigation of ErbB4 reveals 19 sites of Tyr phosphorylation that are unusually selective in their recruitment properties. *Chem. Biol.* **15**, 808-817 (2008).

217. Brinton,C.C. *et al.* Uses of pili in gonorrhoea control: role of bacterial pilin in disease,purification,and properties of gonococcal pili and progress in the development of a gonococcal pilus vaccine for gonorrhoea. (eds. Brooks,G.F., Gotschlich,E.C., Holmes,K.K., Sawyer,W.D. & Young,F.E.) 155-178 (American Society forMicrobiology., Washington, DC , 1978).

218. Khan,E.M. *et al.* Epidermal growth factor receptor exposed to oxidative stress undergoes Src- and caveolin-1-dependent perinuclear trafficking. *J. Biol. Chem.* **281**, 14486-14493 (2006).

219. Zhang,B. *et al.* Caveolin-1 phosphorylation is required for stretch-induced EGFR and Akt activation in mesangial cells. *Cell Signal.*(2007).

220. Burgermeister,E. *et al.* Differential expression and function of caveolin-1 in human gastric cancer progression. *Cancer Res.* **67**, 8519-8526 (2007).

221. Sanguinetti,A.R. & Mastick,C.C. c-Abl is required for oxidative stress-induced phosphorylation of caveolin-1 on tyrosine 14. *Cell Signal.* **15**, 289-298 (2003).

222. Chong,Y.P., Ia,K.K., Mulhern,T.D., & Cheng,H.C. Endogenous and synthetic inhibitors of the Src-family protein tyrosine kinases. *Biochim. Biophys. Acta* **1754**, 210-220 (2005).

223. Capdeville,R., Buchdunger,E., Zimmermann,J., & Matter,A. Glivec (STI571, imatinib), a rationally developed, targeted anticancer drug. *Nat. Rev. Drug Discov.* **1**, 493-502 (2002).

224. Santilman,V., Baran,J., nand-Apte,B., Evans,R.M., & Parat,M.O. Caveolin-1 polarization in transmigrating endothelial cells requires binding to intermediate filaments. *Angiogenesis.* **10**, 297-305 (2007).

225. Hornstein,I., Alcover,A., & Katzav,S. Vav proteins, masters of the world of cytoskeleton organization. *Cell Signal.* **16**, 1-11 (2004).

226. Abe,K. *et al.* Vav2 is an activator of Cdc42, Rac1, and RhoA. *J. Biol. Chem.* **275**, 10141-10149 (2000).

227. Gao,Y., Dickerson,J.B., Guo,F., Zheng,J., & Zheng,Y. Rational design and characterization of a Rac GTPase-specific small molecule inhibitor. *Proc. Natl. Acad. Sci. U. S. A* **101**, 7618-7623 (2004).

228. Janmey,P.A., Hvidt,S., Lamb,J., & Stossel,T.P. Resemblance of actin-binding protein/actin gels to covalently crosslinked networks. *Nature* **345**, 89-92 (1990).

229. Ito,T., Suzuki,A., & Stossel,T.P. Regulation of water flow by actin-binding protein-induced actin gelatin. *Biophys. J.* **61**, 1301-1305 (1992).

230. Clarke,S.C., Haigh,R.D., Freestone,P.P., & Williams,P.H. Virulence of enteropathogenic Escherichia coli, a global pathogen. *Clin. Microbiol. Rev.* **16**, 365-378 (2003).

231. Nougayrede,J.P., Fernandes,P.J., & Donnenberg,M.S. Adhesion of enteropathogenic Escherichia coli to host cells. *Cell Microbiol.* **5**, 359-372 (2003).

232. Craig,L. & Li,J. Type IV pili: paradoxes in form and function. *Curr. Opin. Struct. Biol.* **18**, 267-277 (2008).

233. Virji,M. Pathogenic neisseriae: surface modulation, pathogenesis and infection control. *Nat. Rev. Microbiol.* **7**, 274-286 (2009).

234. Maier,B. *et al.* Single pilus motor forces exceed 100 pN. *Proc. Natl. Acad. Sci. U. S. A* **99**, 16012-16017 (2002).

235. Merz,A.J. & So,M. Attachment of piliated, Opa- and Opc- gonococci and meningococci to epithelial cells elicits cortical actin rearrangements and clustering of tyrosine-phosphorylated proteins. *Infect. Immun.* **65**, 4341-4349 (1997).

236. Neame,S.J., Uff,C.R., Sheikh,H., Wheatley,S.C., & Isacke,C.M. CD44 exhibits a cell type dependent interaction with triton X-100 insoluble, lipid rich, plasma membrane domains. *J. Cell Sci.* **108 (Pt 9)**, 3127-3135 (1995).

237. Tilghman,R.W. & Hoover,R.L. E-selectin and ICAM-1 are incorporated into detergent-insoluble membrane domains following clustering in endothelial cells. *FEBS Lett.* **525**, 83-87 (2002).

238. Couet,J., Sargiacomo,M., & Lisanti,M.P. Interaction of a receptor tyrosine kinase, EGF-R, with caveolins. Caveolin binding negatively regulates tyrosine and serine/threonine kinase activities. *J. Biol. Chem.* **272**, 30429-30438 (1997).

239. Hoffmann,I., Eugene,E., Nassif,X., Couraud,P.O., & Bourdoulous,S. Activation of ErbB2 receptor tyrosine kinase supports invasion of endothelial cells by Neisseria meningitidis. *J. Cell Biol.* **155**, 133-143 (2001).

240. Nagy,P. *et al.* Lipid rafts and the local density of ErbB proteins influence the biological role of homo- and heteroassociations of ErbB2. *J. Cell Sci.* **115**, 4251-4262 (2002).

241. Jay,D., Garcia,E.J., Lara,J.E., Medina,M.A., & de,l.L., I Determination of a cAMP-dependent protein kinase phosphorylation site in the C-terminal region of human endothelial actin-binding protein. *Arch. Biochem. Biophys.* **377**, 80-84 (2000).

242. Jay,D., Garcia,E.J., & de,l.L., I In situ determination of a PKA phosphorylation site in the C-terminal region of filamin. *Mol. Cell Biochem.* **260**, 49-53 (2004).

243. Chen,H.S., Kolahi,K.S., & Mofrad,M.R. Phosphorylation facilitates the integrin binding of filamin under force. *Biophys. J.* **97**, 3095-3104 (2009).

244. Ohta,Y. & Hartwig,J.H. Actin filament cross-linking by chicken gizzard filamin is regulated by phosphorylation in vitro. *Biochemistry* **34**, 6745-6754 (1995).

245. Fielding,P.E., Chau,P., Liu,D., Spencer,T.A., & Fielding,C.J. Mechanism of platelet-derived growth factor-dependent caveolin-1 phosphorylation: relationship to sterol binding and the role of serine-80. *Biochemistry* **43**, 2578-2586 (2004).

246. Head,B.P. & Insel,P.A. Do caveolins regulate cells by actions outside of caveolae? *Trends Cell Biol.*(2006).

247. Ushio-Fukai,M. *et al.* Cholesterol depletion inhibits epidermal growth factor receptor transactivation by angiotensin II in vascular smooth muscle cells: role of cholesterol-rich microdomains and focal adhesions in angiotensin II signaling. *J. Biol. Chem.* **276**, 48269-48275 (2001).

248. Lee,S.W. *et al.* CD46 is phosphorylated at tyrosine 354 upon infection of epithelial cells by Neisseria gonorrhoeae. *J. Cell Biol.* **156**, 951-957 (2002).

249. Naumann,M., Rudel,T., Wieland,B., Bartsch,C., & Meyer,T.F. Coordinate activation of activator protein 1 and inflammatory cytokines in response to Neisseria gonorrhoeae epithelial cell contact involves stress response kinases. *J. Exp. Med.* **188**, 1277-1286 (1998).

250. Radel,C. & Rizzo,V. Integrin mechanotransduction stimulates caveolin-1 phosphorylation and recruitment of Csk to mediate actin reorganization. *Am. J. Physiol Heart Circ. Physiol* **288**, H936-H945 (2005).

251. Lambotin,M. *et al.* Invasion of endothelial cells by Neisseria meningitidis requires cortactin recruitment by a phosphoinositide-3-kinase/Rac1 signalling pathway triggered by the lipo-oligosaccharide. *J. Cell Sci.* **118**, 3805-3816 (2005).

252. Depetris,R.S., Wu,J., & Hubbard,S.R. Structural and functional studies of the Ras-associating and pleckstrin-homology domains of Grb10 and Grb14. *Nat. Struct. Mol. Biol.* **16**, 833-839 (2009).

253. Yang,B., Radel,C., Hughes,D., Kelemen,S., & Rizzo,V. p190Rho GTPase-Activating Protein Links the {beta}1 Integrin/Caveolin-1 Mechanosignaling Complex to RhoA and Actin Remodeling. *Arterioscler. Thromb. Vasc. Biol.*(2010).

254. Peng,F. *et al.* Mechanical stretch-induced RhoA activation is mediated by the RhoGEF Vav2 in mesangial cells. *Cell Signal.* **22**, 34-40 (2010).

255. Rao,D.D., Senzer,N., Cleary,M.A., & Nemunaitis,J. Comparative assessment of siRNA and shRNA off target effects: what is slowing clinical development. *Cancer Gene Ther.* **16**, 807-809 (2009).

256. Elwell,C.A., Ceesay,A., Kim,J.H., Kalman,D., & Engel,J.N. RNA interference screen identifies Abl kinase and PDGFR signaling in Chlamydia trachomatis entry. *PLoS. Pathog.* **4**, e1000021 (2008).

257. Lane,B.J., Mutchler,C., Al,K.S., Grieshaber,S.S., & Carabeo,R.A. Chlamydial entry involves TARP binding of guanine nucleotide exchange factors. *PLoS. Pathog.* **4**, e1000014 (2008).

258. McGee,K., Holmfeldt,P., & Fallman,M. Microtubule-dependent regulation of Rho GTPases during internalisation of Yersinia pseudotuberculosis. *FEBS Lett.* **533**, 35-41 (2003).

259. Merz,A.J., So,M., & Sheetz,M.P. Pilus retraction powers bacterial twitching motility. *Nature* **407**, 98-102 (2000).

260. Hall,A. & Nobes,C.D. Rho GTPases: molecular switches that control the organization and dynamics of the actin cytoskeleton. *Philos. Trans. R. Soc. Lond B Biol. Sci.* **355**, 965-970 (2000).

261. Duan,L. *et al.* Distinct roles for Rho versus Rac/Cdc42 GTPases downstream of Vav2 in regulating mammary epithelial acinar architecture. *J. Biol. Chem.* **285**, 1555-1568 (2010).

262. Hagblom,P., Segal,E., Billyard,E., & So,M. Intragenic recombination leads to pilus antigenic variation in Neisseria gonorrhoeae. *Nature* **315**, 156-158 (1985).

263. Segal,E., Billyard,E., So,M., Storzbach,S., & Meyer,T.F. Role of chromosomal rearrangement in N. gonorrhoeae pilus phase variation. *Cell* **40**, 293-300 (1985).

264. Forest,K.T., Dunham,S.A., Koomey,M., & Tainer,J.A. Crystallographic structure reveals phosphorylated pilin from Neisseria: phosphoserine sites modify type IV pilus surface chemistry and fibre morphology. *Mol. Microbiol.* **31**, 743-752 (1999).

265. Parge,H.E. *et al.* Structure of the fibre-forming protein pilin at 2.6 A resolution. *Nature* **378**, 32-38 (1995).

266. Haas,R., Schwarz,H., & Meyer,T.F. Release of soluble pilin antigen coupled with gene conversion in Neisseria gonorrhoeae. *Proc. Natl. Acad. Sci. U. S. A* **84**, 9079-9083 (1987).

267. Dehio,C., Gray-Owen,S.D., & Meyer,T.F. The role of neisserial Opa proteins in interactions with host cells. *Trends Microbiol.* **6**, 489-495 (1998).

268. Wang,J., Gray-Owen,S.D., Knorre,A., Meyer,T.F., & Dehio,C. Opa binding to cellular CD66 receptors mediates the transcellular traversal of Neisseria gonorrhoeae across polarized T84 epithelial cell monolayers. *Mol. Microbiol.* **30**, 657-671 (1998).

269. Elliott,S.J. *et al.* The complete sequence of the locus of enterocyte effacement (LEE) from enteropathogenic Escherichia coli E2348/69. *Mol. Microbiol* **28**, 1-4 (1998).

270. Mikaty,G. *et al.* Extracellular bacterial pathogen induces host cell surface reorganization to resist shear stress. *PLoS. Pathog.* **5**, e1000314 (2009).

271. Higashi,D.L. *et al.* Dynamics of Neisseria gonorrhoeae attachment: microcolony development, cortical plaque formation, and cytoprotection. *Infect. Immun.* **75**, 4743-4753 (2007).

272. Quest,A.F., Gutierrez-Pajares,J.L., & Torres,V.A. Caveolin-1: an ambiguous partner in cell signalling and cancer. *J. Cell Mol. Med.* **12**, 1130-1150 (2008).

273. Songyang,Z. & Cantley,L.C. Recognition and specificity in protein tyrosine kinase-mediated signalling. *Trends Biochem. Sci.* **20**, 470-475 (1995).

274. Ye,K. *et al.* Phospholipase C gamma 1 is a physiological guanine nucleotide exchange factor for the nuclear GTPase PIKE. *Nature* **415**, 541-544 (2002).

275. Li,S., Wang,Q., Wang,Y., Chen,X., & Wang,Z. PLC-{gamma}1 and Rac1 coregulate EGF-induced cytoskeleton remodeling and cell migration. *Mol. Endocrinol.* **23**, 901-913 (2009).

276. Dodelet,V.C., Pazzagli,C., Zisch,A.H., Hauser,C.A., & Pasquale,E.B. A novel signaling intermediate, SHEP1, directly couples Eph receptors to R-Ras and Rap1A. *J. Biol. Chem.* **274**, 31941-31946 (1999).

277. Sakakibara,A. & Hattori,S. Chat, a Cas/HEF1-associated adaptor protein that integrates multiple signaling pathways. *J. Biol. Chem.* **275**, 6404-6410 (2000).

278. Wojcik,J. *et al.* Sequence analysis identifies a ras-associating (RA)-like domain in the N-termini of band 4.1/JEF domains and in the Grb7/10/14 adapter family. *Biochem. Biophys. Res. Commun.* **259**, 113-120 (1999).

279. Zandy,N.L., Playford,M., & Pendergast,A.M. Abl tyrosine kinases regulate cell-cell adhesion through Rho GTPases. *Proc. Natl. Acad. Sci. U. S. A* **104**, 17686-17691 (2007).

280. Gu,J.J., Ryu,J.R., & Pendergast,A.M. Abl tyrosine kinases in T-cell signaling. *Immunol. Rev.* **228**, 170-183 (2009).

281. Hantschel,O. & Superti-Furga,G. Regulation of the c-Abl and Bcr-Abl tyrosine kinases. *Nat. Rev. Mol. Cell Biol.* **5**, 33-44 (2004).

282. Bradshaw,J.M. & Waksman,G. Molecular recognition by SH2 domains. *Adv. Protein Chem.* **61**, 161-210 (2002).

283. Tomasevic,N. *et al.* Differential regulation of WASP and N-WASP by Cdc42, Rac1, Nck, and PI(4,5)P2. *Biochemistry* **46**, 3494-3502 (2007).

284. Sehgal,P.B., Guo,G.G., Shah,M., Kumar,V., & Patel,K. Cytokine signaling: STATS in plasma membrane rafts. *J. Biol. Chem.* **277**, 12067-12074 (2002).

285. Bond,C.S. & Fox,A.H. Paraspeckles: nuclear bodies built on long noncoding RNA. *J. Cell Biol.* **186**, 637-644 (2009).

286. McConnell,R.E. & Tyska,M.J. Leveraging the membrane - cytoskeleton interface with myosin-1. *Trends Cell Biol.* **20**, 418-426 (2010).

287. Even-Ram,S. & Yamada,K.M. Of mice and men: Relevance of cellular and molecular characterizations of myosin IIA to MYH9-related human disease. *Cell Adh. Migr.* **1**, 152-155 (2007).

288. Chuang,N.N. & Huang,C.C. Interaction of integrin beta1 with cytokeratin 1 in neuroblastoma NMB7 cells. *Biochem. Soc. Trans.* **35**, 1292-1294 (2007).

289. Shack,S. *et al.* Caveolin-induced activation of the phosphatidylinositol 3-kinase/Akt pathway increases arsenite cytotoxicity. *Mol. Cell Biol.* **23**, 2407-2414 (2003).

290. Ono,K. *et al.* Contribution of caveolin-1 alpha and Akt to TNF-alpha-induced cell death. *Am. J. Physiol Lung Cell Mol. Physiol* **287**, L201-L209 (2004).

291. Sedding,D.G. *et al.* Caveolin-1 facilitates mechanosensitive protein kinase B (Akt) signaling in vitro and in vivo. *Circ. Res.* **96**, 635-642 (2005).

292. Cantley,L.C. The phosphoinositide 3-kinase pathway. *Science* **296**, 1655-1657 (2002).

293. Daly,R.J. The Grb7 family of signalling proteins. *Cell Signal.* **10**, 613-618 (1998).

294. Stein,E.G., Ghirlando,R., & Hubbard,S.R. Structural basis for dimerization of the Grb10 Src homology 2 domain. Implications for ligand specificity. *J. Biol. Chem.* **278**, 13257-13264 (2003).

295. Qi,M., Liu,Y., Freeman,M.R., & Solomon,K.R. Cholesterol-regulated stress fiber formation. *J. Cell Biochem.* **106**, 1031-1040 (2009).

296. Peng,F. *et al.* TGFbeta-induced RhoA activation and fibronectin production in mesangial cells require caveolae. *Am. J. Physiol Renal Physiol* **295**, F153-F164 (2008).

297. Yang,B., Radel,C., Hughes,D., Kelemen,S., & Rizzo,V. p190Rho GTPase-Activating Protein Links the {beta}1 Integrin/Caveolin-1 Mechanosignaling Complex to RhoA and Actin Remodeling. *Arterioscler. Thromb. Vasc. Biol.*(2010).

298. Swaney,J.S. *et al.* Focal adhesions in (myo)fibroblasts scaffold adenylyl cyclase with phosphorylated caveolin. *J. Biol. Chem.* **281**, 17173-17179 (2006).

299. Han,J. *et al.* Role of substrates and products of PI 3-kinase in regulating activation of Rac-related guanosine triphosphatases by Vav. *Science* **279**, 558-560 (1998).

300. Mikaty,G. *et al.* Extracellular bacterial pathogen induces host cell surface reorganization to resist shear stress. *PLoS. Pathog.* **5**, e1000314 (2009).

301. Higashi,D.L. *et al.* Influence of type IV pilus retraction on the architecture of the Neisseria gonorrhoeae-infected cell cortex. *Microbiology* **155**, 4084-4092 (2009).

302. Hanisch,J. *et al.* Molecular dissection of Salmonella-induced membrane ruffling versus invasion. *Cell Microbiol.* **12**, 84-98 (2010).

303. Krueger,E.W., Orth,J.D., Cao,H., & McNiven,M.A. A dynamin-cortactin-Arp2/3 complex mediates actin reorganization in growth factor-stimulated cells. *Mol. Biol. Cell* **14**, 1085-1096 (2003).

304. Dowrick,P., Kenworthy,P., McCann,B., & Warn,R. Circular ruffle formation and closure lead to macropinocytosis in hepatocyte growth factor/scatter factor-treated cells. *Eur. J. Cell Biol.* **61**, 44-53 (1993).

305. Orth,J.D., Krueger,E.W., Weller,S.G., & McNiven,M.A. A novel endocytic mechanism of epidermal growth factor receptor sequestration and internalization. *Cancer Res.* **66**, 3603-3610 (2006).

306. Orth,J.D. & McNiven,M.A. Get off my back! Rapid receptor internalization through circular dorsal ruffles. *Cancer Res.* **66**, 11094-11096 (2006).

307. Holz,C., Opitz,D., Mehlich,J., Ravoo,B.J., & Maier,B. Bacterial motility and clustering guided by microcontact printing. *Nano. Lett.* **9**, 4553-4557 (2009).

308. DiDonato,D. & Brasaemle,D.L. Fixation methods for the study of lipid droplets by immunofluorescence microscopy. *J. Histochem. Cytochem.* **51**, 773-780 (2003).

309. Kiernan,J.A. Formaldehyde, formalin, paraformaldehyde and glutaraldehyde: What they are and what they do. *Microscopy Today* **00-1**, 8-12 (2000).

310. Dietrich,M., Mollenkopf,H., So,M., & Friedrich,A. Pilin regulation in the pilT mutant of Neisseria gonorrhoeae strain MS11. *FEMS Microbiol. Lett.* **296**, 248-256 (2009).

APPENDIX

6 Appendix

6.1 Abbreviations

AA	amino acid
APS	ammonium peroxodisulfate
Bfp	bundle-forming pilus
BSA	bovine serum albumin
Cas	Crk-associated substrate
Cav1	caveolin-1
Cav2	caveolin-2
Cav3	caveolin-3
Cdc42	cell division cycle 42
CEACAM	carcinoembryonic antigen cellular adhesion molecule
CSD	caveolin scaffolding domain
Csk	C-terminal Src kinase
Cyt D	cytochalasin D
ddH_20	double distilled water
DGI	disseminated gonococcal infection
DMEM	Dulbecco's modified Eagle medium
DNA	deoxyribonucleic acid
ECL	enhanced chemiluminescence
EDTA	ethylenediaminetetraacetic acid
EGFR	epidermal growth factor receptor
EGTA	ethylene glycol tetraacetic acid
ELISA	enzyme-linked immunosorbent assay
eNOS	endothelial nitric oxide synthase
EPEC	enteropathogenic *Escherichia coli*
Esp	EPEC-secreted protein
FAK	focal adhesion kinase
FCS	fetal calf serum
GAP	GTPase-activating protein
GC	*Neisseria gonorrhoeae*
GEF	guanine nucleotide exchange factors
GFP	green fluorescent protein
Gm^P	gentamicin-protected
gonococci	*Neisseria gonorrhoeae*
Gp96	glycoprotein 96
GPCR	G-protein-coupled receptor
Grb7, 10	growth factor receptor-bound protein 7, 10
GTP	guanosine-5'-triphosphate

HRP	horseradish peroxidase
HSPG	heparan sulfate proteoglycan
IB	immunoblot
ICAM-1	intercellular cell adhesion molecule 1
I-domain	inserted domain
IF	immunofluorescence
IgA	immunoglobulin A
IP	immunoprecipitation
kDa	kilodalton
LEE	locus of enterocyte effacement
LOS	lipooligosaccharide
LPS	lipopolysaccharide
Maldi-MS/MS	matrix-assisted laser desorption/ionization tandem mass spectrometry
MC	microcolony
meningococci	*Neisseria meningitidis*
MOI	multiplicity of infection
MβCD	methyl-β-cyclodextrin
Opa	opacity associated
P^+GC	piliated *Neisseria gonorrhoeae*
p190RhoGAP	p190 Rho GTPase-activating protein
PAGE	polyacrylamide gel electrophoresis
PAK	p21-activated kinase
PBS	phosphate buffered saline
PEG	poly-ethylene glycol
PFA	paraformaldehyde
phospho-Tyr14-Cav1	tyrosine 14-phosphorylated Cav1
PI3K	phosphoinositide 3-kinase
PIKE	phosphatidylinositol-3-OH kinase PI3K enhancer
pilC, D, E, F etc.	pilus-associated proteins C,D,E,F etc.
PIP2	phosphatidylinositol-4,5-bisphosphate
PIP3	phosphatidylinositol-3,4,5-trisphosphate
PIPES	piperazine-N,N'-bis(2-ethanesulfonic acid)
PKA	protein kinase A
PKC	protein kinase C
PLCδ-PH	phospholipase C delta pleckstrin homology domain
PLCγ1	phospholipase C gamma 1
PMN	polymorphonuclear leukocytes
PTB	phosphotyrosine binding
PTP	phosphotyrosine phosphatase
PVDF	polyvinylidene-fluoride

Rac1	Ras-related C3botulinum toxin substrate
RFP	red fluorescent protein
Rho	Ras homolog gene family
RhoA	Ras homolog gene family, member A
Rho-GDI	Rho protein GDP dissociation inhibitor
RNA	ribonucleic acid
RNAi	RNA interference
Rock	Rho-associated serine/threonine kinase
rpm	rounds per minute
RPMI	roswell park memorial institute
SDS	sodium dodecyl sulphate
SFPQ/PSF	splicing factor proline/glutamine rich
SH2	Src-homology 2
SH3	Src-homology 3
shRNA	short hairpin RNA
siRNA	small interfering RNA
Src	sarcoma
STAT	signal transducer and activator of transcription
STI	sexually transmitted infection
Syk	spleen tyrosine kinase
TARP	translocated actin recruiting phosphoprotein
TBS	tris buffered saline
TEM	transmission electron microscopy
TEMED	tetramethylethylenediamine
Tfp	type-IV-pili
Tir	translocated intimin receptor
TNFα	tumor necrosis factor alpha
Tris	tris(hydroxymethyl)aminomethane
TTSS	type III secretion system
Tyr14	tyrosine 14
WASP	Wiskott-Aldrich syndrome protein
WHO	World Health Organization

6.2 Supplementary video material

Live cell movies are provided as supplementary material on the enclosed DVD. All movies are available in two different formats: Divx and Cinepak. The Divx format requires installation of the Divx Codec available at www.divx.com. Cinepak encoded movies can be viewed on any PC but are bigger in size and a little lower in detail.

Movie 1 (Figure 3-2)**:**

Cav1-GFP recruitment to P^+GC

ME-180 cells were transfected with Cav1-GFP and subsequently infected with P^+GC. Images for the movie were acquired every 25 seconds

Movie legend:

Left panel:	Cav1-GFP fluorescence signal
Right panel:	Overlay of phase contrast and the Cav1-GFP fluorescence signal
Green (right panel):	Cav1-GFP
White arrows (right panel):	Early Cav1-GFP recruitment to attached P^+GC

Movie 2 (Figure 3-26)**:**

Infection of fixed cells results in reduced capacity of P^+GC to form MCs on host cells.

Fixed and living ME-180 cells were infected with P^+GC and the infection was monitored using live cell microscopy for 120 min. As an additional control, uninfected cells were also recorded for 120 min. Images for the movie were acquired every 5 seconds.

Movie legend:

Left panel:	Phase contrast: Living ME-180 cells, not infected
Middle panel:	Phase contrast: Living ME-180 cells, P^+GC infected
Right panel:	Phase contrast: Fixed ME-180 cells, P^+GC infected
Boxes (middle panel):	Membrane ruffles following P^+GC infection
White arrows (middle panel):	MC formation on living cells
White arrows (right panel):	MC formation on fixed cells
Black arrows (middle panel):	MC fusion on living cells

Movie 3 (Figure 3-27)**:**

Infection of fixed cells results in reduced capacity of P^+GC to form MCs on host cells and in increased motility speeds of P^+GC over time.

Tracking of individual diplococci residing in or close to MCs. The movie is combined of four parts: part 1 (frame 0-240) was recorded 45 min post infection with P^+GC, part 2 (frame 241-481) was recorded 60 min post infection, part 3 (frame 482-722) was recorded 100 min post infection and part 4 (frame 723-963) was recorded 120 min post infection. Minutes post infections are indicated in the movie. Images for the movie were acquired every 100 milliseconds.

Movie legend:

Left upper panel:	Phase contrast: Fixed ME-180 cells, P^+GC infected
Right upper panel:	Phase contrast: Fixed ME-180 cells, P^+GC infected, magnified excerpt
Left lower panel:	Phase contrast: Living ME-180 cells, P^+GC infected
Right lower panel:	Phase contrast: Living ME-180 cells, P^+GC infected, magnified excerpt
White squares (left panels):	Position of magnified excerpts
White arrows (right panels):	Motility of attached P^+GC

Movie 4 (Figure 3-29)**:**

Tracking of P^+GC-GFP reveals the dependence of P^+GC on host cells to localize into MCs.

ME-180 cells were infected with P^+GC-GFP and the infection was monitored by confocal live cell imaging for 90 min. GFP fluorescent bacteria were tracked and resulting tracks are displayed as vectors. Images for the movie were acquired every 30 seconds.

Movie legend:

Left upper panel:	Phase contrast: Living ME-180 cells, P^+GC-GFP infected
Middle upper panel:	P^+GC-GFP fluorescence signal, Living ME-180 cells, P^+GC-GFP infected
Right upper panel:	Overlay fluorescence signal and P^+GC movement vectors on living cells
Left lower panel:	Phase contrast: Fixed ME-180 cells, P^+GC-GFP infected
Middle lower panel:	P^+GC-GFP fluorescence signal, Fixed ME-180 cells, P^+GC-GFP infected
Right lower panel:	Overlay fluorescence signal and P^+GC movement vectors on fixed cells
Green:	P^+GC-GFP

Movie 5 (Figure 3-30)**:**

Live-cell microscopy demonstrates formation of membrane ruffles on host cells during P^+GC infection which move the bacteria towards the cell center.

Strong membrane movements can be observed as wave-like membrane ruffles pushing P^+GC from the cell poles to the cell centre. Images for the movie were acquired every 30 seconds.

Movie legend:

Green:	P^+GC-GFP
Red arrows:	Membrane ruffling

Movie 6 (Figure 3-31)**:**

P^+GC are exchanged between close MCs.

To observe possible interbacterial communication fusing MCs were followed closely by live-cell imaging. Individual diplococci moved from one MC towards the other, interacted there with other bacteria and finally twitched back to the first MC. Images for the movie were acquired every 3 seconds.

Movie legend:

Black arrows:	MC fusing and exchanging individual P^+GC

6.3 Publications and talks

6.3.1 Publications:

Boettcher J.P., Kirchner M., Churin Y., Kaushansky A., Pompaiah M., Thorn H., Brinkmann V., Macbeath G. and Meyer T.F. Tyrosine-phosphorylated caveolin-1 blocks bacterial uptake by inducing Vav2-RhoA-mediated cytoskeletal rearrangements. *PLoS. Biol.* **8**, (2010).

Asakura H., Churin Y., Bauer B., **Boettcher J.P.**, Bartfeld S., Hashii N., Kawasaki N., Mollenkopf H.J., Jungblut P.R., Brinkmann V. and Meyer T.F. *Helicobacter pylori* HP0518 affects flagellin glycosylation to alter bacterial motility. *Mol. Microbiol.* **78**, 1130-1144 (2010).

Dietrich, M., Munke R., Gottschald M., Ziska E., **Boettcher J.P.**, Mollenkopf H. and Friedrich A. The effect of hfq on global gene expression and virulence in *Neisseria gonorrhoeae*. *FEBS J.* **276**, 5507-5520 (2009).

Peth A., **Boettcher J.P.** and Dubiel W. Ubiquitin-dependent proteolysis of the microtubule end-binding protein 1, EB1, is controlled by the COP9 signalosome: possible consequences for microtubule filament stability. *J. Mol. Biol.* **368**, 550-563 (2007).

Boettcher J.P., Lange C., Rechner C. and Meyer T.F. Microcolony formation of *Neisseria gonorrhoeae* is a multi step process which requires host cell participation. (Manuscript in preparation)

6.3.2 International talks:

14th International Pathogenic Neisseria Conference 2008, Rotterdam: “Caveolin recruitment prevents premature host cell entry of type IV pili producing *Neisseria gonorrhoeae*.”

Spetsai Summer School 2006 - EMBO/FEBS/FEMS Lecture Course. Island of Spetsai, Greece: “Tyrosine phosphorylation of Caveolin-1 is required for recruitment to *Neisseria gonorrhoeae* infection sites.”

6.4 Acknowledgements

First of all I would like to thank Prof. Thomas Meyer for providing this interesting project, his close supervision of my thesis and all scientific discussions and help throughout the years. His advice has been very important for this work and guided me through this formative time of my career.

I am also grateful to Prof. Jörg Hacker and Prof. Thomas Rudel who I could always approach to discuss my project and who kindly agreed to review this thesis.

Many thanks to Dr. Yury Churin, “Jura”, who inspired and supported my work with his brilliant ideas and uncountable contributions to my daily bench work! Also I would like to thank Dr. Marieluise Kirchner who introduced me to the *Neisseria* field and to the work in the lab. Marie and Jura initiated this project and I am very thankful that they decided to collaborate with me.

I would like to express my gratitude to all members of the *Neisseria* group who supported me during all phases of my thesis. Also I wish to sincerely thank all my colleagues and friends at the Department of Molecular Biology who accompanied and helped me throughout this important time.

Most importantly, I would like to express my profound thankfulness to Ana, my parents, my brother and my closest friends for all their support, encouragement, motivation and love.

6.5 Selbstständigkeitserklärung

Hiermit erkläre ich, dass ich die vorliegende Arbeit selbstständig und nur mit den angegebenen Hilfsmitteln erstellt habe.

Berlin, den